Title
Structure-function relations in the intervertebral disc: Age- and disease-mediated changes alter the tensile failure mechanics of the annulus fibrosus

Author
Werbner, Benjamin

Publication Date
2021

Peer reviewed|Thesis/dissertation

Structure-function relations in the intervertebral disc:

Age- and disease-mediated changes alter the tensile failure mechanics of the annulus fibrosus

by

Benjamin Nathan Werbner

A dissertation submitted in partial satisfaction of the

requirements for the degree of

Doctor of Philosophy

in

Engineering – Mechanical Engineering

in the

Graduate Division

of the

University of California, Berkeley

Committee in charge:

Professor Grace D. O'Connell, Chair

Professor Lisa A. Pruitt

Professor Robert J. Full

Fall 2021

Structure-function relations in the intervertebral disc:

Age- and disease-mediated changes alter the tensile failure mechanics of the annulus fibrosus

by

Benjamin Nathan Werbner

Abstract

Structure-function relations in the intervertebral disc: Age- and disease-mediated changes alter the tensile failure mechanics of the annulus fibrosus

by

Benjamin Nathan Werbner

Doctor of Philosophy in Mechanical Engineering

University of California, Berkeley

Professor Grace D. O'Connell, Chair

Back pain is a widespread economic and public health concern, affecting around 70% of the population and incurring annual costs over $100 billion in the US alone. Back pain is frequently associated with degenerative changes to intervertebral discs, including altered biochemical composition, rheology, and mechanics. However, due to the interdependent cascade of degenerative changes occurring *in vivo*, the relative contribution of individual tissue constituents to disc failure remains unclear. Elucidating the fundamental structure-function relations that drive tissue failure aids in the prevention of avoidable injuries, guides the design of protective therapies and tissue repair strategies, and facilitates the development of advanced computational models that may help predict tissue injury.

This dissertation details the development, validation, and implementation an experimental framework to elucidate fundamental tissue-level structure function relations between degeneration- and disease-mediated biochemical changes and annulus fibrosus (AF) failure mechanics. *Chapter 2* reports on the development and validation of a novel method for repeatable failure testing of soft tissues with fibers oriented off-axis from the applied loading, such as AF specimens tested in the circumferential-radial or circumferential-axial orientations. With minor subsequent modification, the method described in *Chapter 2* serves as the basis for the reliable characterization of AF tensile failure mechanics in subsequent chapters. *Chapter 3* describes the effects of enzymatic proteoglycan degradation and concomitant water loss on AF tensile failure mechanics in the circumferential-radial direction at low and high loading rates. *Chapter 4* provides a brief empirical analysis of the relative contribution of the three main AF biochemical constituents to the tensile failure mechanics of AF tissue from a cross-sectional population of human donors

The use of 0.15M phosphate-buffered saline in *Chapters 3* and *4* resulted in hyper-physiologic tissue water contents, which are known to alter the tissue mechanical response. Thus, *Chapter 5* provides a more robust method to target and maintain AF hydration levels, mechanics, and composition at fresh-tissue levels during *in vitro* testing. *Chapter 6* utilizes these methods to provide discrete and continuous descriptions of the role of advanced-glycation end products in AF sub-failure, failure, and post-failure tensile mechanics at quasi-static and dynamic loading rates. Finally, *Chapter 7* addresses the limitations of the current work and suggests possible directions for future investigations that might build on this dissertation work.

Table of Contents

List of Figures

List of Tables

Acknowledgements

First and foremost, I would like to thank my research advisor, mentor, and role model—Professor Grace O'Connell. I applied to the MS/PhD program in Mechanical Engineering at Berkeley with no background or previous experience in the field. Rather than seeing this as a risk or a burden, Professor O'Connell, in her characteristically optimistic and encouraging manner, provided the perfect balance of guidance, support, patience, and independence for me to grow into the scientist that I am proud to be. I hope to achieve even a fraction of your success running a productive and diverse lab while continuing to pursue my extracurricular passions at such an incredibly impressive level.

I would like to acknowledge Professor Lisa Pruitt for her unconditional encouragement, enthusiasm, and insight over the last six years. Not only did your thoughtfully accessible and engaging course provide most of my background in Mechanics, but it also opened my eyes to the value of approaching engineering from a high-level, conceptual, and associative perspective. Your ability to teach to multiple learning styles simultaneously has provided great benefit to your students (as I learned firsthand when I had the honor of teaching this same course alongside you several years later) and is a skill that I hope to take into any teaching that I may do in the future. I would also like to thank Professor Robert Full for sharing his contagious exuberance and excitement for science, particularly the wonders of biology. Helping to teach your course was truly a joy and helped open my eyes to all that engineers stand to learn from nature.

I must also thank all of the past and present members of the Berkeley Biomechanics Lab, particularly my friend and collaborator, Dr Minhao Zhou. From sitting down at the conference table for that first, unintentional collaboration, to teaching and publishing together, and finally giving our PhD exit seminars just a few weeks apart, we've always been on the same wavelength, and I can't imagine my PhD without you. Special thanks also to my colleague and good friend, Emily Lindberg— desk-neighbor, spontaneous Tajo daytripper, and one of the only people who despite significantly shorter legs can consistently outpace me power-walking uphill. Despite our distinct research areas and opposite personalities, our friendship and shared love of the mountains (and coffee) has been a significant part of my PhD experience. I would also like to acknowledge Dr Noah Bonnheim for introducing me to the field of biomechanics—first in theory and shortly thereafter in practice— and for helping to jumpstart my research career with our early collaborative work. I would also like to thank Dr Semih Bezci, Jonathon McKinley, Gabriel Lopez, Tongge Wu, and Shiyin Lim for being integral parts of the wonderfully diverse and close-knit Berkeley Biomechanics community.

My deepest gratitude goes out to my friends Michael Lieb and Colin Wahl for continually keeping me stoked, sane, and safe in the mountains, and for patiently sharing many hours and insights on long drives, cramped belays, and icy skintracks. Special thanks also to my dear friend Dianne Weinthal, who has truly been there for me through it all, knows me better than anyone does, and has always believed in me nonetheless. I am incredibly grateful to have met Jasmine Hennessy and Paul Rezucha just as I embarked on my doctoral journey; thank you both for leading me to nature when I needed it most and for sharing your unique and inspiring energies over the last six years. Finally, I would like to thank my unwaveringly supportive family, without whom, at so many times and in so many ways, this would never have been possible.

1. Background and Motivation

1.1 Back pain and intervertebral disc degeneration

Back pain is a widespread economic and public health problem in industrialized societies worldwide, affecting millions of patients and incurring total costs over $100 billion annually in the United States alone [Maniadakis and Gray, 2000; Katz, 2006]. Primary care providers report that only the common cold exceeds back pain in terms of complaint frequency, with around 70% of the population expected to experience an episode of back pain each year [Hart et al., 1995]. Several etiological factors may contribute to back pain, however accumulating evidence suggests a strong association between back pain and degenerative changes to the intervertebral disc [Buckwalter, 1995; Luoma et al., 2000; Urban and Roberts, 2003; Adams and Roughley, 2006].

While disc degeneration is not always accompanied by pain or other symptoms, severe lumbar disc degeneration that is detectable radiographically has been associated with a two-fold increase in the risk of low back pain [Hicks et al., 2009]. It has also been established that structural disruption or damage to the disc is associated with significant pain and neurologic dysfunction [Jacobs et al., 2011], and that degenerative compositional and structural changes to the disc can alter disc loading conditions and cause joint instability [Cheng and Welch, 2008; Adams et al., 2015], which has been suggested to contribute to the degenerative cascade. However, the mechanisms linking degenerative compositional and structural changes in the disc with gross disc injuries such as annular tears are still being actively studied and are a central focus of this work. The following sections provide essential information on disc composition, structure, and function in order to support the objectives of the current work.

1.2 Intervertebral disc composition and structure

The intervertebral disc is a fibrocartilaginous joint located between adjacent vertebrae in the spine. Discs attach to the vertebral bodies via hyaline cartilage endplates, which facilitate fluid and nutrient diffusion into and out of the disc [Roberts et al., 1989]. The disc is a two-part structure composed of a soft, gel-like center (nucleus pulposus, 'NP') surrounded by a tough, fibrous ring (annulus fibrosus, 'AF'). The NP is composed primarily of water (80-85% by wet weight) and proteoglycans (50% by dry weight) with some type 2 collagen and elastin fibers loosely organized into quasi-homogenous gel [Antoniou et al., 1996; Roughley et al., 2002]. Previous studies have demonstrated minor radial variation in the composition of the nucleus which facilitates a smooth gradient between the outer NP and the inner AF [Iatridis et al., 2007; Bezci et al., 2019].

The AF tissue solid phase is composed primarily of type 1 collagen fiber bundles (55-70% by dry weight) suspended in a hydrated matrix of proteoglycans (10-15% by dry weight. Proteoglycans are macromolecule polysaccharides composed of core proteins bound by chains of anionic mucopolysaccharide molecules such as keratin sulfate and chondroitin sulfate, collectively known as sulfated glycosaminoglycans (GAGs) [Watanabe et al., 1998, Kiani et al., 2002] (**Figure 1A**). These molecules may aggregate and bind to hyaluronan backbone molecules via linker proteins to form aggrecan, the primary proteoglycan of the intervertebral disc [Roughley et al., 2002]. The negatively charged carboxyl and sulfate groups of the GAG sidechains attract positively charged inorganic ions, such as sodium and potassium, generating an osmotic pressure gradient that maintains tissue water content and fluid pressure [Urban and Roberts, 2003]. Other proteoglycans, such as decorin and biglycan, are also present in the disc, albeit in smaller quantities and with less well-studied functions [Melrose et al., 2001].

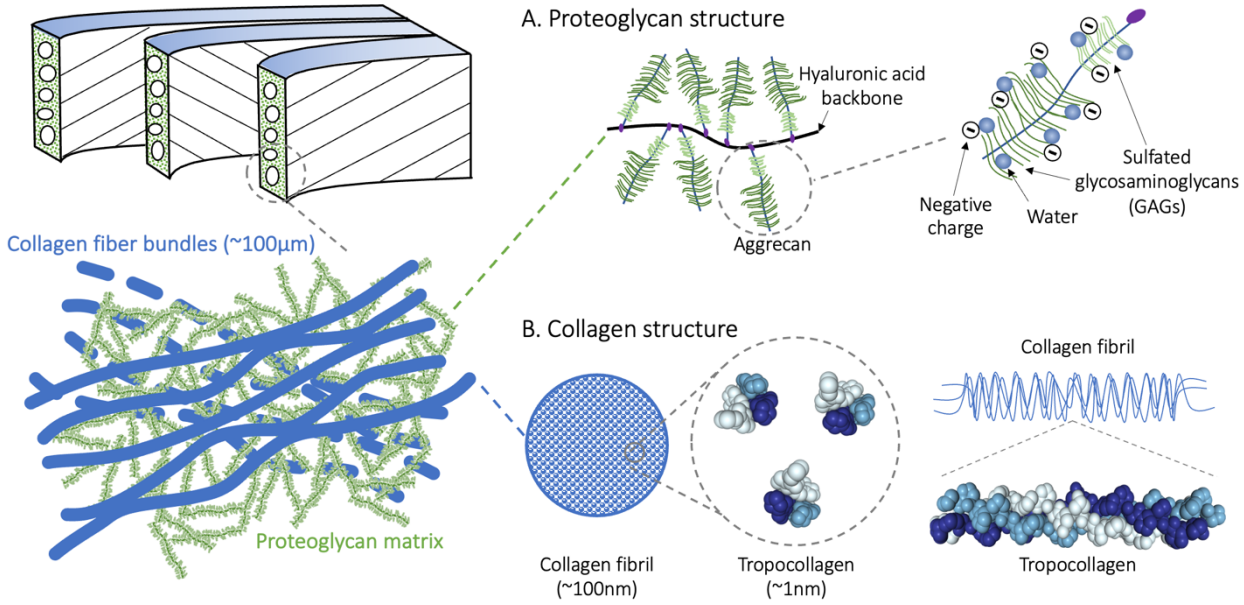

Figure 1: Schematic of annulus fibrosus composition illustrating proteoglycan and collagen structure.

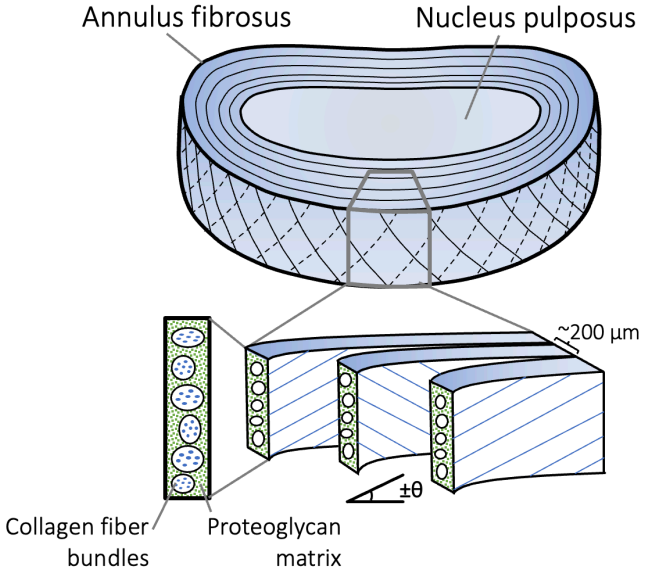

Figure 2: Schematic of annulus fibrosus architecture.

The AF is a highly organized structure composed of 150-200µm layers of unidirectionally aligned populations of collagen fiber bundles, which range in orientation from ±45° in the inner AF to ±30° in the outer AF with respect to the transverse plane and which approximately reverse orientation between adjacent layers [Cassidy et al., 1989; Marchand and Ahmed, 1990] (**Figure 2**). Like other fibril-forming collagen structures, AF type 1 collagen is hierarchically organized in 100µm fiber bundles which are in turn composed of 100nm collagen fibrils, and so on down to the nanometer-scale tropocollagen helix structure (**Figure 1B**). In addition to this structural variation along the disc radius, proteoglycan and water content decrease significantly from inner to outer

AF concurrent with an increase in type 1 collagen and type 1-to-type 2 collagen ratio [Skaggs et al., 1994; Iatridis et al., 2007]. Discs have also been shown to contain smaller amounts of other collagens, including Types III, V, and IX [Wu et al., 1987; Boos et al., 1997] and other macromolecules such as elastin. While the roles of these molecules continue to be explored, it is generally agreed that their mechanical function is minor compared to that of collagen, proteoglycans, and water, which will be the focus of this dissertation.

1.3 Intervertebral disc function

The disc's primary roles are to absorb and distribute multi-axial static and dynamic loads and to facilitate limited compound movements of the spine. The stresses experienced by the disc have been estimated to range between 0.1-2.5 MPa and have been shown to vary between activities such as sitting, walking, or lifting [Nachemson, 1981; Wilke et al., 1999]; these forces are understood to be substantially mediated by muscle contraction in addition to external loads [Panjabi and White, 1990]. At the joint level, the disc experiences compression, tension, bending, torsion, and various combinations of these loading modalities, with forces likely exceeding several times body weight [Panjabi and White, 1990; Bartel et al., 2006]. Additionally, the loading rates experienced by the disc are complex, varied, and difficult to determine experimentally, however it is known that the disc exhibits significant viscoelastic behavior, with distinct mechanical responses varying between low and high loading rates. The mechanical viscoelasticity of the disc is attributable to both solid-component viscoelasticity as well as fluid-mediated effects [Urban and Roberts, 2003; Iatridis et al., 2013].

The two-part structure of the disc imparts its unique ability to redistribute loads. Under most physiological loading conditions, disc loading involves compression and subsequent hydrostatic pressurization of the nucleus pulposus, which in turn exerts outward pressure on the annulus fibrosus, inducing circumferential stresses and strains, and to a lesser extent radial stresses and strains [Bartel et al., 2006] (**Figure 3**). While various alternate mechanisms of loading in the context of disc degeneration and pathology remain an active area of research, it is understood that a loss of fluid pressure in aged and degenerate nucleus pulposus tissue results in diminished nuclear pressurization, which in turn leads to direct compressive, tensile, and torsional loading of the annulus fibrosus [Bartel et al., 2006; Adams and Roughley, 2006; Adams et al., 2015].

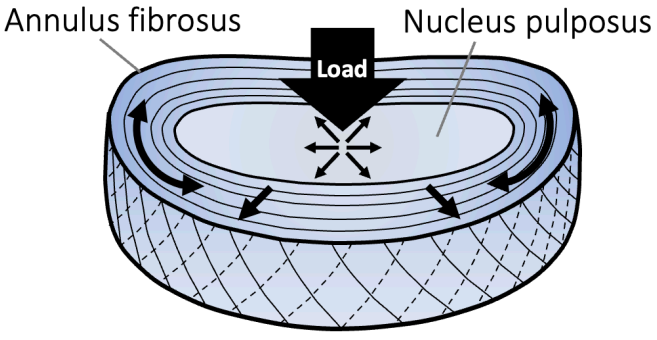

Figure 3: Schematic illustration of disc loading. Nuclear pressurization generates circumferential and radial tensile stresses in the annulus.

1.4 Degenerative compositional changes

Disc degeneration is characterized by altered biochemical composition, including the loss of proteoglycans and water, the loss of disc height, increased non-enzymatic collagen crosslinks, and the accumulation of inter- and intra-lamellar damage, including circumferential and radial tears and lesions [Adams and Roughley, 2006]. Notable compositional changes in the nucleus pulpous include the fragmentation and loss of proteoglycans and the concomitant loss of water content and nuclear depressurization [Urban and Roberts, 2003]. In the inner annulus, replacement of type II collagen fibrils by type I fibers with an overall increase in collagen content has been observed [Adams and Roughley, 2006]. Additionally, collagens throughout the disc become increasingly crosslinked over time [Pokharna and Phillips, 1998; Sivan et al., 2006]. This suite of degenerative compositional changes results in altered disc loading conditions [Adams et al., 2015]. Diminished disc composition combines with altered loading conditions, accumulated structural damage, and adverse cellular remodeling to form a cyclic cascade of degeneration. These biochemical and structural hallmarks of degeneration have been associated with significant alterations in disc mechanical and rheological behavior [Maroudas et al., 1975; Adams et al., 1996] and are expected to alter the viscoelastic and failure properties of the tissue (**Figure 4**).

In addition to the natural process of aging, certain clinical pathologies have been associated with increased rates or extents of disc degeneration. Among risk factors studied in the Nurses' Health Study, diabetes had the highest relative risk of intervertebral disc herniation (relative risk: 1.52, 95% CI: 1.17 to 1.98) after correcting for additional factors such as age, body mass index, level of exercise, *etc.* [Jhawar et al., 2006]. Additionally, previous work showed that diabetes was associated with increased frequency and severity of lower back pain and diminished treatment outcomes [Mäntyselkä et al., 2008; Licciardone et al., 2013; Takahashi et al., 2013; Freedman et al., 2011]. One of the most well-documented changes in connective tissues occurring with diabetes is the accumulation of advanced glycation end-products (AGEs) [Monnier et al., 1986; Singh et al., 2001; Vlassara and Palace, 2002; Ahmed, 2005; Tsai et al., 2014]. Minimal biological turnover and a long half-life makes collagen and proteoglycans in the intervertebral disc particularly susceptible to interaction with glycating metabolites and AGE formation [Pokharna and Phillips, 1998; Vlassara and Palace, 2002; Snedeker and Gautieri, 2014]. AGEs have also been shown to accumulate naturally in the disc with age [Pokharna and Phillips, 1998; Sivan et al., 2006], although the rate and extent of intradiscal AGE accumulation is amplified with diabetes [Tsai et al., 2014].

1.5 Disc structural failure

Degeneration, disease, and injury alter disc biochemical composition and have been shown to adversely impact mechanical and rheological performance [Urban and Roberts, 2003; Adams and Roughley, 2006]. Unfortunately, the disc's avascularity results in minimal self-healing capabilities. As such, accumulated damage, such as annular tears or endplate disruption, tends to catalyze a cascade of degenerative remodeling [Panjabi, 1990]. Histological study of cadaveric disc tissues has distinguished three tear morphologies in the annulus fibrosus: circumferential tears (also called 'delamination'), radial fissures, and peripheral rim tears [Adams and Roughley, 2006]. Incidence of these structural failures has been observed as early as the second decade of life and they are nearly ubiquitous in disc tissues from middle-aged individuals [Boos et al., 2002]. While the relationship between normal, traumatic, and pathological disc loading and the development of specific tear morphologies continues to be researched and debated, it has been suggested that circumferential tears may be attributable to interlaminar shear stresses possibly arising from

stress concentrations in older, degenerate discs [Goel et al., 1995]. In contrast, peripheral rim tears have often been associated with traumatic injuries [Osti et al., 1992]. Radial fissures have been widely observed in cadaveric disc tissues and have been successfully induced *in vitro* by cyclic loading in bending and compression [Adams et al., 2002]. Radial fissures are more strongly associated with degeneration than other tear morphologies [Osti et al., 1992].

Radial fissures that progress to a sufficient extent may allow radial migration of pressurized nucleus pulpous material, disrupting disc bulk morphology and function. Depending on the extent, such a morphological change may be labeled as disc bulging, prolapse, extrusion, or sequestration [Adams et al., 2002]. Interestingly, disc prolapse induced mechanically *in vitro* occurs more readily in 'modestly degenerated' discs than in 'severely degenerated' discs, suggesting that nuclear pressurization is a driving force behind disc herniation [Adams and Hutton, 1982]. Bulging, prolapsed, or herniated discs may all compress nearby nerves or the spinal column, causing debilitating back and leg pain and reducing patient mobility [Luoma et al., 2000].

1.6 Historical approaches to study disc mechanics

Over the last 100 years, intervertebral disc research has sought to develop a deeper understanding of spine biomechanics, the complex relationship between disc health and back pain, and the mechanisms of spinal injury and repair. Unfortunately, inducing joint-level disc failures *in vitro* that mimic *in vivo* herniation morphologies is challenging, requiring multiple simultaneous loading modalities and hyper-physiological loads to be applied [Wilder et al., 1998; Veres et al., 2008; Berger-Roscher et al., 2017; Tavakoli et al., 2018]. Additionally, the relationships between pain, injury, and degeneration are complex and highly interdependent [Luoma et al., 2000]. Therefore, researchers have focused on better understanding tissue-level mechanics, where the role of tissue subcomponents can be more systematically investigated.

Researchers have sought to better understand the mechanisms of disc injury for nearly a century. While many of the fundamental clinical questions remain the same, the experimental approaches utilized to answer them have developed significantly. This progression can be described by two trends: experimentation on smaller length scales due to technological advancements, and an increased emphasis on fundamental, material-level tissue mechanics. As such, experimental research on disc tissues has proceeded cyclically over the years. Important recurring themes include the relationships between age or degeneration and tissue structure, 'structure-function' relationships linking tissue structure and composition with rheology and mechanics, and multiscale relationships between the hierarchical levels of the disc.

Modern study of the disc began in the early 1930s with work that began to address these themes [Beadle, 1931; Göcke, 1932]. As whole-disc mechanics became better understood through the late 1950s, increased interest developed in tissue-level testing to better understand constituent contributions to whole-disc mechanics [Brown et al., 1957; Galante et al., 1967]. Over the subsequent decades, numerous influential studies contributed to an improved understanding of tissue-level rheological structure-function relations, morphological micro-architecture, and tissue permeability [Urban, 1977; Marchand and Ahmed, 1990; Gu et al., 1999]. Improved experimental techniques over the past 20 years have brought about a new era of multiscale mechanics with reliable characterization of single lamellar mechanics, fibrillar mechanics, and micron-scale damage accumulation [Skaggs et al., 2014; Holzapfel et al., 2005; Pezowicz et al., 2006; Tavakoli et al., 2018]. Recent studies have also continued to elucidate tissue-level mechanical structure-function relationships. These studies have shown that water content, collagen content, and collagen

crosslinking all affect sub-failure and failure properties, and that these effects are dependent on the applied loading conditions [Wagner et al., 2006; Isaacs et al., 2014].

Despite these advancements, experimental characterization of tissue mechanics is still limited. For example, there remains a limited supply of healthy human disc tissue that has not experienced degeneration or trauma [Pfirrmann et al., 2001; Vernon-Roberts et al., 2007]. Additionally, complex and variable physiological loads and boundary conditions experienced by the disc *in vivo* are difficult to recapitulate during *in vitro* testing. For this reason, many researchers default to quasi-static mechanical testing in room-temperature physiological saline solutions.

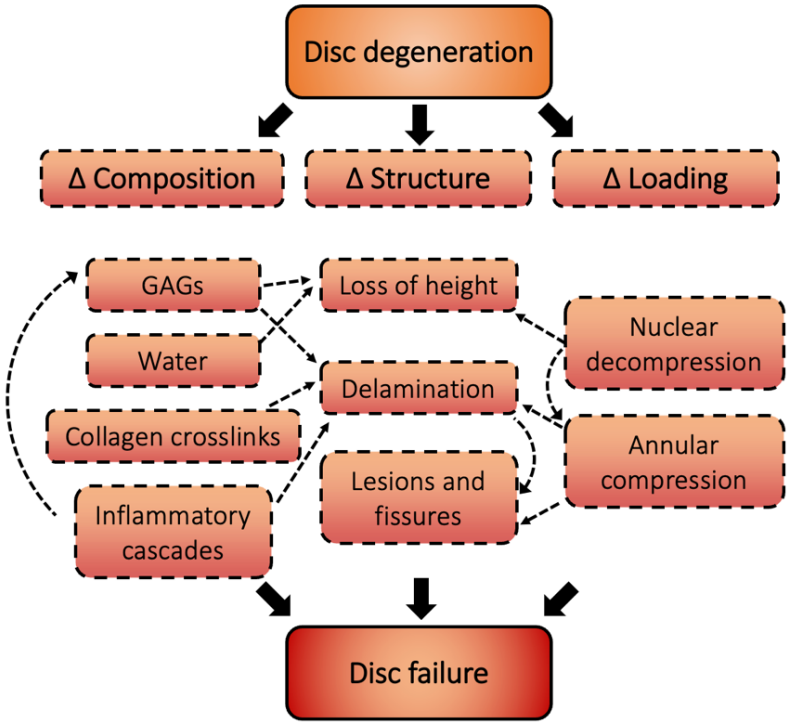

Figure 4: Simplified representation of the disc degenerative cascade.

1.7 In vivo versus in vitro approaches to study disc mechanics

Early studies seeking to understand the relationship between disc degeneration and altered tissue mechanical function tested cadaveric disc tissues from human populations exhibiting a range of degenerative changes [Galante, 1967; Acaroglu et al., 1995; Ebara et al., 1996]. While some studies have reported diminished failure mechanics in degenerate discs, the complex and highly variable cascade of degenerative changes and adaptive remodeling occurring *in vivo* make it difficult to understand the fundamental mechanisms driving alterations in tissue failure properties in the context of degeneration (**Figure 4**). For example, Acaroglu et al. (1995) reported diminished failure stress and strain energy density in degenerate human discs but were not able to provide a mechanistic link between the pathophysiology of disc degeneration and these alterations in mechanics, rendering these early observations phenomenological and limiting translation or interpretation at the joint level, which might provide additional insights into the predisposition of degenerate discs to mechanical failure. Had fundamental structure-function relations been established in these studies, for example by directly correlating variations in various tissue constituents with mechanical properties, mechanisms leading to disc tissue failure might have been

better understood to target preventative and therapeutic strategies aimed at mitigating the biochemical changes deemed most detrimental to disc mechanical function.

1.8 In vitro model systems for establishing structure-function relations

More recent work has sought to investigate tissue constituent contributions to the mechanical failure response by manipulating constituent biomolecules along axes known to be altered by degeneration. For example, Isaacs et al. (2014) used collagenase, chondroitinase, and elastase to selectively degrade annulus fibrosus biomolecules to elucidate the relative contributions of collagen, chondroitin sulfate, and elastin to the lamella-level failure response. As the annulus fibrosus is highly anisotropic, constituent biomolecules are expected to contribute differently to the tissue response in different tissue-level specimen orientations; this study tested a range of specimen orientations to establish a basis for material-level annulus fibrosus structure-function relations. The approach used in this study provided clear evidence for the independent role of each of these important biomolecules in material-level AF failure.

The present work sought to apply a similar framework to build upon these results at the tissue level across a range of loading rates and to develop, validate, and implement methods to conduct repeatable, robust, and physiologically relevant investigations of structure-function relations in the annulus fibrosus. Such a system relies on the selection of an optimal animal model, one or more tissue-level specimen orientations, and a physiologically relevant *in vitro* disease-model that directly and quantifiably targets one or more constituents of interest. Considering the substantially altered boundary conditions present when testing tissue-level specimens *in vitro*, such disease models must aim to appropriately control for as many potentially unphysiological confounders as possible. These include the targeting and maintenance of tissue hydration levels, disease-models that induce physiologically relevant changes in tissue composition, robust and repeatable methods for failure testing and analysis that capture the true tissue mechanical response with minimal measurement variability, and methods of statistical analysis that are appropriate to address the research question and that are compatible with the study design and quality of obtained data. The schematic workflow of such a system has been outlined in **Figure 5**.

1.9 Discussion of the following chapters and previously published material

The following chapters detail the development, validation, and implementation an experimental framework to elucidate fundamental tissue-level structure function relations between degeneration- and disease-mediated biochemical changes and annulus fibrosus failure mechanics. *Chapter 2* reports on the development and validation of a novel method for repeatable failure testing of soft tissues with fibers oriented off-axis from the applied loading, such as AF specimens tested in the circumferential-radial or circumferential-axial orientations. While this study was conducted and originally published as a combined experimental and computational analysis, the computational work was performed by Minhao Zhou and has thus been removed from this dissertation. With minor subsequent modification, the method described in *Chapter 2* serves as the basis for the reliable characterization of AF tensile failure mechanics in subsequent chapters. *Chapter 3* describes the effects of enzymatic proteoglycan degradation and concomitant water loss on AF tensile failure mechanics in the circumferential-radial direction at low and high loading rates. This orientation maximized the contribution of the proteoglycan-rich matrix to the tissue mechanical response; the use of two distinct loading rates varying by three orders of magnitude facilitated exploration of the role of proteoglycan and water content in both the quasi-static and dynamic tensile response of the tissue, which are known to vary and are both critical to

characterize. *Chapter 4* provides a brief empirical analysis of the relative contribution of the three main AF biochemical constituents (*i.e.*, proteoglycans, water, and collagen) to the tensile failure mechanics of AF tissue from a cross-sectional population of human donors, providing direct biochemical-mechanical structure-function relations in human AF. Despite the significant insights gained from *Chapters 3* and *4*, the use of 0.15M phosphate-buffered saline (PBS) resulted in hyper-physiologic tissue water contents, which are known to alter the tissue mechanical response. Thus, *Chapter 5* provides a more robust method to target and maintain AF hydration levels, mechanics, and composition at fresh-tissue levels during *in vitro* testing. *Chapter 6* utilizes these methods to provide discrete and continuous descriptions of the role of advanced-glycation end products in AF sub-failure, failure, and post-failure tensile mechanics at quasi-static and dynamic loading rates. Finally, *Chapter 7* addresses the limitations of the current work and suggests possible directions for future investigations that might build on this dissertation work.

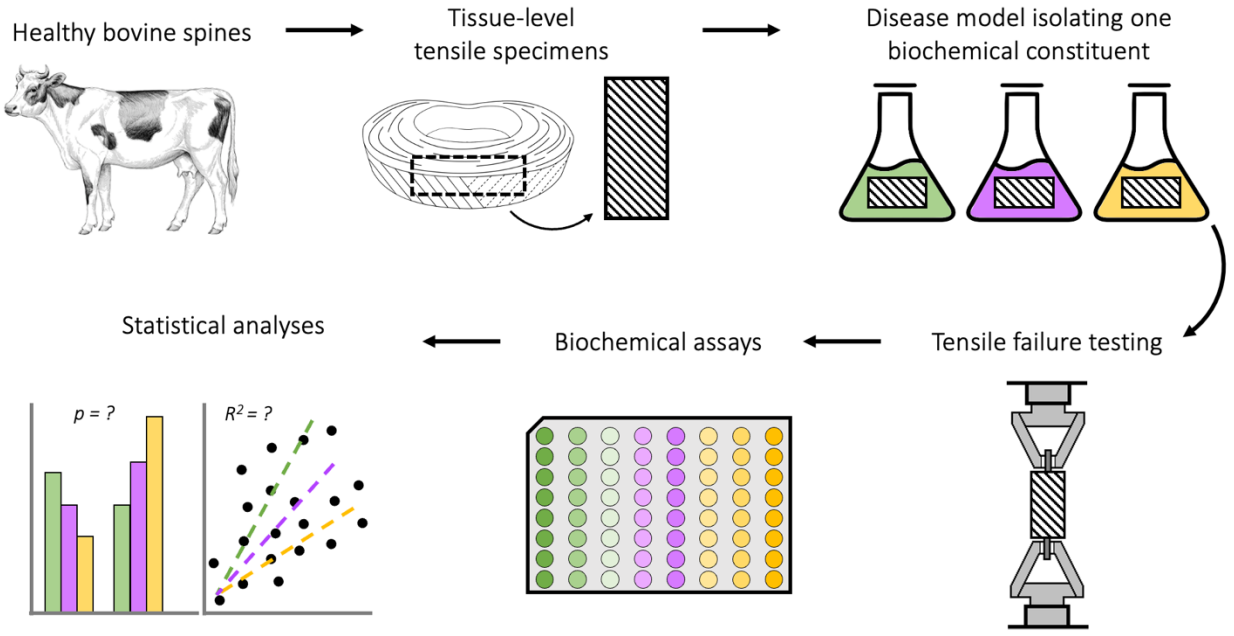

Figure 5: Schematic outline of a disease-model workflow facilitating controlled investigation of tissue biochemical constituent contributions to tensile failure mechanics.

2. A novel method for repeatable failure testing of annulus fibrosus[1]

2.1 Introduction

Fiber-reinforced tissues of the musculoskeletal system, such as the annulus fibrosus in the intervertebral disc, experience large, complex loads during daily activities. Repetitive or excessive loading of these tissues may initiate structural damage and lead to mechanical failure, causing debilitating pain and reduced mobility [Luoma et al., 2000; Iatridis et al., 2005]. Understanding failure mechanisms of tissues with limited self-healing capabilities is of particular importance as the increase in AF tears with age may cause a cascade of damage and degenerative. For example, AF failure can lead to disc herniation, where prolapse of the nucleus pulposus may impinge on the

[1] Adapted from "Werbner B, Zhou M, O'Connell G. A novel method for repeatable failure testing of annulus fibrosus. Journal of biomechanical engineering. 2017 Nov 1;139(11)." Computational aspects have been removed for reproduction in this dissertation.

spinal nerves, causing severe back and leg pain [Adams and Roughley, 2006; Vernon-Roberts et al., 2007].

A comprehensive understanding of soft tissue failure mechanics is important for developing strategies for repairing fiber-reinforced tissues [O'Connell et al., 2015]. Unfortunately, failure mechanics of fiber-reinforced soft tissues is not yet well understood. For example, the significant variability in AF failure properties reported in the literature makes it difficult to interpret and compare experimental results [Green et al., 1993; Skaggs et al., 1994; Acaroglu et al., 1995; Ebara et al., 1996]. This in turn makes design and validation of tissue-repair strategies more difficult. Previous studies have shown that this large variability may be due to limitations in specimen size and premature tissue failure near the testing grips [Acaroglu et al., 1995; Ebara et al., 1996; O'Connell et al., 2007]. In particular, tissue failure near the gripped regions, resulting from undesirable stress and strain concentrations near the testing grips, may yield inconsistent and unreliable failure properties, which do not reflect the true properties of the tissue [Holzapfel et al., 2005; Jacobs et al., 2013; Peloquin et al., 2016]. Recent work by Peloquin et al. identified five different modes of failure in meniscus specimens, with less than 25% of failures occurring at the specimen mid-length [Peloquin et al., 2016]. Furthermore, previous investigators have excluded up to 60% of AF samples due to failure near the gripped region, indicating the inefficient use of limited tissue resources [Skaggs et al., 1994; Ebara et al., 1996; Lechner et al., 2000] (**Figure 6**).

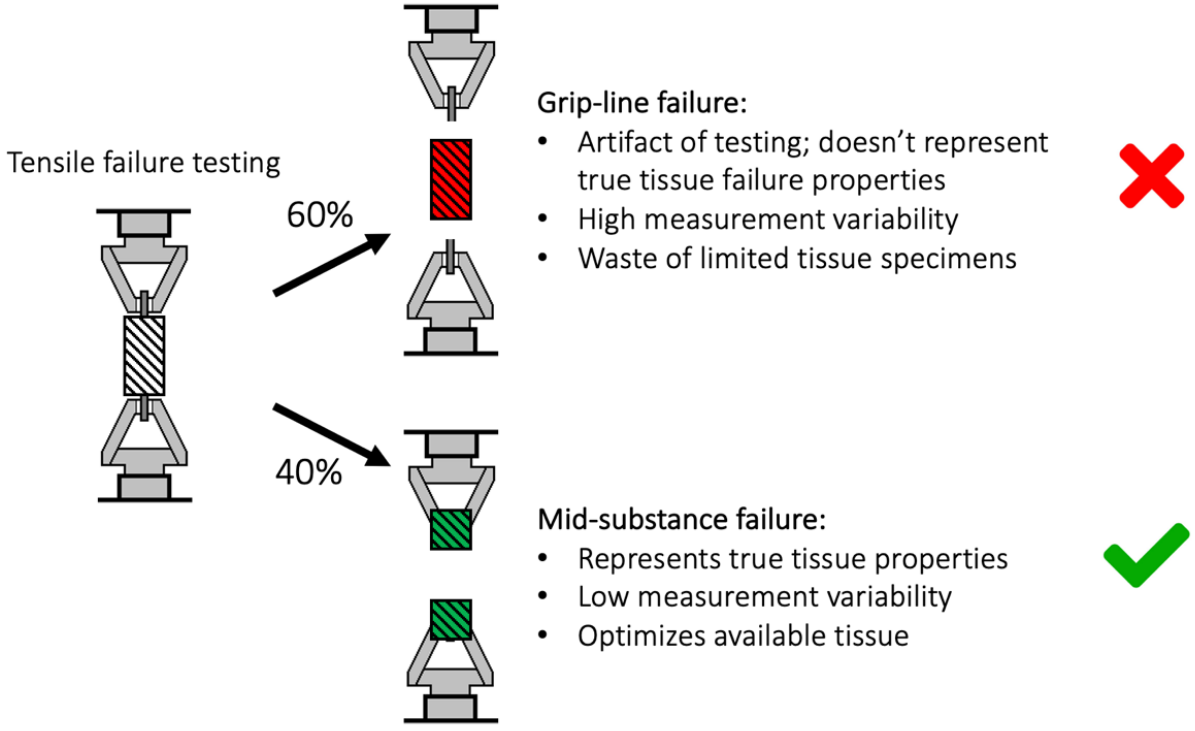

Figure 6: Historical issues with the repeatability of soft, fiber-reinforced tissue tensile failure testing.

Repeatable and predictable failure in a test specimen is largely based on the specimen geometry. ASTM (American Society for Testing and Materials) guidelines for testing the strength of materials suggest using dog-bone shaped specimens to ensure that failure occurs away from the testing grips (i.e. mid-length failure) [ASTM, 2003; ASTM, 2004]. Rectangular and dog-bone shaped specimens have been successful in evaluating failure mechanics of tendons and ligaments, where collagen fibers are aligned along the loading direction [Yamamoto and Hayashi, 1998; Kolz

et al., 2015; Morales-Orcajo et al., 2016]. However, materials with fibers oriented off-axis from the applied loading direction, such as AF (fiber orientation range = 30-45°), often fail unpredictably, even with a dog-bone shaped geometry [Green et al., 1993; Ebara et al., 1996; Peloquin et al., 2016].

The objective of this study was to develop and validate a robust testing protocol for investigating AF failure mechanics. We created several candidate geometries mimicking modified dog-bone geometries at the mid-substance and identified a specimen design that ensured repeatable failure away from the testing grips while reducing mechanical testing measurement variability. While this technique was developed to evaluate AF failure mechanics, which has fibers oriented off-axis from the primary loading direction, the techniques used here can be applied to other soft fiber-reinforced materials.

2.2 Materials and Methods

Caudal spine sections from skeletally mature bovines (18 months) were acquired from a local abattoir. Healthy intervertebral discs were dissected from levels C1 - C5 of the spine using a scalpel. Rectangular tissue sections oriented along the circumferential-radial (n=16) or circumferential-axial (n = 25) directions were isolated from the middle-outer region of the anterior and posterior AF (**Figure 7A-B**). Preliminary work observed no significant differences in mechanical properties between anterior and posterior bovine AF. A freezing stage microtome was used to reduce the specimen thickness to approximately 2 mm and to ensure planar, parallel surfaces. Since disc mechanical properties are known to vary with hydration state, all specimens were soaked in 0.15 M phosphate buffered saline (PBS) overnight at 37 °C before testing. After hydration, all specimens were trimmed using a parallel-block guide and razor blade to ensure uniform width of 5.2 ± 0.6 mm and thickness of 2.1 ± 0.2 mm.

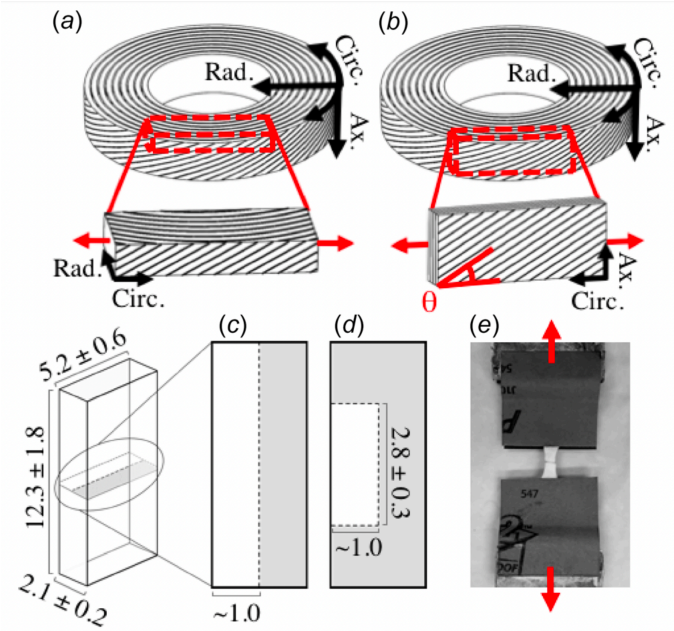

Figure 7: Schematic of (A) circumferential-radial and (B) circumferential-axial specimen orientations. Schematic of (C) half and (D) quarter notch geometries. (E) Sample glued into sandpaper for mechanical testing.

After hydration and trimming, eight Intact specimens were prepared in each orientation. Notched samples were prepared by making a full-width notch at the mid-length with a scalpel (#11 blade) and a depth-stop, which resulted in a remaining specimen thickness of 1 mm ('Half,' **Figure 7C**; n = 8 for each orientation). Additional circumferential-axial samples were notched beyond the Half notch configuration, such that the effective gauge width was approximately half of the full width (2.8 ± 0.3 mm; n = 9; **Figure 7D**).

To ensure that slipping did not occur at the grips, two 5 cm x 5 cm squares of 400 grit waterproof sandpaper were fixed to each end of a 5 cm x 2 cm x 1 cm (length x width x thickness) aluminum block using cyanoacrylate, with the grit sides of the sandpaper facing each other. Approximately 10% of the gauge length of each sample was then glued between the other ends of the sandpaper, such that a gauge length of 12.3 ± 1.8 mm remained between the grips (**Figure 7E**). The glue was allowed to dry for 10 minutes, and samples were rehydrated in 0.15 M PBS for 20 minutes. The aluminum block and sandpaper fixtures were secured to an Instron testing machine (5943, Norwood, MA) using screw-clamp tension grips. The machine was equipped with a custom-built water bath to ensure proper hydration during testing. Slack was removed from the specimen by applying a 0.05 N pre-load. The cross-head extension was zeroed and the specimen was photographed with a scale bar to measure specimen-specific dimensions prior to testing.

An extension-controlled ramp was applied at a rate of 50 mm/min until failure. Engineering strain was calculated as the change in cross-head displacement divided by the initial gauge length (i.e., grip-to-grip distance). Engineering stress was calculated by dividing the measured force by the initial cross-sectional area at the mid-length. The failure stress (σ_f) was defined as the maximum stress, while the failure strain (ε_f) was defined as the strain at which the maximum stress occurred (**Figure 8** - star and red lines). The toe- and linear-region moduli (E_{toe} and $E_{lin.}$, respectively) were calculated using a bi-linear fit to the stress-strain response (**Figure 8** - green lines; custom linear-regression algorithm, Matlab Mathworks Inc.).

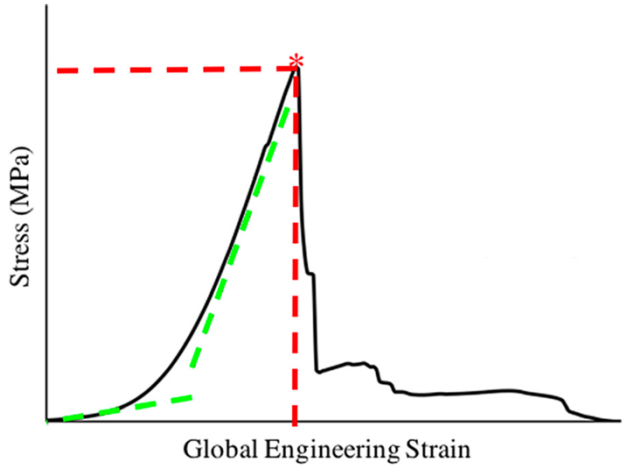

Figure 8: Representative stress–strain curve. Toe- and linear- region moduli (green lines) were calculated using a custom linear-regression optimization technique. The point of failure was defined by the maximum stress achieved (star), and this point was used to define the failure stress and failure strain (red lines).

'Repeatability of failure' was quantified by evaluating the coefficient of variation (or simply 'variation'), which was defined as the standard deviation divided by the mean. Variation

was calculated for toe- and linear-region moduli, failure stress, and global strain at failure, and was used to compare Intact, Half notch, and Quarter notch geometries for circumferential-axial specimens. A one-way ANOVA with a Tukey-Kramer post-hoc analysis was performed on mechanical properties and variation in mechanical properties. A value of $p \leq 0.05$ indicated a significant difference between groups.

2.3 Results

All samples tested exhibited a nonlinear stress-strain response and no slippage between the sample and testing grips was observed for samples that failed at the mid-length (**Figure 8**). For Intact specimens, failure occurred at the grip-line in 100% of circumferential-radial samples (n = 8/8) and 88% of circumferential-axial samples (n = 7/8). For Half notch specimens, failure occurred at the notch-site in 100% of circumferential-radial samples (n = 8/8; **Figure 9**), but in only 25% of circumferential-axial samples (n = 2/8). Conversely, 90% of Quarter notch circumferential-axial specimens failed within 2 mm of the mid-length (n = 8/9).

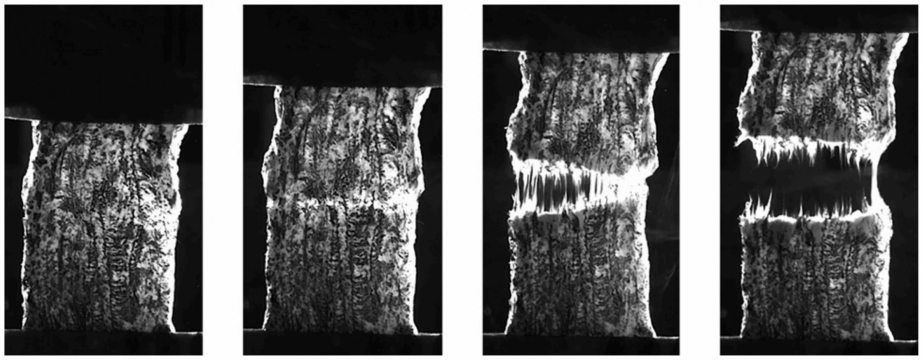

Figure 9: Representative circumferential-radial sample with a half notch geometry failing at the midlength.

Table 1: Measured mechanical properties for specimens failing at the midlength.

	Circ.-Rad.	Circ.-Ax.
$\boldsymbol{E}_{\text{toe}}$ (MPa)	1.39 ± 0.12	1.41 ± 0.07
$\boldsymbol{E}_{\text{lin.}}$ (MPa)	8.26 ± 1.66	15.56 ± 3.59
$\boldsymbol{\sigma}_f$ (MPa)	2.25 ± 0.51	4.67 ± 1.01
$\boldsymbol{\varepsilon}_f$ (mm/mm)	0.47 ± 0.07	0.55 ± 0.10

The linear region modulus and stress at failure for circumferential-radial specimens were approximately half of the values measured for circumferential-axial specimens (**Table 1**). For circumferential-axial samples, there was a significant decrease in linear-region modulus ($p \leq 0.04$) and failure stress ($p \leq 0.02$) with an increase in mid-length cross-sectional area (**Figure 10B & C**). However, there was no significant difference in the toe-region modulus or strain at failure for different notch geometries (**Figure 10A & D**).

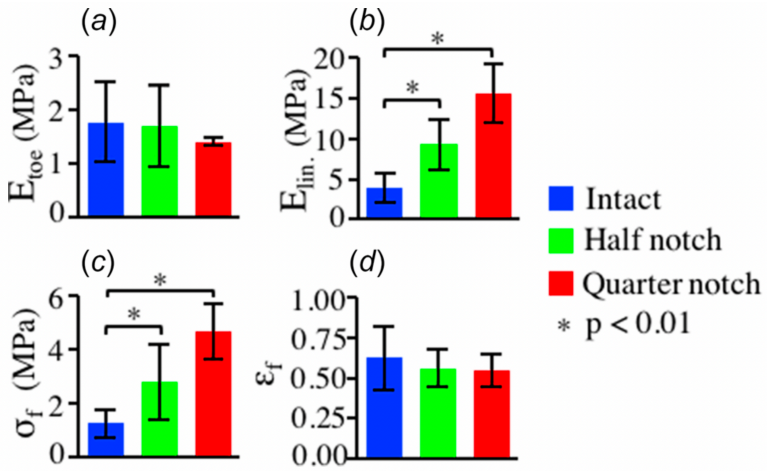

Figure 10: Mechanical properties of circumferential-axial specimens. Data are reported as the mean plus or minus the standard deviation.

The variation of mechanical properties was significantly lower for specimens in which failure occurred at the mid-length rather than at the grip line (p=0.005). For example, the coefficient of variation in failure stress was 0.42 (or 42% of the mean) for the Intact circumferential-axial group and decreased to 0.22 for the Quarter notch group (**Figure 11**). Similar trends were observed for other mechanical properties (circ.-ax. average variation: Intact = 0.41, Half = 0.38, and Quarter = 0.19; **Figure 11**).

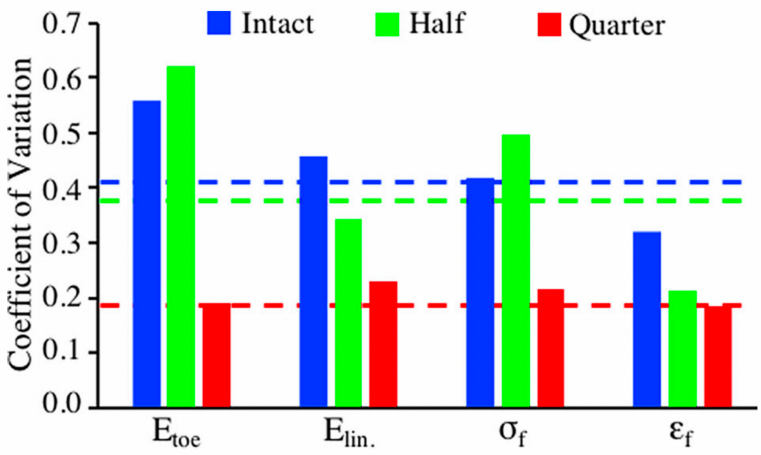

Figure 11: Coefficient of variation for each measured mechanical property.

2.4 Discussion

In this study, we created several candidate geometries mimicking modified dog-bone geometries at the mid-substance and identified a specimen design that ensured repeatable failure away from the testing grips while reducing mechanical testing measurement variability. Adding a simple notch geometry at the mid-length of the specimens (Half) increased the likelihood of failure; however, this effect was dependent on sample orientation. In circumferential-radial specimens, all Half notch samples failed at the notch site. However, samples oriented along the circumferential-axial direction required a Quarter notch geometry. The primary difference between

the two sample orientations is the alignment of collagen fibers, where circumferential-axial specimens have longer continuous fibers that are more aligned with the loading direction.

Repeatable mid-length failure is essential to ensure accurate material properties and efficient use of limited tissue specimens. Previous studies that investigated failure properties of fiber-reinforced tissues (e.g., AF and meniscus) have reported exclusion of up to 60% of samples from the dataset [Acaroglu et al., 1995; Ebara et al., 1996; Lechner et al., 2000], due to failure occurring at the grips even when a dog-bone geometry was employed [Ebara et al., 1996, Peloquin et al., 2016] (**Figure 6**). Our results indicate that Half and Quarter notch geometries increase the likelihood of mid-length failure for circumferential-radial and circumferential-axial specimens, respectively. Both the Half and Quarter notch geometries are modified dog-bone geometries that proved effective in ensuring repeatable mid-length failure during uniaxial tension. We hypothesize that a combination of failures near the grips and at the mid-length likely contributes to the large variability of AF failure data reported in the literature.

Robust failure at the mid-length decreased variability in the measured mechanical properties, leading to more accurate characterizations of tissue failure mechanics. The results of this study indicate that specimens failing at the mid-length exhibit significantly less variability in their measured mechanical properties. For example, the variation in failure stress for Intact samples was nearly twice that of Quarter notch samples (**Figure 11**), suggesting that failure properties measured when the sample fails at the mid-length are more reliable. Variations in mechanical properties for our notched samples were low compared to values reported in the literature. For example, previously reported coefficients of variation for linear-region modulus, failure stress, and failure strain range from 40-100%, 50-90%, and 30-60%, while our values were limited to approximately 22%, 21%, and 19%, respectively [Green et al., 1993; Acaroglu et al., 1995; Ebara et al., 1996]. While the notch does create a stress concentration, which may alter measured mechanical properties, previous studies attempting to initiate crack propagation in fiber-reinforced tissues have observed significant blunting at the notch site rather than propagation [Pelquin et al., 2016; Elliott and Setton, 2001; Wagner and Lotz, 2004].

This study developed and validated a method for sample preparation that ensures repeatable mid-length failure in a fiber-reinforced soft tissue. These results indicated that it is essential to consider strains created at the grips during testing to ensure repeatable failure within the gauge region. The methods presented here may facilitate more efficient and accurate evaluation of the failure properties of both native fiber-reinforced tissues and tissue-engineered constructs.

3. Bovine annulus fibrosus hydration affects rate-dependent failure mechanics in tension[2]

3.1 Introduction

Back pain has been associated with degenerative changes in the intervertebral disc, including altered biochemical composition and an increase in annular tears [Buckwalter, 1995; Luoma et al., 2000; Urban and Roberts, 2003]. Degeneration also has a significant effect on disc mechanical and rheological behavior [Maroudas et al., 1975; Adams et al., 1996]. One of the most significant biochemical changes associated with degeneration is the fragmentation and loss of proteoglycans in the nucleus pulposus and inner AF [Lyons et al., 1981; Roughley et al., 2002]. Proteoglycans are understood to be responsible for water absorption and retention through osmotic pressure induced by negatively charged glycosaminoglycans (GAGs) [Watanabe et al., 1998; Kiani et al., 2002]. High tissue water content helps distribute compressive loads and contributes to

[2] Adapted from "Werbner B, Spack K, O'Connell GD. Bovine annulus fibrosus hydration affects rate-dependent failure mechanics in tension. Journal of biomechanics. 2019 May 24;89:34-9."

the tissue's viscoelastic mechanical properties [Urban and Roberts, 2003; Iatridis et al., 2013]. Thus, proteoglycan fragmentation and loss with degeneration is associated with tissue dehydration and loss of fluid support [Urban and McMullin, 1988; Adams et al., 1996].

In addition to these changes, previous studies have observed a multitude of structural and compositional changes with degeneration, making it difficult to discern the role of individual tissue constituents [Urban and Roberts, 2003; Adams and Roughley, 2006]. Recent work by Isaacs et al. used enzymes to selectively digest individual molecules, isolating the role of each in tissue failure [Isaacs et al., 2014]. However, such studies have typically only evaluated failure mechanics at one loading rate, making it difficult to elucidate the role of viscoelasticity on tissue failure [Green et al., 1993; Acaroglu et al., 1995; Isaacs et al., 2014]. Furthermore, the authors of previous failure studies have consistently reported difficulties in ensuring failure occurred at a point away from the testing grips, which may affect the reliability of the measured mechanics [Acaroglu et al., 1995; Ebara et al., 1996; Peloquin et al., 2016]. Our previous work addressed this issue by developing a method to increase the likelihood of mid-substance failure during uniaxial tensile testing, significantly reducing variability in measured mechanical properties [Werbner et al., 2017].

Since GAG and water content affect the viscoelastic behavior of biological tissues, it is essential to consider potential rate-dependent effects of degeneration on disc failure properties [Elliott et al., 2003]. Studies of similar fiber-reinforced tissues, such as tendons and ligaments, showed that failure stress and strain increased with loading rate [Noyes et al., 1974; Haut, 1983]. Establishing similar structure-function relationships for the AF is important for understanding potential mechanisms of disc herniation [O'Connell et al., 2015]. While several studies have investigated effects of degeneration and loading rate on AF sub-failure mechanics, the relationship between biochemical composition, loading rate, and AF failure mechanics is not yet well defined. With this in mind, the first objective of this study was to determine the effect of loading rate on AF tissue-level failure properties in uniaxial tension. The second objective was to quantify the effects of GAG and water content on AF failure mechanics.

3.2 Materials and Methods

Nineteen caudal spine sections from adult bovines were acquired from a local abattoir. Bovine discs were used to investigate AF mechanics due to their larger disc area and similarities in biochemical and mechanical properties to healthy human discs [Demers et al., 2004; O'Connell et al., 2007; Beckstein et al., 2008]. Musculature was removed from the spine and discs were dissected from levels C1-C4. Rectangular specimens approximately 2 mm thick were prepared from the middle-outer region of the anterior and posterior AF and oriented with the length along the circumferential direction and the width along the radial direction (n=75; **Figure 12**) [Werbner et al., 2017]. This orientation was chosen in part for the greater contribution of the GAG-rich extrafibrillar matrix to the mechanical response [Holzapfel et al., 2005; O'Connell et al., 2009; Isaacs et al., 2014]. Preliminary work ensured no differences in mechanics between anterior and posterior AF (n=6/group, paired t-test $p>0.3$).

Specimens were soaked in saline for 18 hours at 37°C prior to testing. Specimens in the control group (CTL group, n=24) were soaked in 10mL of phosphate-buffered saline (0.15M PBS), while chondroitinase-treated specimens were soaked in 9.75mL of saline with 0.25mL of 10U/mL chondroitinase ABC (chABC group, n=26; enzyme concentration = 0.25U/mL; Sigma-Aldrich, St. Louis, MO). To investigate the effect of water content independent of GAG content, specimens were soaked in a hyperosmotic saline solution (1.43M NaCl, OSM group, n=25). Preliminary work determined the appropriate PBS concentration to match the reduced water content of chABC-

treated specimens using osmotic loading. Twelve outer-middle AF biopsy punches were soaked in PBS solutions varying in concentration from 1.25 to 10 times greater than the control (n=3 per concentration). Tissue weights were measured before and after soaking, and after lyophilization (Labconco 7740021, Kansas City, MO). Water content was calculated by dividing the difference between swollen (ww) and dry weights (dw) by the swollen weight (WC= (ww – dw)/ww). A Pearson correlation was performed to estimate the PBS concentration resulting in the observed chABC group water content (**Figure 13**). Accordingly, OSM specimens were soaked in 1.43M NaCl (~9.5X control concentration).

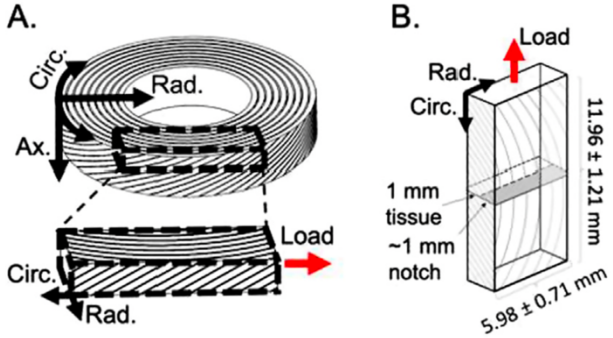

Figure 12: (A) Schematic of circumferential-radial specimen orientation and direction of applied load. (B) Test specimen dimensions and notch geometry.

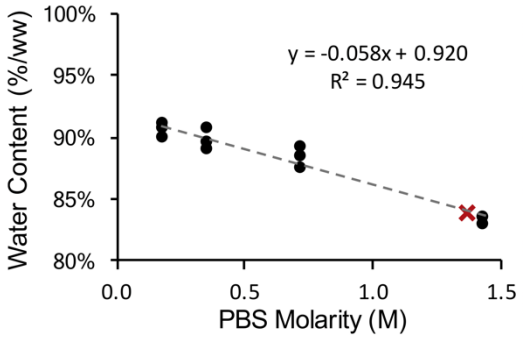

Figure 13: Pearson correlation between PBS concentration and tissue water content after hydration (n = 12; black circles). The regression line was used to determine the PBS concentration needed to match tissue water content of chABC-treated samples (red 'X' = 1.43 M PBS).

After soaking, specimens were trimmed using a parallel-block guide and razor blade to ensure uniform width (final width = 5.98 ± 0.71mm). A full-width, half-depth notch was created to facilitate midlength failure (thickness at midlength = 1mm) [Werbner et al., 2017]. Several studies have reported no significant differences in stiffness or strength between notched and intact fiber-reinforced soft-tissue specimens, suggesting a limited effect of stress concentrations at the notch site [Taylor et al., 2012; Von Forell et al., 2014]. Approximately 10% of the specimen length was glued into waterproof sandpaper; the final specimen length was 11.96 ± 1.21mm. Samples were rehydrated in group-specific solutions for 30 minutes prior to testing. CTL and chABC samples were rehydrated in 0.15 M PBS, while OSM samples were rehydrated in 1.43 M PBS. Preliminary tests confirmed that the initial 18-hour treatment soak with 30 minutes of rehydration was sufficient to achieve steady-state hydration prior to testing (n=6). Specimens were tested in a custom-built water bath containing either 0.15 M PBS (CTL and chABC) or 1.43 M PBS (OSM).

A monotonic 0.1 N preload was applied to remove slack from the tissue. Cyclic preconditioning was not applied to avoid altering pre-testing tissue water content, which could affect different treatment groups differently [Schmidt et al., 2016]. Scale bar photographs were taken to measure sample-specific width and length. Uniaxial tension was applied monotonically along the circumferential direction at either a low or high loading rate until the specimen separated into two pieces (Low = 0.05 mm/min or 6.97 x 10^{-3} %/sec, High = 50 mm/min or 6.97 %/sec). The large difference in loading rates was selected to be within the range of physiological loading conditions and to highlight relative differences, where quasi-static loading minimizes viscoelastic contributions from the tissue solid while facilitating fluid flow and higher rate loading restricts fluid flow and emphasizes solid-component viscoelasticity. Applying uniaxial tension in the

circumferential direction was intended to produce a failure mode representing AF failure by radial fissure.

Engineering strain was calculated as the measured change in displacement divided by the initial gauge length. Engineering stress was calculated as the measured force divided by the initial cross-sectional area at the midlength. Failure stress was defined as the maximum stress, and failure strain as the corresponding strain. The linear-region modulus was calculated using a linear-regression fit to the stress-strain response (Matlab Mathworks Inc.). Strain energy density was determined through numerical integration of the stress-strain response until failure.

After mechanical testing, a 4 mm biopsy punch was taken from the tissue midlength, and specimen water content determined as described above. Lyophilized samples were then digested in 2 mg/mL proteinase K. GAG content was determined using the 1,9-dimethylmethylene blue (DMMB) assay [Farndale et al., 1982]. Solutions from the 18-hour tissue-soak were retained to measure GAGs in the solution, since previous studies reported GAG leaching from tissue during hydration [Urban and Maroudas, 1981; Han et al., 2012]. Each tube of soak solution was centrifuged for 10 minutes at 5000rpm and frozen before 72 hours of lyophilization. Precipitates were digested in proteinase K and the DMMB assay used to determine GAG content. GAG content was normalized by both specimen dry and wet weights.

A two-way ANOVA was performed on mechanical and biochemical properties (factors = soak solution and loading rate). A Bonferroni post hoc analysis was performed where significance was found. Significance was assumed at $p<0.05$. Values are reported as mean ± standard deviation.

3.3 Results

All samples exhibited a nonlinear stress-strain response prior to failure (**Figure 14**). A clear maximum stress, corresponding to the initiation of bulk failure, was observed for all specimens. Mechanical testing data was only analyzed for samples that clearly failed at the midlength (n=66/75). For the low-rate control group (CTL-Low), the average linear-region modulus was 11.31 ± 1.75MPa, strain energy density was 0.40 ± 0.16MPa, failure stress was 2.25 ± 0.63MPa, and failure strain was 0.36 ± 0.09 (**Figure 15** – light blue bars). Since loading rate did not significantly affect GAG or water content, biochemical data for both rates were pooled ($p>0.2$). The average water content for the CTL group was 89.4 ± 5.9%. The average GAG content for controls was 0.98 ± 0.34%/ww normalized by swollen weight and 11.6 ± 5.0%/dw normalized by dry weight (**Figure 16** – blue bars).

Loading rate had a significant effect on both sub-failure and failure properties, including linear-region modulus, strain energy density, and failure stress (all $p<0.001$; **Figure 15** – dark vs light bars). The increase in loading rate resulted in a ~40% increase in linear-region modulus and a ~50% increase in failure stress ($p<0.03$, CTL-Low vs CTL-High). Similarly, mechanical properties of chABC and OSM samples were dependent on loading rate, with significant increases in linear-region modulus, strain energy density, and failure stress (**Figure 15**). Failure strain was not affected by loading rate for any treatment group ($p>0.2$).

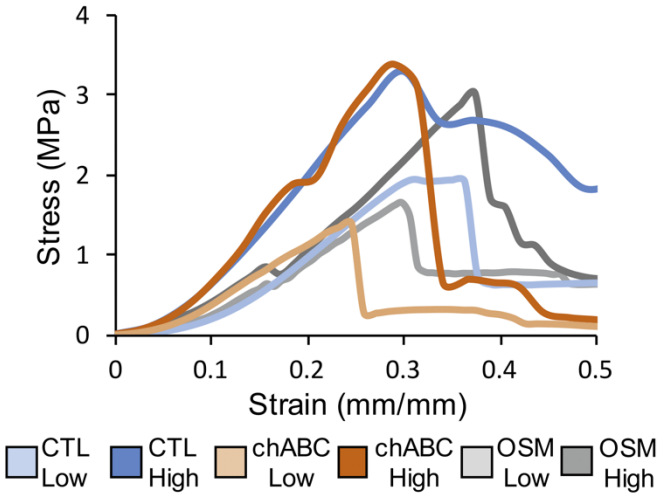

Figure 14: Representative stress-strain curves showing one sample from each group. Each curve shows a non-linear sub-failure response, the point of failure, and post- failure behavior (data truncated at 50% strain for clarity).

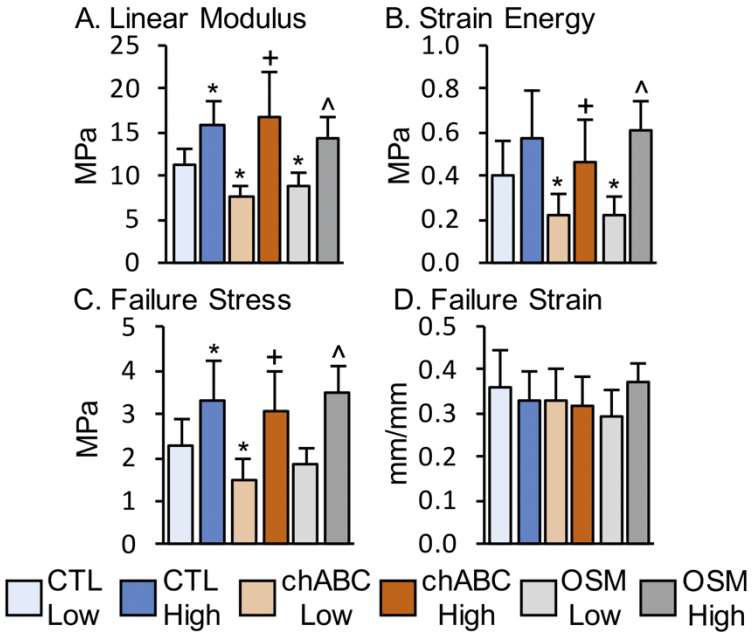

*Figure 15: Summary of mechanical properties in uniaxial tension (Mean + SD; n = 11 per group): (A) linear-region modulus, (B) strain energy density to the point of failure, (C) failure stress, and (D) failure strain. * denotes p < 0.05 vs CTL-Low, + denotes p < 0.05 vs chABC-Low, ^ denotes p < 0.05 vs OSM-Low in post-hoc analysis.*

chABC treatment had a significant effect on mechanical and biochemical properties (**Figures 15 and 16** – blue vs orange bars). In particular, linear-region modulus, strain energy density, and failure stress were significantly affected by soak treatment ($p<0.05$), as were water and GAG contents ($p<0.001$). However, a post-hoc analysis showed that changes in mechanical properties with chABC treatment were only significant at the low loading rate ($p>0.2$ for CTL-High vs chABC-High). At the lower loading rate, chABC treatment resulted in more than a 30%

decrease in linear-region modulus and failure stress and a ~45% decrease in strain energy density ($p<0.04$; **Figure 15**). Failure strain was not affected by chABC treatment ($p>0.2$). The post-hoc analysis also showed that water and GAG contents of chABC-treated samples were significantly lower than the control. We observed a 6% decrease in water content in chABC samples compared to CTL ($p<0.001$; chABC water content = 84%/ww; Figure 5A), corresponding to a ~85% decrease in GAG content ($p<0.001$; chABC GAG content = 0.23 ± 0.12%/ww or 1.46 ± 0.62%/dw; **Figure 16B-C**).

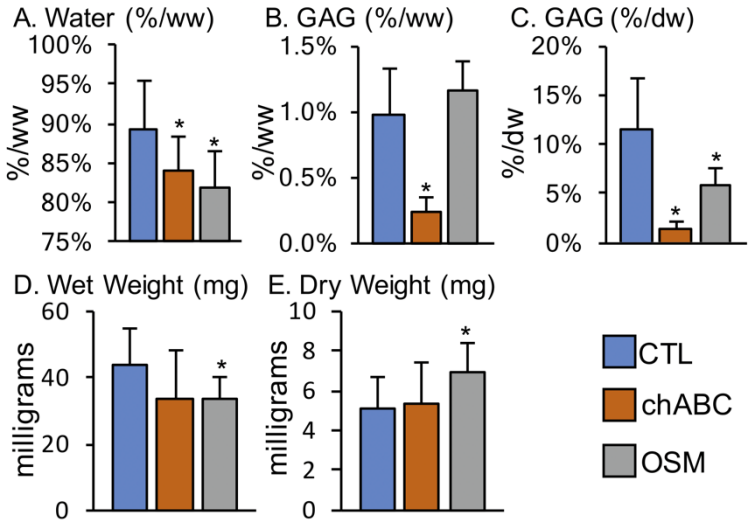

*Figure 16: Summary of biochemical data (Mean + SD; n = 22 per group): (A) water content normalized by swollen weight (ww), (B) GAG content normalized by swollen weight, (C) GAG content normalized by dry weight (dw), and (D) swollen and (E) dry weights of biopsy punches. Biochemical data from low- and high-rate loading groups were pooled. * denotes $p < 0.05$ vs CTL in post-hoc analysis.*

Similar to chABC treatment, osmotic loading altered mechanical and biochemical properties, and significant differences were only observed at the lower loading rate (**Figures 15 and 16**, blue vs grey bars). Osmotic loading resulted in a 22% decrease in linear-region modulus and a 44% decrease in strain energy density versus control ($p<0.04$, CTL-Low vs OSM-Low). Failure stress and failure strain were not affected by osmotic loading ($p>0.2$; **Figure 15**). Water content was 7% lower in OSM samples compared to CTL ($p<0.001$; **Figure 16A**). There were no significant differences in GAG content when normalized by the swollen weight ($p=0.2$; **Figure 16B**), however GAG content normalized by dry weight was 50% lower than the control ($p<0.001$; **Figure 16C**).

Due to conflicting observations of GAG content in the OSM group, we directly compared swollen and dry weights of biopsy punches, assuming that punches had approximately equal tissue volumes. The average swollen weight of biopsy punches from OSM samples was significantly lower than those taken from CTL samples, as expected; however, the average dry weight of OSM specimens was greater than that of CTL specimens ($p=0.02$; **Figure 16D-E**). We also found that GAG content in the OSM soak solutions was not significantly different from that of the CTL soak solutions ($p=0.18$).

3.4 Discussion

The overall aim of this study was to determine the effect of tissue water content on AF failure properties in tension. First, either low- or high-rate loading was applied independently to investigate differences in AF failure behavior under quasi-static and high-rate loading conditions. We employed a modified dog-bone geometry that ensured clear midlength failure in ~90% of specimens. This represents a significant improvement in the failure testing of fiber-reinforced tissues with fibers oriented off-axis to the loading direction, where grip-line and mix-mode failures are commonly observed [Peloquin et al., 2016; Werbner et al., 2017]. Second, we quantified the rate-dependent contribution of GAGs and water content to AF tensile behavior. Controlled GAG depletion was accomplished through enzymatic digestion using chondroitinase ABC. Since enzymatic degradation of GAGs lead to a decrease in water content, the independent effect of tissue hydration on failure behavior was investigated using osmotic loading. Finally, quantitative results regarding the effect of enzymatic digestion on AF GAG and water contents were assessed, since this data has not yet been provided in the literature.

An increase in loading rate significantly altered sub-failure and failure properties, including a ~50% increase in linear-region modulus, strain energy density to failure, and failure stress. Increased moduli and failure stresses at higher loading rates were comparable in magnitude to those previously observed in viscoelastic tissues such as tendons. We believe that this observation is noteworthy considering the significant differences in tissue composition (*e.g.*, GAG content) and subcomponent architecture (*e.g.*, aligned vs off-axis fibers) [Noyes et al., 1974; Haut and Haut, 1997]. Increased tissue strength and energy absorption capacity at high loading rates is essential for protecting against damage during sudden or unexpected loading; our results suggest that AF damage or rupture as a result of sudden, high-speed loads may be attributed to the disc experiencing greater forces during impact rather than the increased loading rate.

Viscoelastic properties of biological tissues were typically attributed to fluid flow [Mow et al., 1984]; more recent studies, however, have also reported viscoelastic contributions from the solid matrix [Elliott et al., 2003; Zitnay and Weiss, 2018]. AF specimens with depleted GAG and/or water contents were still highly sensitive to loading rate, with increases in sub-failure and failure properties that were comparable to or greater than the control. Since similar increases in failure stress were observed for all treatment groups, the rate-dependent increase in failure stress was likely attributable to the collagen component of the solid matrix (*i.e.*, non-GAG and non-water components). The relative increase in linear-region modulus with loading rate was greater for the chABC group than CTL (117% vs 40% increase), also suggesting significant collagen contribution to rate-dependent mechanics.

Samples with depleted GAG and/or water contents showed a significant decrease in both sub-failure and failure properties at the quasi-static loading rate, while no differences were observed at the higher rate. Our high-rate testing results were consistent with data from Isaacs et al. (2014) that reported no change in failure properties after chABC treatment. The lack of differences in mechanical properties between treatment groups at the high loading rate was likely due to restricted water flow during testing [Mow et al., 1984].

The primary mechanism of water retention in the AF is understood to be an osmotic gradient induced by negatively charged GAG molecules. Interestingly, our results showed that a ~90% decrease in GAG content resulted in less than a 10% decrease in water content. That is, the tissue still retained high water content after GAG digestion (water content ~80%/ww), similar to previous observations in ligaments [Lujan et al., 2009]. These findings suggest that GAGs are not the primary mechanism for water absorption and retention; it is possible that tissue permeability

(AF permeability: 0.13-4.5 x 10-15m^4/Ns) and trapped intrafibrillar water may contribute to water retention more than was previously understood [Yao et al., 2002; Périé et al., 2005; Sivan et al., 2006; Schroeder et al., 2007]. Similar mechanisms may also account for high water content of tendons and ligaments despite their low GAG content (water content >65%, GAG content <5%) [Yoon and Halper, 2005; Lujan et al., 2009].

Mechanical properties and GAG content of the control group were consistent with results previously reported for human and bovine AF [Acaroglu et al., 1995; Ebara et al., 1996; Demers et al., 2004]. The decrease in linear-region modulus observed with osmotic loading was contrary to data presented for specimens oriented along the circumferential-axial direction [Han et al., 2012]. This discrepancy was likely due to greater collagen fiber engagement in circumferential-axial specimens, whereas the response from circumferential-radial specimens was dominated by the extra-fibrillar matrix [Holzapfel et al., 2005; O'Connell et al., 2009]. This suggests that structural anisotropy may play an important role in tissue failure properties with respect to hydration.

chABC treatment has been widely used to decrease both GAG and water contents, while osmotic loading has been used to alter hydration levels without changing tissue composition [Bezci and O'Connell, 2018]. Previous work by Han et al. (2012) observed a decrease in tissue GAG content (normalized by dry weight) after osmotic loading. Unlike the current study, Han et al. (2012) did not observe significant changes in tissue dry weight; therefore, the decrease in GAG content was attributed to GAGs leaching into the surrounding solution. In this study, GAGs in the soak solution were measured and no significant differences were observed between CTL and OSM groups ($p = 0.2$). Moreover, GAG content normalized by wet weight showed no significant differences between CTL and OSM. Together, these results suggest that the apparent decrease in GAG content with osmotic loading may be an artifact caused by salt migration into or onto the tissue, increasing tissue density and resulting in a lower apparent GAG content with respect to dry weight. These findings highlight the importance of normalizing biochemical results by both wet and dry weights.

One limitation of this study was our choice to free-swell tissue specimens before mechanical testing, as tissue mechanics are known to change with hydration [Bezci and O'Connell, 2018]. While this resulted in water contents that were greater than values typically reported in the literature, this procedure was chosen to best suit our aims and experimental design; the extended hydration period was largely driven by our GAG depletion protocol, which required 18 hours of submersion in an enzyme solution. A more complete understanding of diurnal changes of *in vivo* water content is required to extrapolate the findings of the current study for clinical purposes; however, joint-level testing and clinical observations suggest that tissue hydration does alter disc mechanics and the risk of spinal injury [Adams et al., 1987; Adams et al., 1990; Belavy et al., 2016]. An additional limitation of this study is that only circumferential-radial specimens were tested, where the mechanical contribution of collagen fibers is limited. This orientation was chosen to represent AF failure by radial fissure, which, in addition to circumferential delamination, has been associated with disc bulging and lower back pain [Veres et al., 2008; Tavakoli et al., 2018; Buirski, 1992].

The current study provides new insights into the structure-function relationship between AF water content and tensile mechanics. Decreases in GAG and water content corresponded with decreases in tissue stiffness, strength, and strain energy density. Osmotic loading resulted in similar decreases in stiffness, strain energy density, and water content. In conclusion, these results suggest that tissue hydration is essential for maintaining bulk tissue stiffness and capacity for

energy absorption, rather than strength. Moreover, hydration altered tissue stiffness and strength at the quasi-static loading rate, where fluid flows more freely, but not at the higher loading rate. This suggests that viscoelasticity of the extrafibrillar matrix plays an important role in stress distribution between fibers and the resistance to bulk tissue failure. These findings are important for defining design criterion for biological repair strategies that recapitulate the behavior of healthy native tissues and for understanding mechanisms of annular tears with injury and degeneration.

4. Human annulus fibrosus failure mechanics are correlated with tissue composition

4.1 Introduction

Lower back pain and intervertebral disc herniation are widespread public health problems associated with degenerative changes to the disc, including altered biochemical composition and an increase in annular tears [Buckwalter, 1995; Luoma et al., 2000; Urban and Roberts, 2003]. While previous studies have observed a multitude of structural, compositional, and mechanical changes with aging and degeneration, the role of individual tissue constituents in disc failure mechanics remains unclear [Urban and Roberts, 2003; Adams and Roughley, 2006]. Researchers have selectively digested individual biomolecules to isolate the role of each constituent in tissue failure [Isaacs et al., 2014], however this *in vitro* model does not account for the myriad of compositional changes that occur during disc degeneration [Grunhagen et al., 2006]. Furthermore, establishing quantitative structure-function relationships for the annulus fibrosus (AF) is important for understanding mechanisms of disc herniation [O'Connell et al., 2015]. Thus, the objective of this study was to determine relationships between human AF biochemical composition and failure mechanics in uniaxial tension.

4.2 Materials and Methods

16 human lumbar intervertebral discs were obtained from 10 cadaver donors (age 38-73 years; 58.4 ± 9.4 years; IRB exempt - Category 4). 34 rectangular specimens ~2 mm thick were prepared from the anterior AF and oriented along the circumferential-axial direction (**Figure 17A**) [Werbner et al., 2017]. Specimens were soaked in 0.15M saline for 18 hours and a midlength notch was introduced to facilitate repeatable failure (**Figure 17B**) [Werbner et al., 2017]. Uniaxial tension to failure was applied in the circumferential direction at 0.1 mm/min. Linear-region modulus ('modulus,' E_{lin}) was calculated using an optimized linear-regression fit to the stress-strain response. Failure stress (σ_f) was defined as the maximum engineering stress, and failure strain was defined as the corresponding engineering strain. Total strain energy density ('total energy,' U_T) was determined through numerical integration of the complete stress-strain response.

After testing, tissue from the failure location was analyzed for water content (WC = ((Wet-Dry)/Wet)*100), glycosaminoglycan content (sGAG) [Farndale et al., 1986], collagen content (COL) [Woessner, 1961], and advanced glycation end-product content (AGE). sGAG, COL, and AGE contents were normalized to tissue dry weight ('dw'). Mechanical and biochemical properties are reported as mean ± standard deviation (SD). Preliminary stepwise regression analysis suggested implementation of a multivariate linear regression (MVLR) model with all four biochemical properties as predictor variables (WC, sGAG, COL, and AGE) and mechanical properties as response variables (modulus, failure stress, failure strain, and total energy; JMP, SAS Institute). Significance was defined as $p < 0.05$. Correlation strength was determined on the basis of R^2 (Weak: 0.10-0.29, Moderate: 0.30-0.49, Strong: ≥ 0.50). Insignificant predictors were removed from the model and the reduced model was re-analyzed. The contribution of each significant biochemical predictor was assessed based on its calculated standardized coefficient,

which represents the predicted change in the mechanical response (units of SD) given a one SD increase in the predictor.

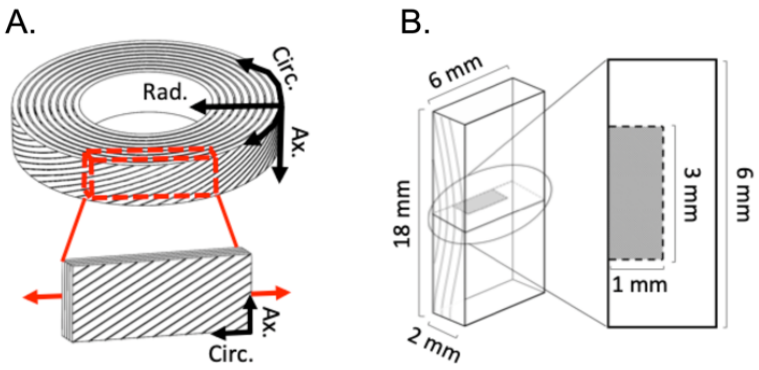

Figure 17: Schematic of (A) specimen orientation and (B) notch geometry [Werbner et al., 2017].

4.3 Results

All samples exhibited a clear maximum stress corresponding to bulk failure initiation, and no slippage was observed at the grips. The average linear-region modulus was 29.4 ± 18.3 MPa, failure stress was 4.4 ± 3.3 MPa, failure strain was 25 ± 9%, and total strain energy density was 0.98 ± 1.02 MPa. Average water content was 80.5 ± 3.4%, sGAG content was 125.9 ± 38.5 µg/mg dw, collagen content was 539.5 ± 114.2 µg/mg dw, and AGE content was 498.0 ± 94.6 ng fl/mg dw (0.97 ± 0.31 ng fl/mg collagen).

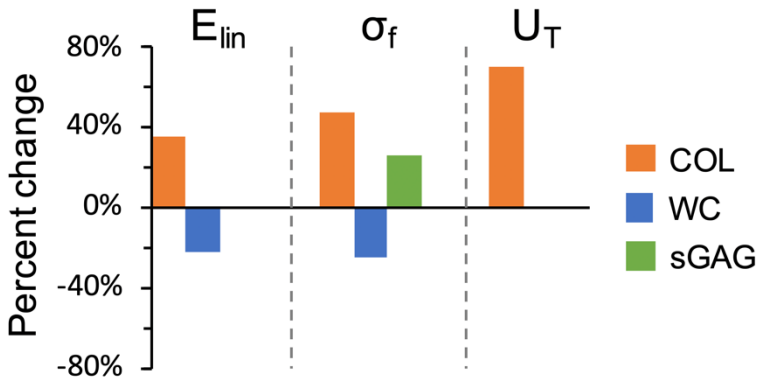

Figure 18: Predicted change in each mechanical property attributable to a one SD increase in each significant biochemical predictor.

MVLR established strong correlations for modulus ($R^2 = 0.66$, $p < 0.0001$), failure stress ($R^2 = 0.59$, $p < 0.0001$), and total energy ($R^2 = 0.51$, $p = 0.0003$) with over 99% post-hoc power (G*Power). Collagen content was a strong predictor of modulus, failure stress, and total energy ($p < 0.001$). Water content was also a strong predictor of modulus and failure stress ($p < 0.002$). sGAG was only a significant predictor of failure stress ($p = 0.04$). AGE content was not a significant predictor of any mechanical property ($p > 0.098$). The reduced multivariate regression equations were: $E_{lin} = 135.35 + 0.09(COL) – 1.92(WC)$, $\sigma_f = 18.56 + 0.02(COL) – 0.35(WC) + 0.03(sGAG)$, and $U_T = -2.27 + 0.006(COL)$. **Figure 18** illustrates the relative contribution of each significant biochemical component to the tissue mechanics by showing the predicted percent

change in mechanics attributable to a one SD increase in each significant biochemical property. For example, a one SD increase in collagen content (~115 μg/mg) is predicted to increase the average modulus by 35% (10.4 MPa), while a one SD increase in water content (3.4%) is predicted to decrease the average failure stress by 27% (1.2 MPa).

4.4 Discussion

This study quantified the contribution of AF biochemical constituents to the tensile failure mechanics. As expected, collagen was the dominant contributor to elastic and failure behaviors (**Figure 18**). In particular, our findings show that collagen content was important for maintaining bulk tissue stiffness, strength, and energy absorption capacity. Water content, on the other hand, was negatively correlated with tissue stiffness and strength (**Figure 18**), agreeing with previous studies testing in the circumferential-axial orientation [Han et al., 2012]. One limitation of this study was our choice to free-swell specimens before testing to ensure repeatable stress-strain behavior, resulting in WC values that were higher than previously reported [Iatridis et al., 2007]. As water and proteoglycan loss are often observed with age and degeneration [Urban and Roberts, 2003], it is essential to understand how these changes affect tissue failure. Although a previous study showed that AGEs affect disc mechanics [Wagner et al., 2006], our findings did not show a significant contribution of AGEs to elastic or failure mechanics. This difference was likely due to the discs in our study having a relatively narrow range of AGEs. Evaluating the effects of AGEs due to advanced degeneration or disease will be assessed in future work. The current study provides strong evidence that AF biochemical composition plays a crucial role in tissue failure.

5. Saline-polyethylene glycol blends preserve annulus fibrosus hydration and mechanics in vitro[3]

5.1 Introduction

Water content is known to have a significant effect on tissue mechanics across length scales [Costi et al., 2002; Screen et al., 2006; Han et al., 2012; Bezci et al., 2015; Żak and Pezowicz, 2016; Werbner et al., 2019; Bloom et al., 2021]. Thus, buffer solutions have been used to maintain hydration levels during mechanical testing, achieve target water content values, and as treatment carriers for *in vitro* disease models [Skaggs et al., 1994; Acaroglu et al., 1995; Ebara et al., 1996; Screen et al., 2005; Lujan et al., 2009; Han et al., 2012; Isaacs et al., 2014; Bezci et al., 2015; Żak and Pezowicz, 2016; Werbner et al., 2019; Werbner et al., 2021b]. Additionally, buffer solutions may be used for short-term tissue storage during sample preparation and to correct minor dehydration occurring during dissection, sample preparation, or imaging [Galante, 1967; Skaggs et al., 1994; Pflaster et al., 1997; Costi et al., 2002; Pezowicz et al., 2005; Żak and Pezowicz, 2016]. Precise control of tissue hydration levels is essential for ensuring accurate, repeatable, and physiologically relevant measurements of tissue mechanics and biochemical composition [Costi et al., 2021].

This is particularly important for joint-, tissue-, and sub-tissue level specimens that have been removed from larger, more constrained structures, as progressive dissection alters residual stresses and removes fluid-mediating barriers such as the cartilaginous endplate and longitudinal ligament. Thus, while 'physiological saline' (0.15M or 0.9%w/v phosphate-buffered saline,

[3] Adapted from "Werbner B, Zhou M, McMindes N, Lee A, Lee M, O'Connell GD. Saline-polyethylene glycol blends preserve in vitro annulus fibrosus hydration and mechanics: An experimental and finite-element analysis. Journal of the Mechanical Behavior of Biomedical Materials. 2021 Nov 2:104951." Computational aspects have been removed for reproduction in this dissertation.

'PBS') maintains intervertebral disc hydration *in vivo*, removal of the vertebral bodies and cartilage endplates dramatically alters tissue boundary conditions, leading to excessive swelling in both the annulus fibrosus (AF) and the nucleus pulposus (**Figure 19**) [Urban and Maroudas, 1981; Skaggs et al., 1994; Acaroglu et al., 1995; Ebara et al., 1996; Pflaster et al., 1997; Han et al., 2012; Huyghe and Jongeneelen, 2012; Bezci et al., 2015; Bezci et al., 2020]. Furthermore, when tissue-level specimens are removed from the whole disc, additional swelling occurs, with outer AF specimens approximately doubling in size when allowed to free-swell in 0.9%w/v PBS [Han et al., 2012; Żak and Pezowicz, 2016; Werbner et al., 2019; Bezci et al., 2020]. This highlights the importance of developing solutions that maintain physiological hydration levels based on specific *in vitro* boundary conditions for a given experiment [Urban and Maroudas, 1981; Costi et al., 2002; Lujan et al., 2009; Huyghe and Jongeneelen, 2012].

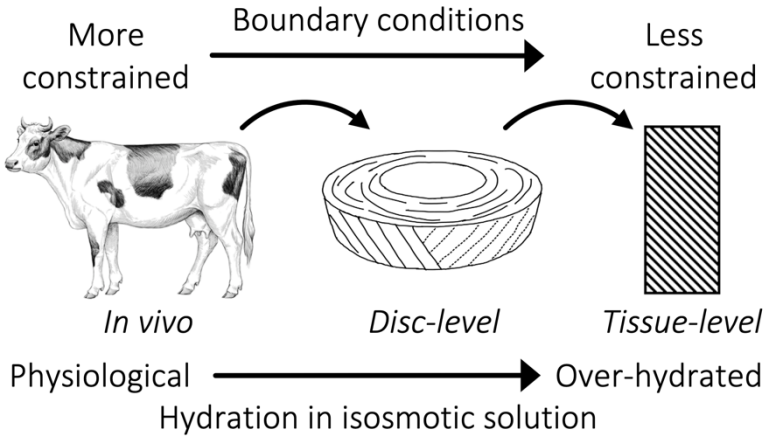

Figure 19: As anatomically constraining boundary conditions are removed, tissue hydration increases from physiological to over-hydrated levels in isosmotic solutions.

To this end, previous studies have used hyperosmotic saline and sucrose solutions in an attempt to maintain physiological tissue hydration levels during long-duration mechanical testing experiments [Han et al., 2012; Bezci et al., 2015; Buckley et al., 2016; Safa et al., 2017]. These studies and others showed that hyperosmotic saline solutions cause significant solute diffusion into the tissue, altering the biochemical environment, potentially affecting measured mechanics, and artificially inflating tissue dry weights, which confounds calculation of normalized biochemical components [Davey and Skegg, 1971; Safa et al., 2017; Werbner et al., 2019, Bezci et al., 2020]. Previous studies found that large molecular weight hydrophilic polymers, such as polyethylene glycol (PEG), were effective at controlling tissue hydration levels without significant solute deposition, likely because the large molecular weight prohibits the molecule from diffusing into the tissue [Davey and Skegg, 1971; Katz and Li, 1973; Robinson, 1978; Sverdlik and Lanir, 2002; Lujan et al., 2009; Huyghe and Jongeneelen, 2012; Safa et al., 2017; Bloom et al., 2021]. In particular, solutions containing a mixture of saline and PEG have been shown to robustly control tendon and ligament hydration levels with minimal solute deposition [Lujan et al., 2009; Safa et al., 2017; Bloom et al., 2021].

This work has yet to be extended to annulus fibrosus, which experiences even greater alterations in boundary conditions and swelling capacity than tendon when tested at the tissue level. Additionally, previous studies have not investigated the effects of such buffer solutions on tissue constituent composition after extended soak times, such as those required when using

solutions as treatment carriers for disease-models (~18 hours). Thus, the objective of this study was to determine and validate an optimal buffer solution for targeting and maintaining hydration levels in tissue-level AF specimens. This was accomplished by measuring transient swelling behavior of bovine AF specimens in saline and PEG buffers across a wide range of concentrations. Sub-failure, failure, and post-failure uniaxial tensile mechanics were measured to determine the relationship between buffer solution induced changes in tissue hydration and tensile mechanical response. The effect of each buffer solution on tissue biochemical constituent composition was also assessed. Fresh-frozen bovine AF tissue was used as the control for swelling, mechanical, and biochemical analyses.

5.2 Materials and Methods

Three fresh coccygeal spine sections from skeletally mature bovines (age ~18-24 months) were acquired from a local abattoir. Musculature was removed and discs were dissected from levels C2-C5 with a scalpel. Eight to ten middle-outer AF specimens were removed from each disc using a 4 mm biopsy punch and immediately massed to determine fresh tissue weight ('FW'); care was taken to produce specimens of nearly equal mass (198 ± 19.7 mg). Specimens were randomized and soaked at room temperature in 5 ml of buffer solution (n = 4 samples per solution concentration). Candidate buffer solutions were created by mixing a range of concentrations of PBS and PEG (**Table 2**). In particular, three solution compositions were investigated at each of the following concentration levels: 0.9, 5, 10, 15, and 20%w/v PBS ('PBS1'-'PBS20', respectively); 5, 10, 15, and 20%w/v PEG ('PEG5'-'PEG20', respectively), and one-to-one mixtures of 5, 10, 15, and 20%w/v PBS and 5, 10, 15, and 20%w/v PEG ('SPEG5'-'SPEG20', respectively). For example, SPEG10 was a mixture of equal parts 10%w/v PBS with 10%w/v PEG, resulting in a final concentration of 5%w/v PBS and 5%w/v PEG. All solutions were pH-balanced to 7.4. Solution compositions are detailed in **Table 2**.

Table 2: Weight/volume (w/v) and molar concentrations of buffer solutions: phosphate- buffered saline (PBS), polyethylene glycol (PEG), and saline-PEG blend (SPEG).

Solution	PBS Concentration		PEG Concentration	
Name	%w/v	mol/L	%w/v	mmol/L
PBS1	0.9	0.154	0	0
PBS5	5.0	0.856	0	0
PBS10	10.0	1.711	0	0
PBS15	15.0	2.567	0	0
PBS20	20.0	3.422	0	0
PEG5	0	0	5.0	2.5
PEG10	0	0	10.0	5.0
PEG15	0	0	15.0	7.5
PEG20	0	0	20.0	10.0
SPEG5	2.5	0.428	2.5	1.25
SPEG10	5.0	0.856	5.0	2.50
SPEG15	7.5	1.283	7.5	3.75
SPEG20	10.0	1.711	10.0	5.00

To provide insight into the transient swelling behavior, specimens were briefly removed from their solutions, blotted dry to remove surface liquid, and weighed periodically during 18 hours of free swelling ($TW_{x\ min}$ = transient weight at minute *x*). Swelling ratio was defined as the percent mass increase divided by the initial fresh weight (*e.g.*, swelling ratio at 120min = (TW_{120min}-FW)/FW*100). After 18 hours of free swelling, specimens were massed and lyophilized to determine tissue dry weight (DW), which was used to calculate water content (WC) during the fresh, transient, and soaked states (*e.g.*, WC_{120min} = (TW_{120min}-DW)/TW_{120min}).

Mechanical testing was performed for the best-performing candidate buffer solution (alongside fresh-frozen and PBS controls) to investigate whether the optimal swelling-limiting solution also maintained tensile mechanics. Thus, three additional fresh coccygeal spine sections were acquired from the same abattoir and discs were dissected from levels C2-C5. Rectangular specimens 2 mm thick and 5 mm wide were prepared from the middle-outer region of the anterior and posterior AF using a freezing stage microtome and oriented with the length along the circumferential direction and the width along the axial direction. Preliminary work ensured no differences in mechanics between anterior and posterior bovine AF (n = 6/group, $p > 0.3$; not shown). Specimen cross-sectional area (CSA) at the midlength was reduced to 1 mm thickness and 1.25 mm width using a series of custom cutting jigs [Werbner et al., 2021b]. That is, the initial cross-sectional area ('pre-CSA') was assumed to be 1.25 mm^2 for all mechanical test specimens. A similar notch geometry was previously developed and validated by our lab using a combined experimental and computational approach to ensure tissue failure properties were robustly and consistently measured [Werbner et al., 2017].

Samples in the SPEG group were soaked in a solution containing 6.25%w/v PBS and 6.25%w/v PEG pH-balanced to 7.4 (n = 6, 'SPEG') and specimens in the PBS group were soaked in 0.9%w/v PBS pH-balanced to 7.4 (n = 6, 'PBS'); all samples were soaked for 18 hours at 25°C prior to testing. Fresh-frozen samples were thawed at room temperature in damp gauze for 15 minutes immediately prior to testing (n = 6, 'Fresh'). Specimens were gripped for mechanical testing using custom-made, serrated screw-clamp grips. A monotonic 0.1 N preload was applied to remove slack from the tissue. Cyclic preconditioning was not applied to avoid altering pre-testing tissue water content, which could affect treatment groups differently [Schmidt et al., 2016]. High-resolution scale bar photographs were taken to measure sample-specific post-swelling cross-sectional area ('post-CSA') and gauge length (average gauge-length 10.1 ± 0.3 mm; ANOVA $p > 0.5$ between groups).

Uniaxial tension was applied monotonically along the circumferential direction at 6 mm/min (~1%/sec) until the specimen separated into two pieces with no load-bearing components between them (end-of-test load threshold = 0.2N). Engineering strain was calculated as the measured change in test-machine crosshead displacement divided by the initial gauge length. Engineering stress was calculated as the measured force divided by the initial cross-sectional area at the midlength. The linear-region modulus was calculated using a custom, sequential linear-regression optimization to the stress-strain response to ensure exclusion of the toe- and yield-regions. Briefly, the algorithm sequentially narrowed a window in which to fit the stress-strain response with a linear regression until the goodness of fit ceased to improve beyond a calibrated threshold. Failure stress was defined as the maximum stress and failure strain as the corresponding strain. Strain energy density was determined through numerical integration of the stress-strain response. The 'failure energy ratio' was defined as the strain energy density up to the point of failure divided by the total strain energy density (*i.e.*, until the end-of-test load threshold was

achieved). Immediately after testing, two small tissue samples were removed from near the notch site, massed, and lyophilized to determine water content, as described above.

All lyophilized samples were digested in 1 ml of 2 mg/mL proteinase K. Glycosaminoglycan (GAG) content was determined using the 1,9-dimethylmethylene blue assay [Farndale et al., 1982]. An aliquot of each digest was hydrolyzed in 6N HCl at 120°C for 24 hours, after which the HCl solution was allowed to evaporate completely under low heat (~40° C). Lysates were resuspended and assayed for hydroxyproline using the chloramine-T spectrophotometric method [Stegemann and Stalder, 1967]. Collagen content was calculated assuming a 1:7.5 OHP-to-collagen mass ratio [Hollander et al., 1994]. Lysates were also assayed for advanced glycation end-product content (AGEs) as measured by total fluorescence using a quinine sulfate standard at excitation/emission wavelengths of 370 nm/440 nm.

Values are reported as medians (first quartile: third quartile). Figure error bars indicate interquartile ranges. Bivariate linear correlations were established between solution concentrations and hydration levels and considered valid for correlation coefficients $R^2 > 0.70$. One-way ANOVA analyses were performed on all mechanical and biochemical properties; significance for ANOVA was assumed at $p < 0.05$. Dunnett's method was applied for multiple pairwise comparisons where significance was found, with the fresh-frozen group as the control (post-hoc significance assumed at $p < 0.05$).

5.3 Results

A nonlinear transient swelling response was observed for all AF specimens soaked in PBS, PEG, and SPEG solutions (**Figure 20**). Experimental transient swelling data for each solution was curve-fit with a logarithmic function ($R^2 > 0.93$ for all but SPEG20). Median and interquartile swelling data at select time points are reported in **Table 3**. Curve-fit coefficients and goodness of fits for each solution are given in **Table 4**.

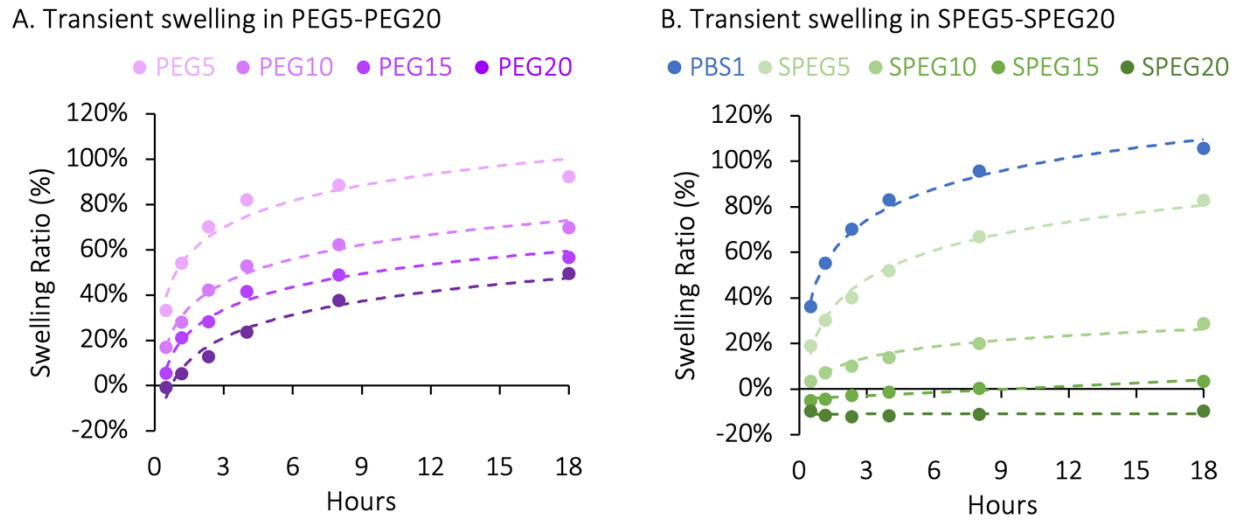

Figure 20: Transient swelling trends for specimens in (A) PEG and (B) SPEG buffer solutions. PBS1 is shown for comparison. Each point represents the median of 4 EXP samples and dotted lines represent logarithmic best-fits.

Apparent equilibrium tissue water content after soaking in PBS, PEG, and SPEG is presented in **Figure 21**. The relationship between solution concentration and measured post-soak water content was curve fit with a linear function ($R^2 > 0.97$ for all). Linear interpolation determined that the solution concentration required to achieve the median fresh-frozen tissue water

content level was 15.7%w/v for PBS, 21.7%w/v for PEG, and 6.25%w/v PBS + 6.25%w/v PEG for SPEG. Despite similar initial weights for all samples ($p > 0.2$), specimen dry weights increased significantly and progressively for PBS concentrations above 5%w/v (Dunnett's $p < 0.001$ versus fresh-frozen; **Figure 22**). This increase in dry weights indirectly suggests solute deposition within the tissue, which may cause water content values to appear lower than true values for these groups [Safa et al., 2017]. Dry weights for PEG and SPEG specimens were not significantly different from controls for any solution concentration ($p > 0.4$; **Figure 22**).

Table 3: Transient swelling values in PBS, PEG, and SPEG for a range of concentrations. Values represent the median (interquartile range) of 4 samples.

Solution	30min	8hr	18hr
PBS1	**36%** (32:39%)	**96%** (91:99%)	**106%** (97:113%)
PBS5	**27%** (26:28%)	**99%** (94:105%)	**110%** (108:117%)
PBS10	**19%** (18:20%)	**93%** (89:98%)	**110%** (107:114%)
PBS15	**20%** (18:21%)	**89%** (84:95%)	**103%** (99:108%)
PBS20	**8.7%** (8.2:11%)	**70%** (68:76%)	**92%** (90:97%)
PEG5	**33%** (32:34%)	**89%** (83:93%)	**92%** (89:97%)
PEG10	**17%** (14:20%)	**62%** (57:66%)	**70%** (63:72%)
PEG15	**5.6%** (4.1:7.2%)	**49%** (43:55%)	**57%** (50:64%)
PEG20	**-0.7%** (-2.0:0.4%)	**38%** (33:42%)	**50%** (45:53%)
SPEG5	**19%** (17:21%)	**67%** (63:68%)	**83%** (78:85%)
SPEG10	**3.4%** (3.0:4.4%)	**20%** (18:22%)	**29%** (28:30%)
SPEG15	**-5.1%** (-5.5:-4.3%)	**0.4%** (-0.8:3.0%)	**3.4%** (2.3:6.3%)
SPEG20	**-9.7%** (-11:-9.5%)	**-11%** (-13:9.2%)	**-9.6%** (-12:-8.1%)

Table 4: Coefficients and R^2 values for logarithmic best-fits of the transient swelling response in PBS, PEG, and SPEG over a range of concentrations. Swelling ratio = $\alpha \cdot \ln(t) + \beta$ where t is the free-swelling time in hours.

Solution	α	β	R^2
PBS1	0.198	0.507	0.989
PBS5	0.247	0.415	0.987
PBS10	0.269	0.325	0.983
PBS15	0.243	0.340	0.993
PBS20	0.241	0.173	0.963
PEG5	0.169	0.513	0.931
PEG10	0.155	0.282	0.985
PEG15	0.145	0.176	0.982
PEG20	0.147	0.050	0.969
SPEG5	0.172	0.284	0.992
SPEG10	0.068	0.065	0.962
SPEG15	0.028	0.037	0.960
SPEG20	0.001	0.113	0.008

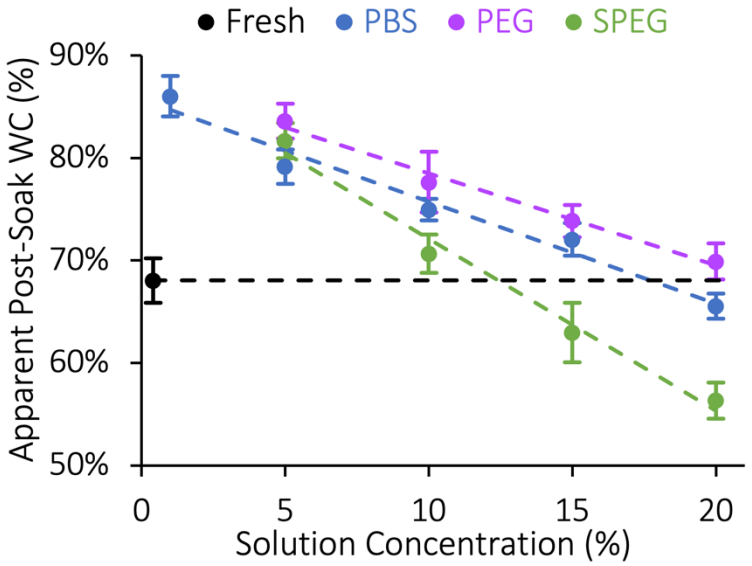

Figure 21: Median apparent tissue water content after 18 h in solution (n = 4 per data point). Some values, particularly in the PBS group, may appear lower than true values due to inferred solute deposition. Trendlines represent linear regression ($R^2 > 0.97$).

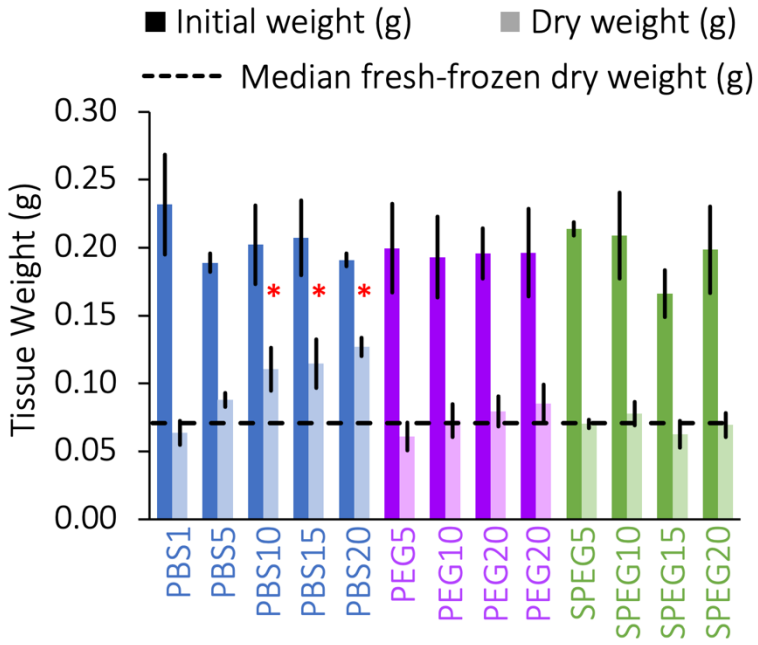

*Figure 22: Median and interquartile range of initial and dry weights (n = 4 per group). For the PBS groups, dry weights increased with osmolarity despite similar initial weights, indirectly suggesting solute deposition in these groups. * indicates Dunnett's $p < 0.001$ vs fresh-frozen dry weights.*

Mechanical testing results are summarized in **Table 5** and **Figure 23** and representative stress-strain curves for experimental and computational samples are given in **Figure 24**. A one-way ANOVA indicated significant differences in linear-region modulus, failure stress, and failure energy ratio ($p < 0.001$), but not failure strain ($p = 0.47$) between solution types. Specimens soaked

in 0.9%w/v PBS exhibited an 81% decrease in modulus ($p < 0.0001$), a 79% decrease in failure stress ($p < 0.0001$), and a 27% decrease in failure energy ratio ($p = 0.001$) versus fresh-frozen controls (**Figure 23A, B, and D** – red stars), concurrent with an 82% increase in gauge cross-sectional area (**Figure 25**). In contrast, none of the mechanical properties of SPEG specimens were significantly different from fresh-frozen controls ($p > 0.10$; **Figures 23 and 24**); gauge cross-sectional area was decreased by 5% after soaking (**Figure 25**).

Table 5: Linear-region modulus (E), failure stress (σ_f), failure strain (ε_f), failure energy ratio (FER), and percent change in gauge cross-sectional area (Δ-CSA). Values represent the median (interquartile range) of 6 samples.

Solution	E (MPa)	σ_f (MPa)	ε_f (%)	FER (%)	Δ-CSA (%)
Fresh	66 (54:71)	18 (16:20)	52 (49:56)	66 (61:75)	-2% (-9:6%)
PBS	13 (9:14)	3.8 (2.4:4.0)	53 (46:58)	48 (43:51)	82% (68:95%)
SPEG	74 (71:76)	20 (20:21)	49 (48:51)	64 (60:72)	-5% (-8:-1%)

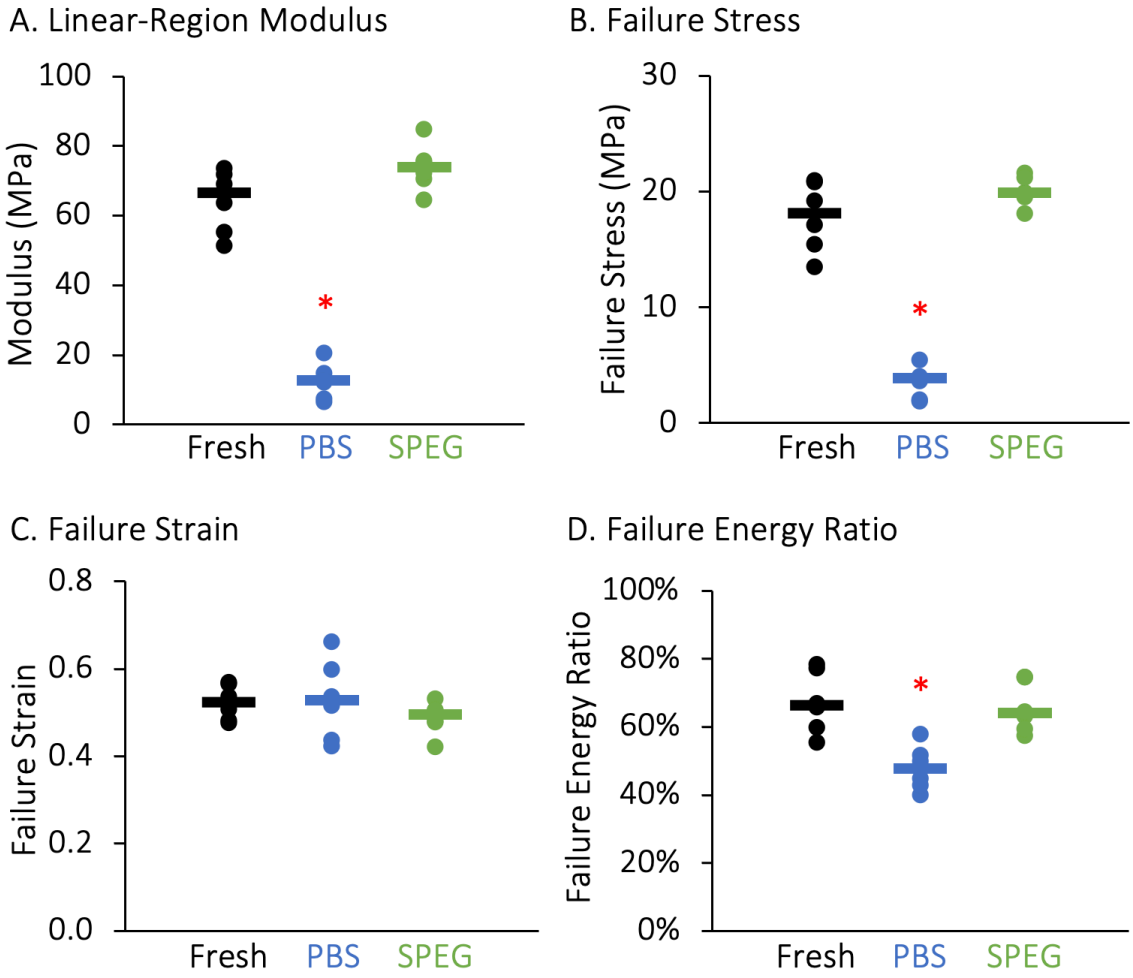

*Figure 23: (A) Linear-region modulus, (B) failure stress, (C) failure strain, and (D) failure energy ratio for each mechanical testing group. Bars represent group medians. * indicates Dunnett's $p < 0.001$ vs fresh-frozen control.*

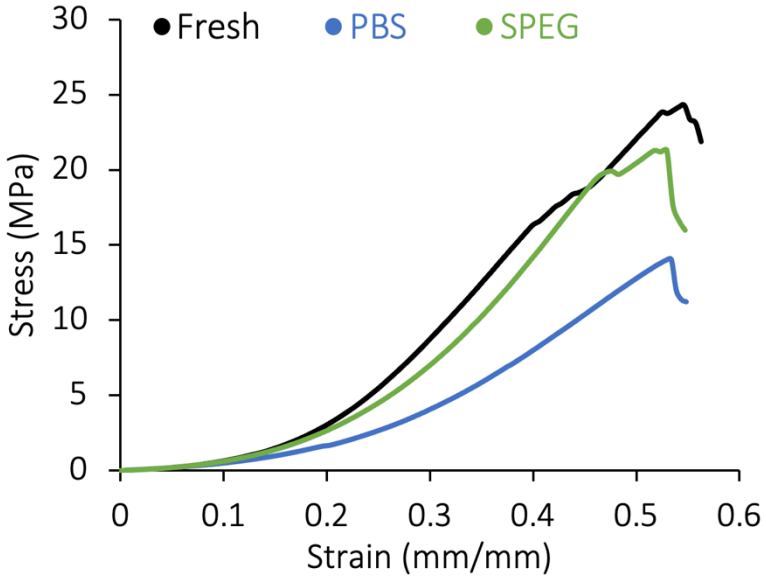

Figure 24: Representative stress-strain curves, truncated after failure for clarity.

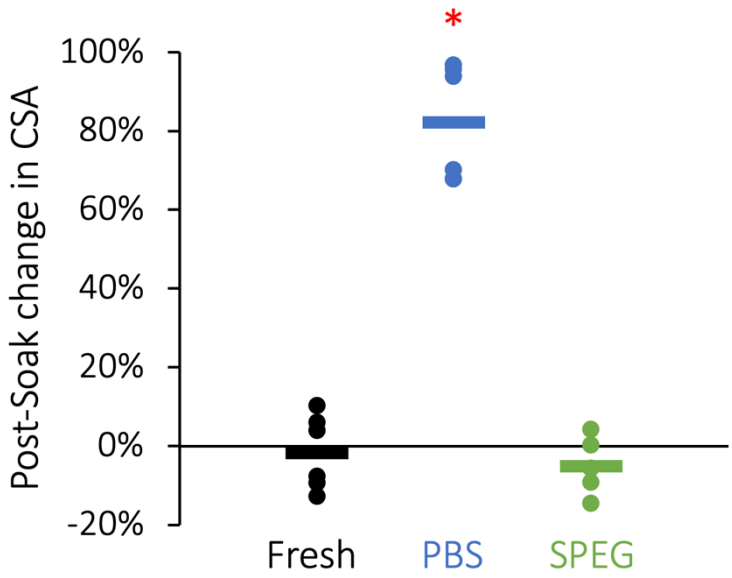

Figure 25: Percent change in mechanical test specimen gauge cross-sectional area (CSA) after 18 h in solution. Bars represent group medians.

Collagen content normalized by tissue fresh weight was not significantly different from fresh-frozen controls for any buffer solution ($p > 0.09$; **Figure 26A**). However, when normalized by tissue dry weight, collagen content appeared to decrease by up to 58% for hyperosmotic PBS solutions versus fresh-frozen controls ($p < 0.001$), likely due to artificially elevated tissue dry weights caused by inferred solute deposition (**Figure 22**). In contrast, GAG contents for specimens soaked in all buffer solutions were significantly lower than fresh-frozen controls, regardless of normalization method ($p < 0.05$ for GAG%/FW, $p < 0.02$ for GAG%/DW), indicating the likelihood of significant GAG leaching in all solutions (**Figure 26B** – red stars). When normalized

by tissue fresh weight, which would not be influenced by solute deposition, GAG leaching ranged from 18-42% versus fresh-frozen controls. AGE content normalized by tissue fresh weight was not significantly different from fresh-frozen controls for any buffer solution ($p > 0.18$), nor was AGE content normalized by collagen mass ($p > 0.40$).

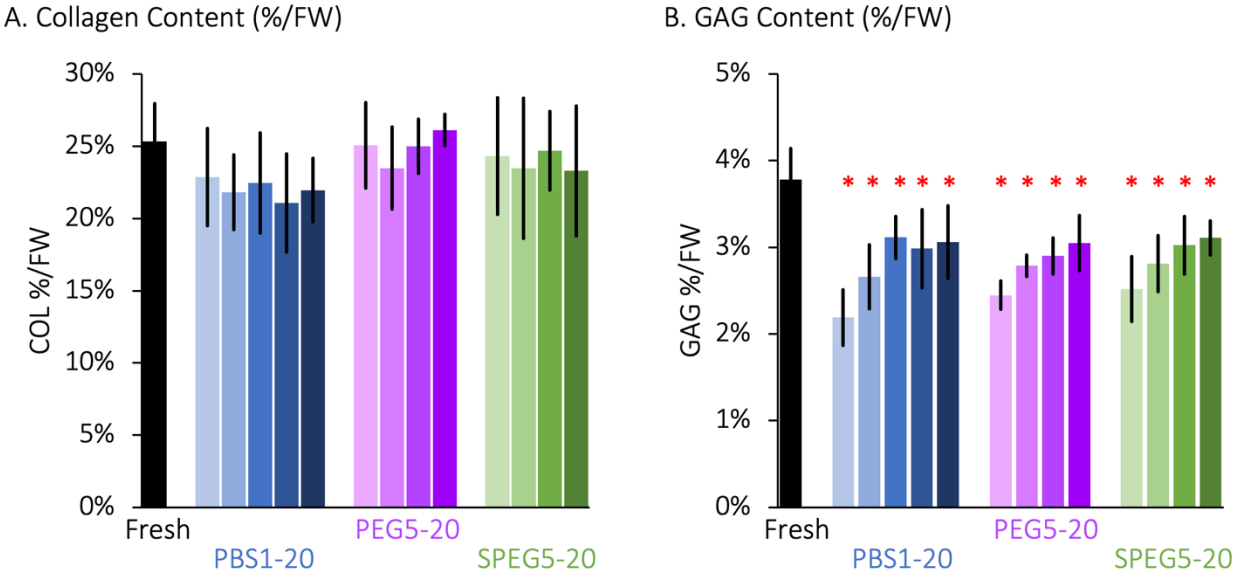

*Figure 26: (A) Collagen content and (B) GAG content normalized by tissue fresh weight. Each bar represents the median of 4 samples and error bars denote the interquartile range. * indicates Dunnett's $p < 0.001$ vs fresh-frozen.*

5.4 Discussion

This study investigated the effects of saline, PEG, and saline-PEG buffer solutions on AF transient and equilibrium swelling behavior and tensile mechanical properties. Buffer solution compositions and concentrations targeting a range of tissue-level AF hydration levels– including the maintenance of fresh-frozen hydration levels– were identified and tested *in vitro* to assess tissue swelling, mechanics, and biochemical composition.

We found that a 6.25%w/v PBS and 6.25%w/v PEG solution (adjusted to pH 7.4) effectively maintained fresh-frozen AF tissue hydration levels, even after 18 hours in solution (**Table 3, Figures 20-21**). In addition to maintaining physiologic hydration levels, this solution also maintained tissue cross-sectional area, as well as sub-failure, failure, and post-failure tensile mechanics at fresh-frozen levels (**Table 5, Figures 23-25**). In contrast, specimens soaked in 0.9%w/v PBS for 18 hours experienced over 100% swelling (*i.e.*, absorbed more than their fresh weight in additional water), concurrent with an 80% increase in gauge cross-sectional area. Linear-region modulus and failure stress decreased nearly two-fold for these samples versus fresh-frozen controls.

It appears that changes in water content likely influence tissue mechanics both by altering bulk specimen geometry due to swelling and by additional sub-tissue scale mechanisms not measured in the current study. At the tissue-level, the 80% increase in cross-sectional area for samples soaked in 0.9%w/v PBS would be expected to decrease the apparent modulus to ~37 MPa (from ~66 MPa for fresh tissue). However, we observed a significantly lower linear-region modulus for PBS-soaked specimens (~13 MPa), agreeing well with results reported by Żak and Pezowicz (2016) and adding to the emerging evidence that sub-tissue scale mechanisms likely contribute to diminished tissue stiffness with overhydration [Screen et al., 2006; Han et al., 2012;

Żak and Pezowicz, 2016]. Such effects likely include: the leaching of GAGs, which has been shown to diminish AF single- and multi-lamellar tensile mechanics [Han et al., 2012; Isaacs et al., 2014; Werbner et al., 2019], increased distance between collagen fibrils [Screen et al., 2005; Screen et al., 2006; Han et al., 2012], and increased collagen fibril diameter, which has been associated with decreased tensile stiffness [Roeder et al., 2002; Bueler and Wong, 2007; Aladin et al., 2010]. Additionally, understanding the fundamental mechanisms driving altered failure mechanics is important as the field progresses towards a more comprehensive multi-scale understanding of multi-phasic tissue mechanics. However, it has proven difficult to determine the sub-tissue level mechanisms that drive the initiation of bulk tissue failure.

None of the buffer solutions investigated in this study altered tissue collagen content when normalized by specimen fresh weight (**Figure 26**). However, elevation of tissue dry weights in hyperosmotic saline solutions, presumably due to solute deposition, caused a significant decrease in apparent collagen content. For this reason, biochemical measurements from tissues exposed to hyperosmotic solutions should be normalized to specimen fresh weight [Bezci et al., 2019; Werbner et al., 2019]. A similar discrepancy between fresh and dry weight normalizations was observed for tissue AGE contents; it remains preferable to normalize AGE content to total collagen mass to avoid artifacts of solute deposition and account for inter-species differences in tissue collagen content [Showalter et al., 2012; Werbner et al., 2021b]. GAG contents were observed to decrease for all buffer solutions, regardless of normalization method, suggesting significant leaching of GAGs during extended soak times, agreeing well with previous observations [Urban and Maroudas, 1979; Maroudas et al., 1985; Perie et al., 2006; Han et al., 2012; Bezci et al., 2019; Bezci et al., 2020]. GAG content of specimens soaked in 0.9%w/v PBS suggest almost 50% loss in GAG content compared to fresh-frozen controls, while specimens soaked in SPEG20 lost less than 20% compared to fresh-frozen controls (**Figure 26**). Thus, high-concentration saline-PEG blends provide the additional utility of limiting GAG leaching in addition to preserving fresh-frozen hydration levels and mechanical properties, consistent with previous literature reporting that 20 kDa PEG was used to help limit tissue GAG loss [Urban and Maroudas, 1979].

The main results of this study are consistent with recent tendon studies, which found that saline-PEG blends maintained hydration at fresh-frozen levels and limited the significant decrease in modulus observed after soaking in 0.9%w/v PBS [Safa et al., 2017; Bloom et al., 2021]. Additionally, Safa et al. (2017) showed that both NaCl and PEG have the same proportionate effect on lowering tendon water content at increasing concentrations, as indicated by the slopes in Table 3 and Figure 4 of that study; while absolute water content values differ between tissue types (~55% in fresh tendon versus ~75% in fresh AF), this is directionally consistent with the results of this study (**Figure 21**). Furthermore, the increased slope of the SPEG curve compared to NaCl and PEG in Safa et al. (2017) suggests that there is a substantial synergistic effect of combining these two solutes, consistent with the greater slope of the green line in **Figure 21**. This important result is also consistent with older work by Davey and Skegg (1973) showing that media containing NaCl and PEG reduced kidney tissue water content *in vitro* by ~20-45% (depending on incubation time) compared to PEG- or NaCl-containing media alone. These results also corroborate work by Schiller et al. (1988) suggesting that PEG might reduce the availability of water to interact with other osmotic solutes within the same solution.

The current study expands upon these results for the AF by presenting comprehensive transient swelling trends for a broad range of buffer solution compositions and concentrations across an extended timescale (18 hours). Despite these advances, this study had its limitations in the relatively small intra-group sample size for swelling experiments (n=4 per solution

concentration), the single specimen orientation used for mechanical testing (circumferential-axial), and single loading rate (~1%/sec), as previous studies have shown that AF mechanical response is orientation- and rate- dependent [Gregory and Callaghan, 2010; Isaacs et al., 2014; Werbner et al., 2017]. An additional limitation of the study was our choice to limit the study size by investigating only one-to-one mixtures of PBS and PEG. This choice arose from preliminary work which found that, even when paired with high concentrations of PEG, mixtures of 0.9%w/v NaCl were insufficient to limit tissue-level AF swelling (not shown). The discrepancy between this result and those observed previously in tendons and ligaments for 0.9%w/v NaCl + 8%w/v PEG solutions [Sverdlik and Lanir, 2002; Lujan et al., 2009; Safa et al., 2017; Bloom et al., 2021] may be due to the substantially higher GAG content of AF samples (8-12%/DW in AF versus 1-5%/DW in tendon) [Demers et al., 2004; Thorpe and Screen, 2016], as well as potentially greater residual stresses in the AF due to *in situ* boundary conditions [Huyghe and Jongeneelen, 2012]. Additional work is needed to evaluate whether different ratios of PBS and PEG would produce similar (or possibly better) results in AF swelling.

This study determined and validated a saline-PEG buffer solution that maintained AF tissue-level hydration and mechanics *in vitro* at fresh-frozen tissue levels. The results from this study suggest that 0.9%w/v PBS should not be used to maintain tissue-level AF specimen hydration during preparation, treatment, or testing if physiological relevance is to be considered regarding hydration and mechanics. Instead, a solution generating sufficient osmotic pressure to maintain physiological hydration levels in tissue-level specimens should be used. While a 6.25%w/v PBS + 6.25%w/v PEG solution proved effective for healthy bovine AF tissues commonly used in the field, inter-species differences and tissue health status are known to influence swelling and mechanical behavior; thus, future work should seek to determine optimal solution compositions to maintain hydration levels and mechanics in the specific tissues being studied. As the field develops a deeper understanding of the central role of tissue hydration in maintaining proper mechanical and biological function, it is essential for future studies investigating the relationship between tissue hydration, aging, injury, and disease to prepare, treat, and test tissues in solutions that allow precise control of hydration levels.

6. Non-enzymatic glycation of annulus fibrosus alters tissue-level failure mechanics in tension[4]

6.1 Introduction

Fiber-reinforced tissues of the musculoskeletal system, such as the annulus fibrosus (AF) in the intervertebral disc, experience large, complex loads during daily activities. Repetitive or excessive loading may initiate structural damage and lead to mechanical failure, causing debilitating pain and reduced mobility [Buckwalter, 1995; Luoma et al., 2000]. Additionally, disc tissue structure and composition change with age and disease, which alters mechanical behavior and may predispose the disc and surrounding structures to damage [Urban and Roberts, 2003; Adams and Roughley, 2006]. Thus, it is essential to comprehensively characterize tissue structure-function relationships and failure mechanisms to better understand and prevent avoidable injuries, including those occurring due to age and disease.

In addition to the natural aging process, several clinical conditions have been linked to accelerated degeneration and herniation of the intervertebral disc. Among cardiovascular risk

[4] Adapted from "Werbner B, Lee M, Lee A, Yang L, Habib M, Fields AJ, O'Connell GD. Non-enzymatic glycation of annulus fibrosus alters tissue-level failure mechanics in tension. Journal of the Mechanical Behavior of Biomedical Materials. 2021 Nov 20:104992."

factors studied in the Nurses' Health Study, diabetes had the highest relative risk of intervertebral disc herniation (relative risk: 1.52, 95% CI: 1.17 to 1.98) after correcting for additional risk factors such as age, body mass index, level of exercise, and several other important factors [Jhawar et al., 2006]. Additionally, previous work showed that diabetes was associated with increased frequency and severity of lower back pain and diminished treatment outcomes [Mäntyselkä et al., 2008; Licciardone et al., 2013; Takahashi et al., 2013; Freedman et al., 2011]. Approximately 10.5% of Americans are diabetic and with 1.5 million new cases diagnosed every year and total annual costs estimated at $327 billion, diabetes and the associated complications represent one of the most significant healthcare issues in the United States [CDC, 2020].

One of the most well-documented changes in connective tissues occurring with diabetes is the accumulation of advanced glycation end-products (AGEs) [Monnier et al., 1986; Singh et al., 2001; Vlassara and Palace, 2002; Ahmed, 2005; Tsai et al., 2014]. Research in this group of post-translational protein crosslinks and adducts has grown in recent years, as they exhibit a wide range of chemical, cellular, and tissue-level effects that have been strongly implicated in diabetes-related complications [Singh et al., 2001; Vlassara and Palace, 2002; Ahmed, 2005]. Minimal biological turnover and a long half-life makes collagen and proteoglycans in the intervertebral disc particularly susceptible to interaction with glycating metabolites and AGE formation [Pokharna and Phillips, 1998; Vlassara and Palace, 2002; Snedeker and Gautieri, 2014]. AGEs have also been shown to accumulate naturally in the disc with age [Pokharna and Phillips, 1998; Sivan et al., 2006], although the rate and extent of intradiscal AGE accumulation is amplified with diabetes [Tsai et al., 2014].

Previous studies of soft tissues in the musculoskeletal system, such as articular cartilage, tendon, and the intervertebral disc, have probed the effects of AGEs on tissue mechanics using animal models of diabetes or *in vitro* crosslinking with ribose or methylglyoxal (MGO) [Reddy et al., 2002; Verzijl et al., 2002; Reddy, 2004; Wagner et al., 2006; de Oliveira et al., 2011; Fox et al., 2011; Li et al., 2013; Jazini et al., 2012; Gautieri et al., 2017; Svensson et al., 2018]. More recently, studies have also begun to investigate structural and functional effects of controlled *in vivo* AGE accumulation through animal models fed AGE-rich diets [Illien-Jünger et al., 2015; Krishnamoorthy et al., 2018; Hoy et al., 2020]. These studies reported noteworthy alterations to tissue structure and function across multiple length scales. The most widely reported alterations to connective tissue mechanics include increased tissue stiffness, failure strength, energetic toughness, and reduced viscoelasticity [Reddy et al., 2002; Verzijl et al., 2002; Reddy, 2004; Wagner et al., 2006; Li et al., 2013; Snedeker and Gautieri, 2014; Gautieri et al., 2017; Svensson et al., 2018]. However, a few studies in diabetic animals have reported decreases in tissue stiffness [de Oliveira et al., 2011; Fox et al., 2011]. Additional studies have also observed significant changes in disc-adjacent tissues, such as vertebral bodies and endplates, which are known to play an important role in load-distribution and nutrient transport [Viguet-Carrin et al., 2006; Fields et al., 2015; Illien-Jünger et al., 2015; Acevedo et al., 2018; Dolor et al., 2019; Zhou et al., 2021].

Despite these advances, the effects of AGEs on AF tensile failure mechanics have not yet been reported. Additionally, *in vitro* soak treatments applied in previous studies tend to cause tissue swelling, which is known to alter tissue mechanics and potentially confound mechanical testing results [Han et al., 2012; Bezci et al., 2015; Safa et al., 2017; Werbner et al., 2019; Werbner et al., 2021]. Thus, the specific aim of this study was to quantify the relationship between physiological, glycation-induced biochemical changes and AF tensile failure mechanics while maintaining physiological tissue hydration levels. The broader aim of this study was to provide a more complete understanding of mechanisms that may help explain the increased propensity for disc degeneration

and herniation with diabetes. Thus, the current study evaluated pre-failure, failure, and post-failure properties of normal and *in vitro* glycated bovine caudal AF tissue by comparing measured mechanics between control, moderate glycation, and high glycation groups, and by correlating biochemical composition, including AGE content, to mechanical properties at two distinct loading rates. Furthermore, human cadaver AF tissue from a cross-sectional population of donors of both sexes and a range of ages was assayed to provide a physiologically relevant range of AGEs in adult humans as a target for *in vitro* glycation.

6.2 Materials and Methods

Fresh bovine coccygeal spine sections were acquired from a local abattoir (n = 19, age 18-24 months). Bovine discs were used to investigate AF mechanics due to their larger disc area and similarities in biochemical and mechanical properties to healthy human discs [O'Connell et al., 2007; Demers et al., 2004; Beckstein et al., 2008]. Musculature was removed from the spine and discs were dissected from levels CC2-CC5. Rectangular specimens 2 mm thick and 5 mm wide were prepared from the middle-outer region of the anterior and posterior AF using a freezing stage microtome and oriented with the length along the circumferential direction and the width along the axial direction (**Figure 27A**). Preliminary work ensured no differences in mechanics between anterior and posterior bovine AF (n=6/group, Student's $p > 0.3$).

A full-width, half-depth notch was created using a custom cutting jig that ensured 1 mm thickness at the midlength; the width of the notch area was then further reduced to 1.25 mm using another custom cutting jig (**Figure 27B**). A similar notch geometry was previously developed and validated by our lab using a combined experimental and computational approach to ensure tissue failure properties were robustly and consistently measured [Werbner et al., 2017]. Previous studies reported no significant differences in stiffness or strength between notched and intact fiber-reinforced soft-tissues, suggesting a limited effect of stress concentrations at the notch site [Taylor et al., 2012; Von Forell et al., 2014].

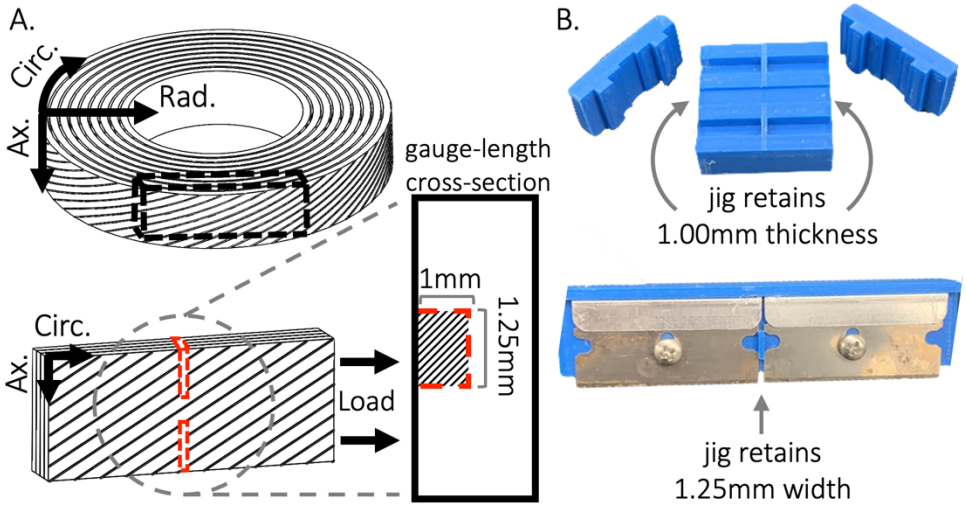

Figure 27: (A) Disc schematic showing circumferential-axial specimen orientation and loading direction. Inset shows reduced cross-sectional area at the midlength, which was notched to ensure repeatable failure. (B) Custom cutting jigs used to ensure that the tissue remaining at the notch site had repeatable dimensions of 1 × 1.25 mm.

Preliminary work was conducted to determine the appropriate concentration and soak temperature of the glycation solution to achieve two distinct, physiologically relevant levels of AGEs. The range of physiological AGE concentrations was determined by assaying the AGE content of unfixed human lumbar AF tissues obtained from 10 cadaveric spines (**Table 6;** mean age 58.4 ± 9.4 years; IRB exempt - Category 4). Briefly, 36 AF specimens were dissected, lyophilized, digested in papain, hydrolyzed in 6N HCl at 120°C, neutralized, and assayed for total fluorescence using a quinine sulfate standard at excitation/emission wavelengths of 370 nm/440 nm to estimate total AGE content.

Table 6: Human tissue donor information and disc AGE contents.

Donor Age	Donor Sex	Donor BMI	Disc Level	Disc Grade	AGE Content (ngQ/mgDW)
38	Male	27	L4-L5	III	422.23
			L5-S1	III	437.62
52	Male	25	L3-L4	III	452.96
55	Male	26	L3-L4	II	416.57
			L4-L5	II	459.40
56	Male	23	L3-L4	II	432.65
57	Male	29	L4-L5	IV	647.32
64	Male	16	L3-L4	III	503.87
60	Female	31	L3-L4	III	507.26
			L4-L5	III	598.57
63	Female	25	L2-L3	IV	410.83
			L4-L5	IV	416.41
66	Female	22	L3-L4	III	562.58
			L4-L5	III	551.23
73	Female	24	L3-L4	III	506.65
			L4-L5	III	629.29

Bovine AF samples in the control group (CTL, n=26) were soaked for 18 hours at 25°C in 10 mL of a solution containing 5% phosphate-buffered saline (PBS) and 5%w/v polyethylene glycol (PEG) pH-balanced to 7.4. Previous studies found that this solution avoided excessive tissue swelling caused by traditional 0.9% PBS treatments as well as excessive solute deposition caused by hyperosmotic saline solutions [Safa et al., 2017; Werbner et al., 2019; Bezci et al., 2020; Bloom et al., 2021; Werbner et al., 2021]. Based on the human data from our preliminary work, glycated specimens were soaked in 0.3 M methylglyoxal pH-balanced to 7.4 at either 25°C or 50°C for 18 hours immediately prior to testing (GLY25 (n=26) and GLY50 (n=26), respectively). Previous work from our lab analyzed the thermal profile of bovine annulus fibrosus tissue using differential scanning calorimetry and did not observe any measurable deviations in the trace until 65-70°C, consistent with previous studies of similar connective tissues [Domán and Illés, 2004; Bálint et al., 2009; Chae et al., 2009; Samouillan et al., 2011]. Thus, it was assumed that incubation at 50°C did not affect the bulk tissue composition or mechanical response.

Specimens were gripped for mechanical testing using custom-made, serrated screw-clamp grips. Specimens were tested in a custom-built water bath containing the previously mentioned PBS-PEG mixture to maintain tissue hydration during testing (total testing time up to 150 minutes for low-rate testing). A monotonic 0.1 N preload was applied to remove slack from the tissue. Cyclic preconditioning was not applied to avoid altering pre-testing tissue water content, which

could affect treatment groups differently [Schmidt et al., 2016]. Scale bar photographs were taken to measure sample-specific length (9.90 ± 2.03 mm). Uniaxial tension was applied monotonically along the circumferential direction at either a low (0.1 mm/min, 0.017%/sec, 'Lo') or high (50 mm/min, 8.33%/sec, 'Hi') loading rate until the specimen separated into two pieces with no load-bearing components between them (end-of-test load threshold = 0.2N). Physiological loading rates experienced by the AF are complex, varied, and difficult to determine, in part because they are mitigated by a myriad of muscle contractions [White and Panjabi, 1990]. The low and high loading rates used here were selected to be within a reasonable range of physiological loading conditions and to highlight potential rate-sensitive differences in mechanics [Gregory and Callaghan, 2010; Werbner et al., 2019].

Engineering strain was calculated as the measured change in test-machine crosshead displacement divided by the initial gauge length. Engineering stress was calculated as the measured force divided by the initial cross-sectional area at the midlength. The linear-region modulus was calculated using a custom, sequential linear-regression optimization to the stress-strain response to ensure exclusion of the toe- and yield-regions. Failure stress was defined as the maximum stress and failure strain as the corresponding strain. Strain energy density was determined through numerical integration of the engineering stress-strain response. The 'failure energy ratio' was defined as the strain energy density up to the point of failure divided by the total strain energy density (*i.e.*, until the end-of-test load threshold was achieved). While Lagrangian or Eulerian strain descriptions might provide a more accurate characterization of the strain energy density at large deformations, most tissue mechanics studies use the area under the engineering stress-strain curve due to experimental limitations in collecting accurate local deformation data around and beyond bulk failure [Reddy et al., 2002; Reddy, 2004; de Oliveira et al., 2011; Fox et al., 2011; Li et al., 2013; Gautieri et al., 2017]. Thus, the engineering stress-strain response was used in this study to facilitate comparison to previous literature.

After mechanical testing, two small tissue samples adjacent to the notch site were removed with a scalpel and weighed before (wet weight, 'WW') and after (dry weight, 'DW') lyophilization to determine water content ('WC', WC = (WW-DW)/WW). Dried specimens were hydrolyzed in 6N HCl at 120°C for 24 hours, after which the HCl solution was allowed to evaporate completely under low heat (40°C). Lysates were resuspended and assayed for hydroxyproline using the chloramine-T spectrophotometric method [Stegemann and Stalder, 1967]. Collagen content ('Col') was calculated assuming a 1:7.5 OHP-to-collagen mass ratio and reported as a percentage of tissue dry weight (mgCol/mgDW) [Hollander et al 1994]. Lysates were also assayed for total fluorescence using a quinine sulfate standard at excitation/emission wavelengths of 370 nm/440 nm. Total fluorescence was reported as equivalent nanograms of quinine normalized by tissue dry weight (ngQ/mgDW) and equivalent micrograms of quinine normalized by tissue collagen content (ugQ/mgCol).

All values are reported as mean ± standard deviation. A two-way ANOVA on means was performed for all mechanical and biochemical properties (factors = treatment and loading rate); significance for the ANOVA was assumed at $p < 0.05$. A Tukey HSD post-hoc analysis for multiple pairwise comparisons was performed where significance was found. Significance was assumed at $p < 0.05$ for the post-hoc analysis. Bivariate linear correlations were established between each pair of biochemical and mechanical properties. Correlation strength was determined based on the correlation coefficient R (weak: $|R| < 0.5$, moderate: 0.50-0.69, strong: ≥ 0.70).

6.3 Results

All samples exhibited a nonlinear stress-strain response prior to failure and a clear maximum stress corresponding to the initiation of bulk failure (**Figure 28**). Mechanical testing data was only included for samples that clearly failed at the midlength (n=78/84 *i.e.,* 93%).

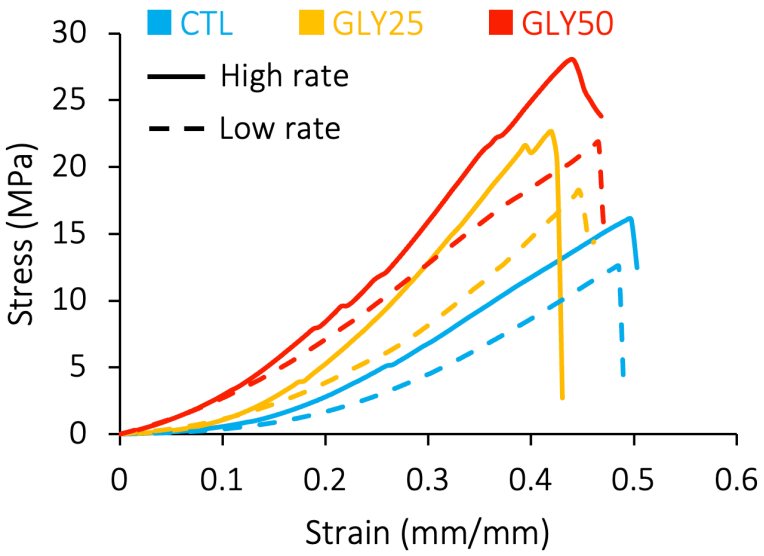

Figure 28: Representative stress-strain curves for control (CTL) and glycated (GLY25 and GLY50) specimens at the low and high loading rates.

For the low-rate control group, the mean linear-region modulus was 27.47 ± 6.60 MPa, failure stress was 11.19 ± 2.36 MPa, failure strain was 0.54 ± 0.07 mm/mm, and failure energy ratio was 0.64 ± 0.10. For the high-rate control group, the mean linear-region modulus was 38.35 ± 12.42 MPa, failure stress was 14.12 ± 3.66 MPa, failure strain was 0.49 ± 0.09 mm/mm, and failure energy ratio was 0.67 ± 0.10. Modulus and failure stress increased at the higher loading rate across treatment groups (ANOVA $p < 0.0002$; **Figure 29A-B**, light vs dark). In particular, modulus increased 40-44% (HSD $p < 0.0001$) and failure stress increased 18-28% (HSD $p = 0.0002$) while failure strain decreased 9-16% at the higher loading rate (ANOVA $p = 0.001$, HSD $p = 0.001$; **Figure 29A-C**). Failure energy ratio was not different between loading rates (ANOVA $p = 0.84$; **Figure 29D**).

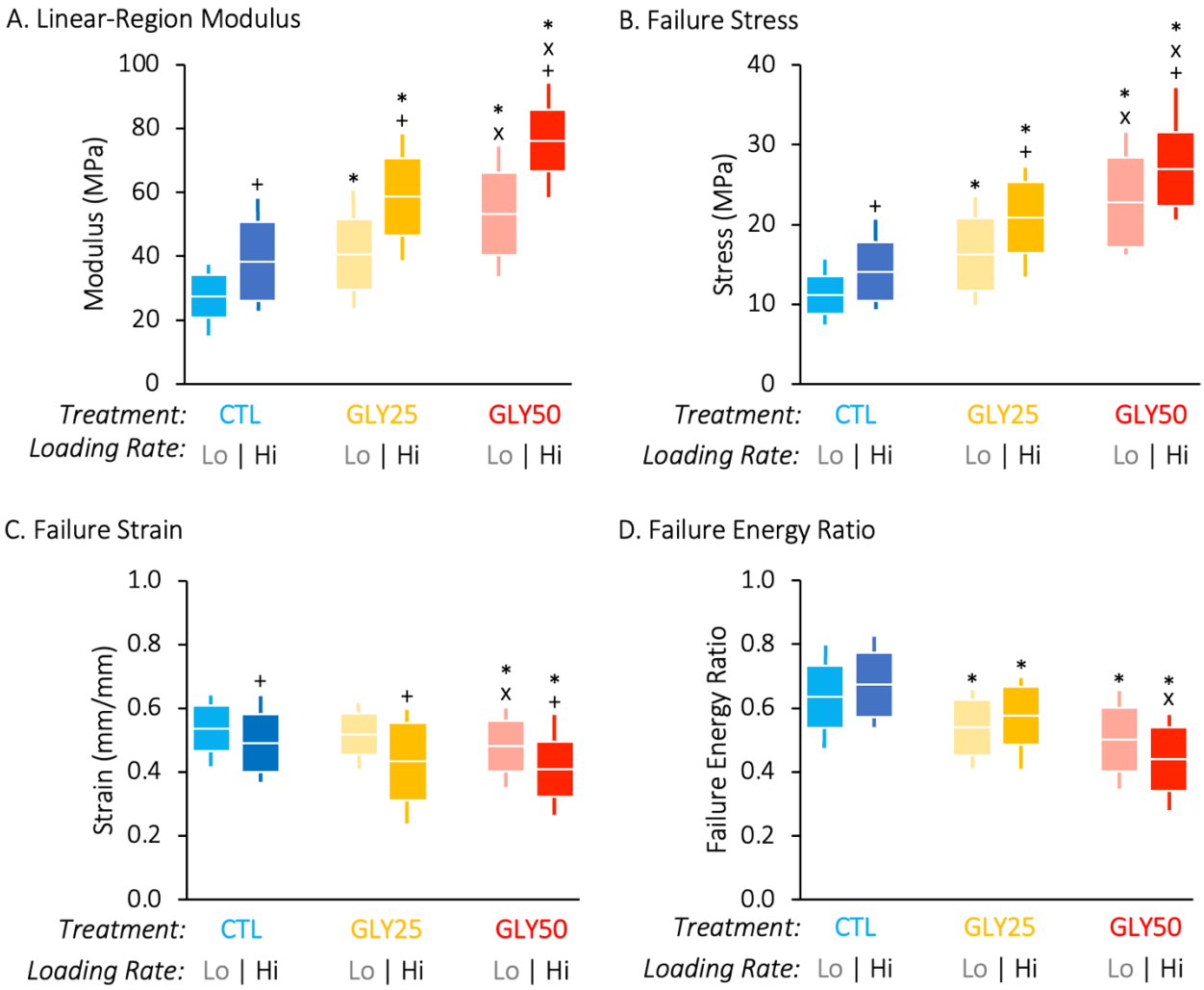

Figure 29: (A) Linear-region modulus, (B) failure stress, (C) failure strain, and (D) failure energy ratio at each glycation level and loading rate (mean ± standard deviation ± range, n = 13 per group). Statistics highlight the effect of glycation (indicates $p < 0.01$ vs CTL and x indicates $p < 0.01$ vs GLY25) and loading rate (+indicates $p < 0.05$ vs Lo).*

In vitro glycation had significant effects on pre-failure, failure, and post-failure mechanical properties (**Figure 29**). Increasing extent of glycation was associated with higher modulus and failure stress values at both loading rates (ANOVA $p < 0.0001$; **Figure 29A-B**, blue vs orange vs red). In particular, glycation increased mean tensile modulus versus control by 48-94% at the low rate and 53-99% at the high rate (HSD $p < 0.0001$). Glycation increased failure stress by 45-104% at the low rate and 48-91% at the high rate (HSD $p < 0.0001$). Glycation decreased failure strain by 10% at the low rate and 17% at the high rate (ANOVA $p = 0.02$, HSD $p = 0.02$). Glycation decreased the failure energy ratio by 15-21% at the low rate and 15-35% at the high rate (ANOVA $p < 0.0001$; HSD $p < 0.006$).

Biochemical measurements are summarized in **Figure 30**. As only methylglyoxal treatment, and not loading rate, was hypothesized to alter tissue composition, biochemical measurements within treatment groups were pooled between loading rates. The rate-pooled mean water content for the CTL group was 75 ± 3%/WW, collagen content was 70 ± 4%/DW, and AGE content was 175 ± 36 ngQ/mgDW and 250 ± 54 ugQ/mgCol (**Figure 30**).

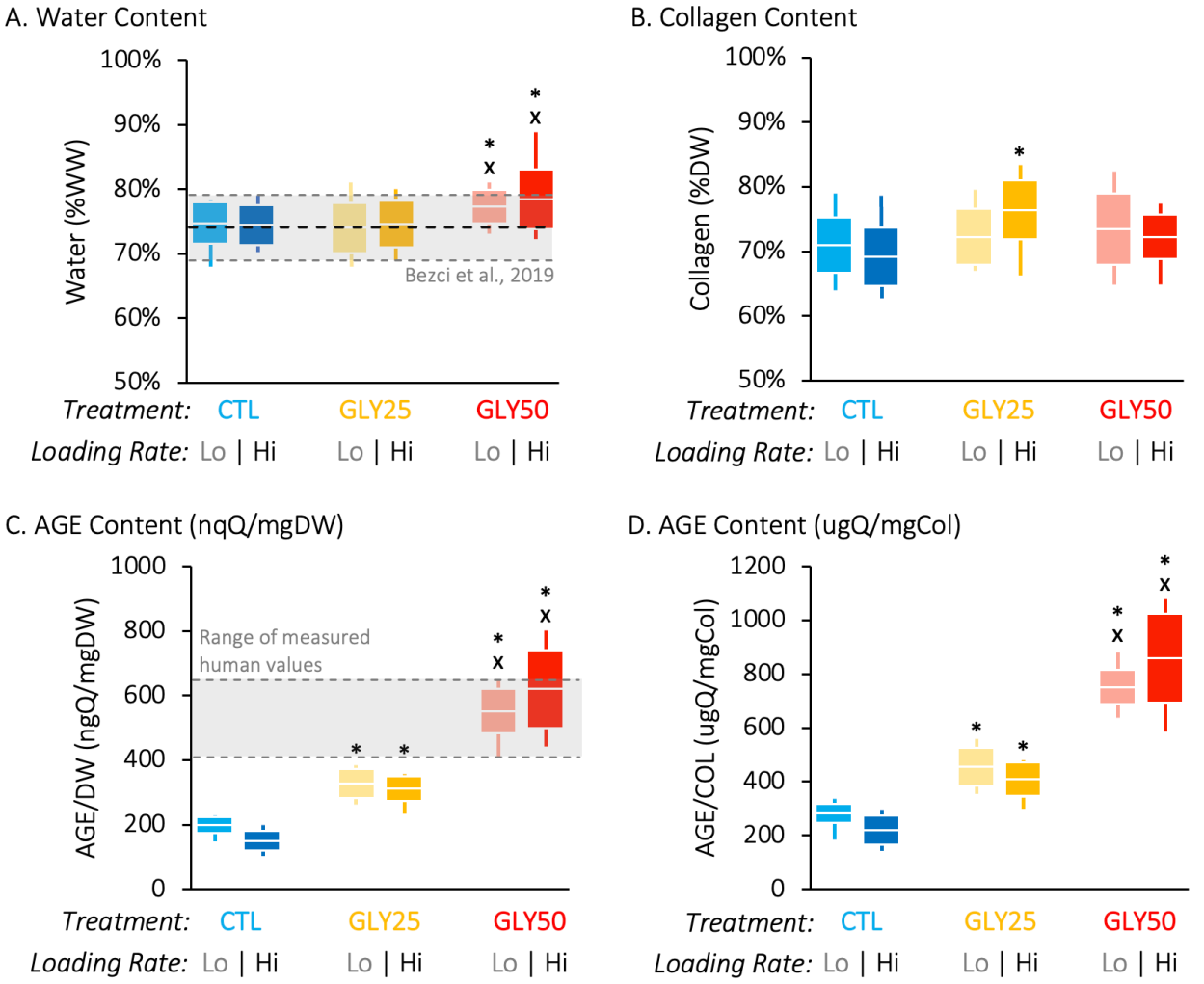

*Figure 30: (A) Water content, (B) collagen content, and (C–D) AGE content at each glycation level and loading rate (mean ± standard deviation ± range, n = 13 per group). Fresh AF water content level (mean ± standard deviation) from Bezci et al. (2019) shown for reference in (A). Range of human AF AGE levels measured in the current study shown for reference in (C). * indicates $p < 0.05$ vs CTL and x indicates $p < 0.05$ vs GLY25.*

AGE content normalized by dry weight increased 83% and AGE content normalized by collagen content increased 73% in the GLY25 group (ANOVA $p < 0.0001$, HSD $p < 0.0001$). AGE content normalized by dry weight increased 236% and AGE content normalized by collagen content increased 222% in the GLY50 group (ANOVA $p < 0.0001$, HSD $p < 0.0001$). Water content increased 4% in the GLY50 group versus control (ANOVA $p = 0.0008$, HSD $p = 0.005$). AGE contents for the human AF specimens were normally distributed (Shapiro-Wilk $p = 0.125$) with a mean of 498 ± 94 ngQ/mgDW; donor-specific values are presented in **Table 6**.

AGE content was strongly positively correlated with modulus (R = 0.74, $p < 0.0001$) and failure stress (R = 0.70, $p < 0.0001$) (**Figure 31A-B**). AGE content was moderately negatively correlated with failure energy ratio (R = -0.62, $p < 0.0001$) (**Figure 31C**). Linear-region modulus was strongly positively correlated with failure stress (R = 0.85, $p < 0.0001$) (**Figure 31D**).

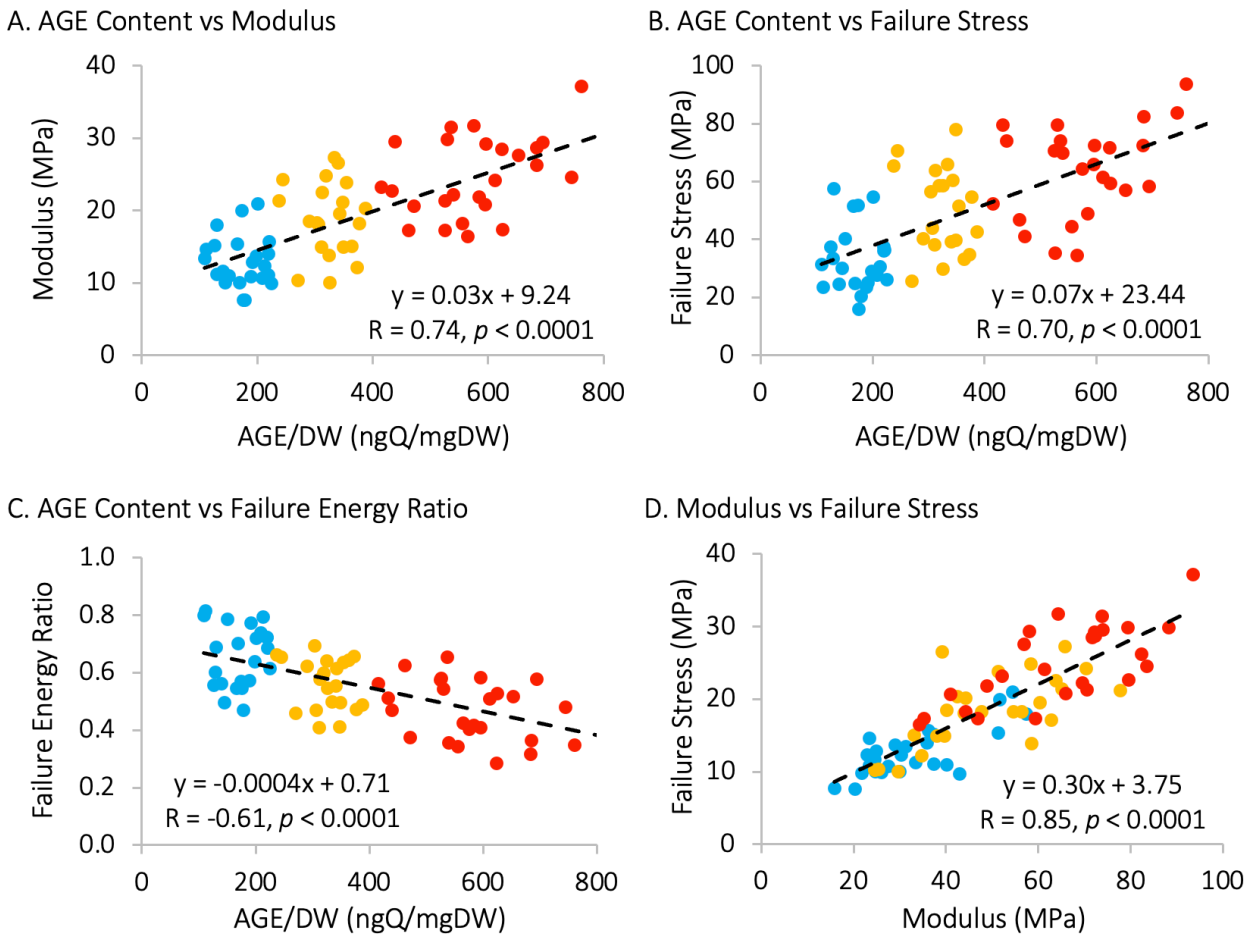

Figure 31: (A–C) Bivariate linear correlations between AGE content and measured mechanics. (D) Bivariate linear correlation between linear-region modulus and failure stress. Colors indicate rate-pooled glycation treatment groups.

6.4 Discussion

The specific aim of this study was to determine the relationship between AF advanced glycation end-product content and tissue-level tensile mechanics at two distinct loading rates. *In vitro* glycation treatments were designed to minimize changes in water content and induce two distinct levels of AGEs based on measurements from human cadaver AF tissues (donor age range: 38-73 years). Changes in AF mechanics between glycation groups were reported, as well as correlations between tissue AGE content and mechanics.

In vitro glycation increased linear-region modulus and failure stress at both loading rates (**Figure 29A-B**). The increases in mechanical properties were more pronounced at the higher loading rate, which may be attributed to the solid-tissue component having a greater contribution to mechanics at higher loading rates. Increases in modulus and failure stress with glycation are consistent with previous studies that investigated the effects of AGEs on collagenous connective tissue mechanics [Reddy et al., 2002; Verzijl et al., 2002; Reddy, 2004; Wagner et al., 2006; Li et al., 2013; Snedeker and Gautieri, 2014; Gautieri et al., 2017; Svensson et al., 2018]. Moreover, increases in modulus and failure stress and decreases in failure strain at the higher loading rate are consistent with first principles of fiber-reinforced triphasic tissues and previous observations of the AF [Gregory and Callaghan, 2010; Werbner et al., 2019]. In synthetic materials, an increase in modulus and failure stress generally increases embrittlement. However, despite a concurrent

decrease in failure strain, we observed an increase in post-failure energy absorption capacity with glycation (**Figure 29D**). This shift in energy absorption may be attributable to non-enzymatic crosslinks between collagen molecules remaining intact after the initiation of bulk failure [Svensson et al., 2013].

In addition to significant group dependent differences in mechanics, we found moderate to strong linear correlations between biochemical and mechanical properties. Specifically, AGE contents were moderately to strongly correlated with tissue mechanics. Additionally, we observed a strong linear correlation between linear-region modulus and failure stress. While previously unpublished for the AF, this has been a consistent finding in our work and has significant implications for understanding tissue failure mechanisms. In particular, it may suggest that the rate-dependent mechanical response of connective tissues serves a protective role against failure: failure stress increases proportionately with tissue stiffness, which both increase at higher loading rates associated with potentially traumatic impacts.

While AGE accumulation is known to occur with aging, diabetes, chronic kidney disease, and AGE-rich diets, there are conflicting reports regarding the impact of *in vivo* versus *in vitro* AGE accumulation on soft tissue mechanics. For example, two studies found that tendon stiffness decreased in rats with diabetes induced *in vivo* [de Oliveira et al., 2011; Fox et al., 2011], in contrast to most *in vitro* studies that observed increases in stiffness with AGE accumulation [Reddy et al., 2002; Verzijl et al., 2002; Reddy, 2004; Wagner et al., 2006; Li et al., 2013; Snedeker and Gautieri, 2014; Gautieri et al., 2017; Svensson et al., 2018]. One limitation of *in vitro* models is that exogenous AGE formation is uncoupled from normal tissue remodeling and adaptation, which may include processes that mitigate the effects of AGE formation [Fields et al., 2015; Dolor et al., 2019]. Additionally, it is possible that the specific AGE profile generated from incubation in methylglyoxal differs from that generated from glucose *in vivo*, which may contribute to the discrepancy between *in vivo* and *in vitro* alterations in mechanics with glycation.

While there is a clear clinical predisposition to soft-tissue injury in diabetics, it remains unclear how the changes reported here and elsewhere, namely increased stiffness, strength, and post-failure energy absorption capacity, might predispose diabetic discs to herniation. Despite similar observed alterations in mechanics with glycation, previous investigators have not been able to explain the apparent paradox between increased stiffness and strength without brittleness in lab-tested tissue and the clinical predisposition of diabetics to connective tissue injury. This may be due to increased stresses experienced by diabetic patients, altered disc loading conditions, or stress redistribution. It is also possible that the glycated tissue response is anisotropic, with decreases in failure properties in the radial or axial directions [Guerin and Elliott, 2007; O'Connell et al., 2009; Isaacs et al., 2014; Werbner et al., 2017; Andriotis et al., 2019].

Collagen contents were in the range of previous bovine AF data across treatment groups [Bezci et al., 2019]. 18 hours in 0.3M methylglyoxal at 25°C and 50°C were found to be sufficient for inducing distinct levels of AGEs that were comparable to the human AF tissues measured in this study. The AGE content of the bovine control in this study is likely lower than adult human AGE levels, highlighting the benefit of animal models to provide a wider range of biochemical parameters. Normalizing total fluorescence measurements by tissue dry weight helped promote a clear comparison between species with different amounts of collagen and proteoglycans [Showalter et al., 2012; Bezci et al., 2019]. Tissue water contents remained near or just above values reported for fresh tissue, which is a significant improvement from previous studies using 0.15 M saline [Isaacs et al., 2014; Bezci et al., 2019; Werbner et al., 2019; Bezci et al., 2020]. Our recent work determined the composition and concentration of buffer needed to minimize AF tissue

swelling and solute deposition during the treatment process (*i.e.,* 18-hour soak period) [Werbner et al., 2021]. This approach was largely successful in maintaining fresh tissue hydration levels, as the mean water content across all groups in this study was 76 ± 4%, which was only slightly higher than values for fresh bovine tissue reported by Bezci et al. 2019 (74 ± 5%). The slightly elevated water content in the MGO50 group (4% higher than control) is likely due to greater fluid diffusion into tissue at 50°C and not due to non-enzymatic crosslinking, as Jazini et al. (2012) noted a decrease in AF water content with increasing glycation.

Preserving fresh-tissue hydration conditions makes comparisons to previous studies more complicated, as they have largely used 0.15 M PBS as a buffer solution during testing. Previous studies showed that prolonged exposure of tissue samples to 0.15 M PBS significantly increases water content [Galante, 1967; Acaroglu et al., 1995; Ebara et al., 1996; Werbner et al., 2019; Bezci et al., 2020] and may lower modulus by over 80% [Han et al., 2012; Werbner et al., 2019; Werbner et al., 2021]. This in part explains why the modulus values reported here are significantly higher than many values reported for tissue-level AF specimens in the literature [Acaroglu et al., 1995; Ebara et al., 1996; Han et al., 2012; Werbner et al., 2019]. Additionally, the notch geometry employed in this study reduced specimen cross-sectional area beyond those typically applied, which may also have resulted in higher apparent modulus values [Adams and Green 1993; Werbner et al., 2017]. An additional limitation of this study is that only circumferential-axially oriented specimens were tested to maximize the contribution of collagen fibers (the constituent targeted by the applied disease-model) to the mechanical response.

This study sought to determine the relationship between AF advanced glycation end-product content and pre-failure, failure, and post-failure tensile mechanics at the tissue-level at two distinct loading rates. This was accomplished using an *in vitro* glycation treatment that induced two distinct, physiological AGE levels while maintaining hydration levels comparable to fresh tissue. We observed an increase in modulus, strength, and post-failure energy absorption capacity with increasing levels of glycation at both loading rates. AGE contents from a cross-sectional population of human cadaver discs were also presented. Results from this study may be used in development of advanced computational models that aim to study disc disease progression and to provide a deeper understanding of altered structure-function relationships that may lead to tissue dysfunction and failure.

7. Limitations, future directions, and concluding remarks

7.1 Limitations of in vitro, tissue-level testing

Despite the advantages enumerated in *Chapter 1*, *in vitro* tissue-level testing is accompanied by significant limitations, including reliability and translatability. While the aim of tissue-level testing is not necessarily to mimic *in vivo* failure modes, but rather to independently characterize the material-level tissue mechanical response, the boundary conditions of *in vitro* testing will always pose a challenge to physiological translatability. Regardless of the level of rigor applied to establish a robust testing framework of consistent and physiologically relevant conditions, *in vitro* boundary conditions are expected to significantly impact the measurement and interpretation of mechanical and rheological testing results. Such boundary conditions include the residual mechanical stresses and fluid pressures generated from the removal of anatomical constraints, such as the vertebral bodies and endplates during dissections, as well as from the removal of tissue-level AF specimens from the constraining structure of the intact disc [Huyghe and Jongeneelen, 2012]. Additional considerations of boundary conditions include the choice of

specimen orientation, gripping method, and loading conditions (temperature, hydration environment, loading rate, *etc.*).

These effects are evident during the preparation of AF specimens of different orientations (*e.g.*, circumferential-radial vs circumferential-axial). Circumferential-radial specimens contain more GAG- and water-rich inner AF material compared to circumferential-axial specimens; circumferential-radial specimens also contain minimal continuous fiber populations compared to circumferential-axial specimens. Thus, despite preparing specimens of identical geometry in these two orientations, the residual mechanical stresses and fluid pressures are expected to vary, which will impact specimen composition, swelling, hydration, and mechanical testing results beyond the structural anisotropy being directly investigated by comparing these orientations. Given the significant compositional, structural, mechanical, and rheological anisotropy of the disc, numerous such boundary conditions are expected to impact the measured tissue mechanical response, making it difficult to compare and interpret mechanical testing results across studies, and in the context of the anticipated tissue response *in vivo*. The current work has sought to develop and validate methods to minimize the effects of varying boundary conditions, and yet to maintain an interpretation of the results that considers such effects.

7.2 Future directions for in vitro, tissue-level testing

7.2.1 Standardized testing protocols

Many of the significant advances in AF tissue-level experimental testing were facilitated by newly developed or translated methods, while other advances arose from progressive development of existing techniques. Experimental design over the last several decades has produced a variety of robust and repeatable methods yielding more complete and reliable datasets, yet little has been done to develop a consensus across the field regarding standardizing testing procedures. Numerous factors suggest the benefit of developing and implementing standardized protocols for tissue-level mechanical and rheological testing. Standardizing test protocols that minimize variations due to experimental boundary conditions will yield more translatable, higher-impact studies, and more cohesive datasets. This is precisely the basis for numerous organizations working to standardize testing protocols for traditional engineering materials, such as the American Society for Testing and Materials or the International Organization for Standardization. Given that the effect of experimental conditions can be large for biological tissues when compared to traditional engineering materials, this is a particularly salient issue for the field, and thus a concerted effort toward the standardization of mechanical testing protocols for fiber-reinforced biological tissues would be of great benefit.

7.2.2 Maintenance of physiological hydration levels

Water content has a significant effect on tissue mechanics across length scales, and thus precise control of tissue hydration levels is essential for ensuring accurate, repeatable, and physiologically relevant measurements of tissue mechanics and biochemical composition. This should motivate the development of robust methods to maintain physiological hydration levels based on specific *in vitro* boundary conditions for a given experiment. *Chapter 5* extended such a method for tissue-level bovine AF specimens that had been previously developed for the maintenance of tendon hydration levels *in vitro*. The accumulating body of literature on *in vitro* connective tissue testing suggests that ‘physiological saline’ should not be used to maintain tissue-level specimen hydration during preparation, treatment, or testing if physiological relevance is to be considered regarding hydration and mechanics. Instead, a solution generating sufficient osmotic

pressure to maintain physiological hydration levels in tissue-level specimens should be used. While a 6.25%w/v PBS + 6.25%w/v PEG solution proved effective for healthy bovine AF tissues commonly used in the field, inter-species differences and tissue health status are known to influence swelling and mechanical behavior; thus, future studies should seek to determine optimal solution compositions to maintain hydration levels and mechanics in the specific tissues being studied. As the field develops a deeper understanding of the central role of tissue hydration in maintaining proper mechanical and biological function, it is essential for future studies investigating the relationship between tissue hydration, aging, injury, and disease to prepare, treat, and test tissues in solutions that allow precise control of hydration levels, facilitating more robust translation to *in vivo* tissue behavior.

7.2.3 Anisotropy and loading-rate considerations

Within each chapter of this dissertation, only one specimen orientation was tested when investigating each biochemical constituent contribution to the tissue mechanical response. For example, the effect of proteoglycan degradation described in *Chapter 3* was studied only in the circumferential-radial orientation to elucidate the effect on the GAG-rich matrix, which dominates the mechanical response in that orientation. In contrast, *Chapter 6* investigated alterations in tissue mechanics in the circumferential-axial orientation after non-enzymatic collagen crosslinking to emphasize the contribution of the collagen fiber populations that dominate in that orientation. While these choices were made to maximize the effect size for each study, providing a first-order structure-function relationship for each targeted constituent, tissue responses are known to be highly anisotropic, and it remains important to characterize the tissue response in other orientations than those described above.

Additionally, the two loading rates applied in the current work were selected to be within the range of physiological loading conditions and to highlight relative differences, where quasi-static loading is believed to minimize viscoelastic contributions from the tissue solid while facilitating fluid flow, while higher rate loading restricts fluid flow and emphasizes solid-component viscoelasticity. However, these two disparate and isolated rates are not sufficient to characterize the tissue response across the range of all loading rates. Particularly as the results of *Chapter 3* indicate a differential degenerate tissue response between quasi-static and dynamic loading rates, it remains important to quantify the tissue response at rates between these two to deepen our understanding of the mechanisms underlying this loading-rate dependent transition in tissue failure behavior.

7.3 Concluding remarks

This dissertation work explored the relationship between age- and disease-mediated biochemical changes and annulus fibrosus tensile failure mechanics. This was achieved by applying simplified but physiologically relevant model systems to isolate the material-level contribution of specific degenerative changes to tissue failure *in vitro*. Quantitative relationships were established between annulus fibrosus proteoglycan, water, and collagen crosslink content and the sub-failure, failure, and post-failure tensile mechanical response of tissue-level specimens across a range of specimen orientations and loading rates. In pursuit of these aims, novel methods for targeting and maintaining tissue hydration, mechanics, and composition *in vitro* were developed, validated, and implemented alongside a novel method for repeatable failure testing of tissue-level annulus fibrosus specimens. In addition to contributing these robust and translatable

methods for *in vitro* tissue testing, this work provided novel insights regarding the structure-function relations that drive soft-tissue failure in the spine.

8. References

Acaroglu ER, Latridis JC, Setton LA, Foster RJ, Mow VC, Weidenbaum M. Degeneration and aging affect the tensile behavior of human lumbar anulus fibrosus. Spine. 1995 Dec 15;20(24):2690-701.

Acevedo C, Sylvia M, Schaible E, Graham JL, Stanhope KL, Metz LN, Gludovatz B, Schwartz AV, Ritchie RO, Alliston TN, Havel PJ. Contributions of material properties and structure to increased bone fragility for a given bone mass in the UCD-T2DM rat model of type 2 diabetes. Journal of bone and mineral research. 2018 Jun;33(6):1066-75.

Adams MA, Bogduk N, Burton K, Dolan P. The Biomechanics of Back Pain-E-Book. Elsevier health sciences; 2012 Nov 19.

Adams MA, Dolan P, Hutton WC, Porter RW. Diurnal changes in spinal mechanics and their clinical significance. The Journal of bone and joint surgery. British volume. 1990 Mar;72(2):266-70.

Adams MA, Dolan P, Hutton WC. Diurnal variations in the stresses on the lumbar spine. Spine. 1987 Mar 1;12(2):130-7.

Adams MA, Hutton WC. Prolapsed intervertebral disc: a hyperflexion injury. Spine. 1982 May 1;7(3):184-91.

Adams MA, Lama P, Zehra U, Dolan P. Why do some intervertebral discs degenerate, when others (in the same spine) do not?. Clinical anatomy. 2015 Mar;28(2):195-204.

Adams MA, McNally DS, Dolan P. 'Stress distributions inside intervertebral discs: the effects of age and degeneration. The Journal of bone and joint surgery. British volume. 1996 Nov;78(6):965-72.

Adams MA, Roughley PJ. What is intervertebral disc degeneration, and what causes it?. Spine. 2006 Aug 15;31(18):2151-61.

Ahmed N. Advanced glycation endproducts—role in pathology of diabetic complications. Diabetes research and clinical practice. 2005 Jan 1;67(1):3-21.

Aladin DM, Cheung KM, Ngan AH, Chan D, Leung VY, Lim CT, Luk KD, Lu WW. Nanostructure of collagen fibrils in human nucleus pulposus and its correlation with macroscale tissue mechanics. Journal of Orthopaedic Research. 2010 Apr;28(4):497-502.

Allen MR, Newman CL, Chen N, Granke M, Nyman JS, Moe SM. Changes in skeletal collagen cross-links and matrix hydration in high-and low-turnover chronic kidney disease. Osteoporosis International. 2015 Mar;26(3):977-85.

Antoniou J, Steffen T, Nelson F, Winterbottom N, Hollander AP, Poole RA, Aebi M, Alini M. The human lumbar intervertebral disc: evidence for changes in the biosynthesis and denaturation of the extracellular matrix with growth, maturation, ageing, and degeneration. The Journal of clinical investigation. 1996 Aug 15;98(4):996-1003.

ASTM, 2003, "Standard Test Method for Tensile Properties of Plastics," ASTM International, West Conshohocken, PA, Standard No. ASTM D638-14.

ASTM, 2004, "Standard Test Methods for Tension Testing of Metallic Materials," ASTM, West Conshohocken, PA, Standard No. ASTM E8/E8M-13.

Bálint G, Than P, Domán I, Wiegand N, Horváth G, Lőrinczy D. Calorimetric examination of the human meniscus. Journal of thermal analysis and calorimetry. 2009 Mar;95(3):759-61.

Bartel DL, Davy DT. Orthopaedic biomechanics: mechanics and design in musculoskeletal systems. Prentice Hall; 2006.

Beadle OA. The intervertebral disc: observations on their normal and morbid anatomy in relation to certain spinal deformities. Med Res Counc Spec Rep Ser. 1931;161:7-7.

Beckstein JC, Sen S, Schaer TP, Vresilovic EJ, Elliott DM. Comparison of animal discs used in disc research to human lumbar disc: axial compression mechanics and glycosaminoglycan content. Spine. 2008 Mar 15;33(6):E166-73.

Belavy DL, Adams M, Brisby H, Cagnie B, Danneels L, Fairbank J, Hargens AR, Judex S, Scheuring RA, Sovelius R, Urban J. Disc herniations in astronauts: What causes them, and what does it tell us about herniation on earth?. European Spine Journal. 2016 Jan 1;25(1):144-54.

Berger-Roscher N, Casaroli G, Rasche V, Villa T, Galbusera F, Wilke HJ. Influence of complex loading conditions on intervertebral disc failure. Spine. 2017 Jan 15;42(2):E78-85.

Bezci SE, Nandy A, O'Connell GD. Effect of hydration on healthy intervertebral disk mechanical stiffness. Journal of biomechanical engineering. 2015 Oct 1;137(10).

Bezci SE, O'Connell GD. Osmotic pressure alters time-dependent recovery behavior of the intervertebral disc. Spine. 2018 Mar 15;43(6):E334-40.

Bezci SE, Torres K, Carraro C, Chiavacci D, Werbner B, Lim S, O'Connell GD. Transient swelling behavior of the bovine caudal disc. Journal of the Mechanical Behavior of Biomedical Materials. 2020 Dec 1;112:104089.

Bezci SE, Werbner B, Zhou M, Malollari KG, Dorlhiac G, Carraro C, Streets A, O'Connell GD. Radial variation in biochemical composition of the bovine caudal intervertebral disc. JOR spine. 2019 Sep;2(3):e1065.

Bloom ET, Lee AH, Elliott DM. Tendon Multiscale Structure, Mechanics, and Damage Are Affected by Osmolarity of Bath Solution. Annals of Biomedical Engineering. 2021 Mar;49(3):1058-68.

Boos N, Nerlich AG, Wiest I, von der Mark K, Aebi M. Immunolocalization of type X collagen in human lumbar intervertebral discs during ageing and degeneration. Histochemistry and cell biology. 1997 Dec 1;108(6):471-80.

Boos N, Weissbach S, Rohrbach H, Weiler C, Spratt KF, Nerlich AG. Classification of age-related changes in lumbar intervertebral discs: 2002 Volvo Award in basic science. Spine. 2002 Dec 1;27(23):2631-44.

Brown T, Hansen RJ, Yorra AJ. Some mechanical tests on the lumbosacral spine with particular reference to the intervertebral discs: a preliminary report. JBJS. 1957 Oct 1;39(5):1135-64.

Buckwalter JA. Aging and degeneration of the human intervertebral disc. Spine. 1995 Jun 1;20(11):1307-14.

Buehler MJ, Wong SY. Entropic elasticity controls nanomechanics of single tropocollagen molecules. Biophysical journal. 2007 Jul 1;93(1):37-43.

Buirski G. Magnetic resonance signal patterns of lumbar discs in patients with low back pain. A prospective study with discographic correlation. Spine. 1992 Oct 1;17(10):1199-204.

Cassidy JJ, Hiltner A, Baer E. Hierarchical structure of the intervertebral disc. Connective tissue research. 1989 Jan 1;23(1):75-88.

Centers for Disease Control and Prevention. National diabetes statistics report, 2020. Atlanta, GA: Centers for Disease Control and Prevention, US Department of Health and Human Services. 2020 Sep 21:12-5.

Chae Y, Protsenko D, Lavernia E, Wong B. Effect of water content on enthalpic relaxations in porcine septal cartilage. Journal of thermal analysis and calorimetry. 2009 Mar 1;95(3):937-43.

Cheng BC, Welch WC. Initial Observations in the Validation of a Hybrid Test Protocol for Motion Preservation Devices on a Biomechanical Spine Tester. InSummer Bioengineering Conference 2008 Jun 25 (Vol. 43215, pp. 107-108). American Society of Mechanical Engineers.

Costi JJ, Hearn TC, Fazzalari NL. The effect of hydration on the stiffness of intervertebral discs in an ovine model. Clinical biomechanics. 2002 Jul 1;17(6):446-55.

Costi JJ, Ledet EH, O'Connell GD. Spine biomechanical testing methodologies: The controversy of consensus vs scientific evidence. JOR spine. 2021 Mar;4(1):e1138.

Davey KJ, Skegg DC. The effects of high concentrations of an electrolyte on the swelling of non-metabolizing tissue slices. The Journal of physiology. 1971 Feb 1;212(3):641-53.

de Oliveira RR, de Lira KD, de Castro Silveira PV, Coutinho MP, Medeiros MN, Teixeira MF, de Moraes SR. Mechanical properties of achilles tendon in rats induced to experimental diabetes. Annals of biomedical engineering. 2011 May;39(5):1528-34.

Demers CN, Antoniou J, Mwale F. Value and limitations of using the bovine tail as a model for the human lumbar spine. Spine. 2004 Dec 15;29(24):2793-9.

Dolor A, Sampson SL, Lazar AA, Lotz JC, Szoka FC, Fields AJ. Matrix modification for enhancing the transport properties of the human cartilage endplate to improve disc nutrition. PloS one. 2019 Apr 10;14(4):e0215218.

Domán I, Illés T. Thermal analysis of the human intervertebral disc. Journal of biochemical and biophysical methods. 2004 Oct 29;61(1-2):207-14.

Ebara S, Iatridis JC, Setton LA, Foster RJ, Mow VC, Weidenbaum M. Tensile properties of nondegenerate human lumbar anulus fibrosus. Spine. 1996 Feb 15;21(4):452-61.

Elliott DM, Robinson PS, Gimbel JA, Sarver JJ, Abboud JA, Iozzo RV, Soslowsky LJ. Effect of altered matrix proteins on quasilinear viscoelastic properties in transgenic mouse tail tendons. Annals of biomedical engineering. 2003 May;31(5):599-605.

Elliott DM, Setton LA. Anisotropic and inhomogeneous tensile behavior of the human anulus fibrosus: experimental measurement and material model predictions. Journal of biomechanical engineering. 2001 Jun 1;123(3):256-63.

Farndale RW, Sayers CA, Barrett AJ. A direct spectrophotometric microassay for sulfated glycosaminoglycans in cartilage cultures. Connective tissue research. 1982 Jan 1;9(4):247-8.

Fields AJ, Berg-Johansen B, Metz LN, Miller S, La B, Liebenberg EC, Coughlin DG, Graham JL, Stanhope KL, Havel PJ, Lotz JC. Alterations in intervertebral disc composition, matrix homeostasis and biomechanical behavior in the UCD-T2DM rat model of type 2 diabetes. Journal of Orthopaedic Research. 2015 May;33(5):738-46.

Fox AJ, Bedi A, Deng XH, Ying L, Harris PE, Warren RF, Rodeo SA. Diabetes mellitus alters the mechanical properties of the native tendon in an experimental rat model. Journal of Orthopaedic Research. 2011 Jun;29(6):880-5.

Freedman MK, Hilibrand AS, Blood EA, Zhao W, Albert TJ, Vacarro A, Oleson CV, Morgan TS, Weinstein JN. The impact of diabetes on the outcomes of surgical and nonsurgical

treatment of patients in the spine patient outcomes research trial. Spine. 2011 Feb 15;36(4):290.

Galante JO. Tensile properties of the human lumbar annulus fibrosus. Acta Orthopaedica Scandinavica. 1967 May 1;38(sup100):1-91.

Gautieri A, Passini FS, Silván U, Guizar-Sicairos M, Carimati G, Volpi P, Moretti M, Schoenhuber H, Redaelli A, Berli M, Snedeker JG. Advanced glycation end-products: Mechanics of aged collagen from molecule to tissue. Matrix Biology. 2017 May 1;59:95-108.

Göcke C. Das verhalten der Bandscheiben bei Wirbelverletzungen. Archiv für orthopädische und Unfall-Chirurgie, mit besonderer Berücksichtigung der Frakturenlehre und der orthopädisch-chirurgischen Technik. 1932 Dec;31(1):42-80.

Goel VK, Monroe BT, Gilbertson LG, Brinckmann P. Interlaminar shear stresses and laminae separation in a disc: finite element analysis of the L3-L4 motion segment subjected to axial compressive loads. Spine. 1995 Mar 15;20(6):689-98.

Green TP, Adams MA, Dolan P. Tensile properties of the annulus fibrosus. European Spine Journal. 1993 Dec;2(4):209-14.

Gregory DE, Callaghan JP. An examination of the influence of strain rate on subfailure mechanical properties of the annulus fibrosus. Journal of biomechanical engineering. 2010 Sep 1;132(9).

Grunhagen T, Wilde G, Soukane DM, Shirazi-Adl SA, Urban JP. Nutrient supply and intervertebral disc metabolism. JBJS. 2006 Apr 1;88(suppl_2):30-5.

Gu WY, Mao XG, Foster RJ, Weidenbaum M, Mow VC, Rawlins BA. The anisotropic hydraulic permeability of human lumbar anulus fibrosus: influence of age, degeneration, direction, and water content. Spine. 1999 Dec 1;24(23):2449.

Guerin HL, Elliott DM. Quantifying the contributions of structure to annulus fibrosus mechanical function using a nonlinear, anisotropic, hyperelastic model. Journal of orthopaedic research. 2007 Apr;25(4):508-16.

Han WM, Nerurkar NL, Smith LJ, Jacobs NT, Mauck RL, Elliott DM. Multi-scale structural and tensile mechanical response of annulus fibrosus to osmotic loading. Annals of biomedical engineering. 2012 Jul;40(7):1610-21.

Hart LG, Deyo RA, Cherkin DC. Physician office visits for low back pain. Frequency, clinical evaluation, and treatment patterns from a US national survey. Spine. 1995 Jan 1;20(1):11-9.

Haut RC. Age-dependent influence of strain rate on the tensile failure of rat-tail tendon.

Hicks GE, Morone N, Weiner DK. Degenerative lumbar disc and facet disease in older adults: prevalence and clinical correlates. Spine. 2009 May 20;34(12):1301.

Hollander AP, Heathfield TF, Webber C, Iwata Y, Bourne R, Rorabeck C, Poole AR. Increased damage to type II collagen in osteoarthritic articular cartilage detected by a new immunoassay. The Journal of clinical investigation. 1994 Apr 1;93(4):1722-32.

Holzapfel GA, Schulze-Bauer CA, Feigl G, Regitnig P. Single lamellar mechanics of the human lumbar anulus fibrosus. Biomechanics and modeling in mechanobiology. 2005 Mar;3(3):125-40.

Hoy RC, D'Erminio DN, Krishnamoorthy D, Natelson DM, Laudier DM, Illien-Jünger S, Iatridis JC. Advanced glycation end products cause RAGE-dependent annulus fibrosus collagen disruption and loss identified using in situ second harmonic generation imaging in mice intervertebral disk in vivo and in organ culture models. JOR spine. 2020 Dec;3(4):e1126.

Huyghe JM, Jongeneelen CJ. 3D non-affine finite strains measured in isolated bovine annulus fibrosus tissue samples. Biomechanics and modeling in mechanobiology. 2012 Jan;11(1):161-70.

Iatridis JC, MacLean JJ, O'Brien M, Stokes IA. Measurements of proteoglycan and water content distribution in human lumbar intervertebral discs. Spine. 2007 Jun 15;32(14):1493.

Iatridis JC, MacLean JJ, Ryan DA. Mechanical damage to the intervertebral disc annulus fibrosus subjected to tensile loading. Journal of biomechanics. 2005 Mar 1;38(3):557-65.

Iatridis JC, Nicoll SB, Michalek AJ, Walter BA, Gupta MS. Role of biomechanics in intervertebral disc degeneration and regenerative therapies: what needs repairing in the disc and what are promising biomaterials for its repair?. The spine journal. 2013 Mar 1;13(3):243-62.

Illien-Jünger S, Lu Y, Qureshi SA, Hecht AC, Cai W, Vlassara H, Striker GE, Iatridis JC. Chronic ingestion of advanced glycation end products induces degenerative spinal changes and hypertrophy in aging pre-diabetic mice. PLoS One. 2015 Feb 10;10(2):e0116625.

Illien-Jünger S, Torre OM, Kindschuh WF, Chen X, Laudier DM, Iatridis JC. AGEs induce ectopic endochondral ossification in intervertebral discs. European cells & materials. 2016 Nov 18;32:257.

Isaacs JL, Vresilovic E, Sarkar S, Marcolongo M. Role of biomolecules on annulus fibrosus micromechanics: Effect of enzymatic digestion on elastic and failure properties. Journal of the mechanical behavior of biomedical materials. 2014 Dec 1;40:75-84.

Jacobs JV, Henry SM, Jones SL, Hitt JR, Bunn JY. A history of low back pain associates with altered electromyographic activation patterns in response to perturbations of standing balance. Journal of neurophysiology. 2011 Nov;106(5):2506-14.

Jacobs NT, Cortes DH, Vresilovic EJ, Elliott DM. Biaxial tension of fibrous tissue: using finite element methods to address experimental challenges arising from boundary conditions and anisotropy. Journal of biomechanical engineering. 2013 Feb 1;135(2).

Jazini E, Sharan AD, Morse LJ, Dyke JP, Aronowitz EA, Chen LK, Tang SY. Alterations in magnetic resonance imaging T2 relaxation times of the ovine intervertebral disc due to non-enzymatic glycation. Spine. 2012 Feb 15;37(4):E209.

Jhawar BS, Fuchs CS, Colditz GA, Stampfer MJ. Cardiovascular risk factors for physician-diagnosed lumbar disc herniation. The spine journal. 2006 Nov 1;6(6):684-91.

Katz EP, Li ST. The intermolecular space of reconstituted collagen fibrils. Journal of molecular biology. 1973 Jan 19;73(3):351-69.

Katz JN. Lumbar disc disorders and low-back pain: socioeconomic factors and consequences. JBJS. 2006 Apr 1;88(suppl_2):21-4.

Kiani C, Liwen CH, Wu YJ, Albert JY, Burton BY. Structure and function of aggrecan. Cell research. 2002 Mar;12(1):19-32.

Kolz CW, Suter T, Henninger HB. Regional mechanical properties of the long head of the biceps tendon. Clinical Biomechanics. 2015 Nov 1;30(9):940-5.

Krishnamoorthy D, Hoy RC, Natelson DM, Torre OM, Laudier DM, Iatridis JC, Illien-Jünger S. Dietary advanced glycation end-product consumption leads to mechanical stiffening of murine intervertebral discs. Disease models & mechanisms. 2018 Dec 1;11(12):dmm036012.

Lechner K, Hull ML, Howell SM. Is the circumferential tensile modulus within a human medial meniscus affected by the test sample location and cross-sectional area?. Journal of orthopaedic research. 2000 Nov;18(6):945-51.

Li Y, Fessel G, Georgiadis M, Snedeker JG. Advanced glycation end-products diminish tendon collagen fiber sliding. Matrix Biology. 2013 Apr 24;32(3-4):169-77.

Licciardone JC, Kearns CM, Minotti DE. Outcomes of osteopathic manual treatment for chronic low back pain according to baseline pain severity: results from the OSTEOPATHIC Trial. Manual therapy. 2013 Dec 1;18(6):533-40.

Lujan TJ, Underwood CJ, Jacobs NT, Weiss JA. Contribution of glycosaminoglycans to viscoelastic tensile behavior of human ligament. Journal of applied physiology. 2009 Feb;106(2):423-31.

Luoma K, Riihimäki H, Luukkonen R, Raininko R, Viikari-Juntura E, Lamminen A. Low back pain in relation to lumbar disc degeneration. Spine. 2000 Feb 15;25(4):487-92.

Lyons G, Eisenstein SM, Sweet MB. Biochemical changes in intervertebral disc degeneration. Biochimica et Biophysica Acta (BBA)-General Subjects. 1981 Jan 1;673:443-53.

Maniadakis N, Gray A. The economic burden of back pain in the UK. Pain. 2000 Jan 1;84(1):95-103.

Mäntyselkä P, Miettola J, Niskanen L, Kumpusalo E. Chronic pain, impaired glucose tolerance and diabetes: a community-based study. PAIN®. 2008 Jun 30;137(1):34-40.

Marchand F, Ahmed AM. Investigation of the laminate structure of lumbar disc anulus fibrosus. Spine. 1990 May 1;15(5):402-10.

Maroudas A, Stockwell RA, Nachemson A, Urban J. Factors involved in the nutrition of the human lumbar intervertebral disc: cellularity and diffusion of glucose in vitro. Journal of anatomy. 1975 Sep;120(Pt 1):113.

Maroudas A, Ziv I, Weisman N, Venn M. Studies of hydration and swelling pressure in normal and osteoarthritic cartilage. Biorheology. 1985 Jan 1;22(2):159-69.

Melrose J. Cartilage and smooth muscle cell proteoglycans detected by affinity blotting using biotinylated hyaluronan. InProteoglycan Protocols 2001 (pp. 53-66). Humana Press.

Monnier VM, Sell DR, Genuth SA. Glycation products as markers and predictors of the progression of diabetic complications. ANNALS-NEW YORK ACADEMY OF SCIENCES. 2005 Jun 1;1043:567.

Morales-Orcajo E, de Bengoa Vallejo RB, Iglesias ML, Bayod J. Structural and material properties of human foot tendons. Clinical Biomechanics. 2016 Aug 1;37:1-6.

Mow VC, Holmes MH, Lai WM. Fluid transport and mechanical properties of articular cartilage: a review. Journal of biomechanics. 1984 Jan 1;17(5):377-94.

Nachemson AL. Disc pressure measurements. Spine. 1981 Jan 1;6(1):93-7.

Noyes FR, DeLucas JL, Torvik PJ. Biomechanics of Anterior Cruciate Ligament Failure: An Analysis of. J. Bone Joint Surg. Am. 1974;56:236-53.

O'Connell GD, Leach JK, Klineberg EO. Tissue engineering a biological repair strategy for lumbar disc herniation. BioResearch open access. 2015 Nov 1;4(1):431-45.

O'Connell GD, Guerin HL, Elliott DM. Theoretical and uniaxial experimental evaluation of human annulus fibrosus degeneration.

O'Connell GD, Vresilovic EJ, Elliott DM. Comparison of animals used in disc research to human lumbar disc geometry. Spine. 2007 Feb 1;32(3):328-33.

Osti OL, Vernon-Roberts B, Moore R, Fraser RD. Annular tears and disc degeneration in the lumbar spine. A post-mortem study of 135 discs. The Journal of bone and joint surgery. British volume. 1992 Sep;74(5):678-82.

Panjabi MM. Physical properties and functional biomechanics of the spine. Clinical Biomechnics of the Spine. 1990:1-84.

Paul Buckley C, Samuel Salisbury ST, Zavatsky AB. Viscoelasticity of tendons under transverse compression. Journal of Biomechanical Engineering. 2016 Oct 1;138(10).

Peloquin JM, Santare MH, Elliott DM. Advances in quantification of meniscus tensile mechanics including nonlinearity, yield, and failure. Journal of biomechanical engineering. 2016 Feb 1;138(2):021002.

Périé D, Korda D, Iatridis JC. Confined compression experiments on bovine nucleus pulposus and annulus fibrosus: sensitivity of the experiment in the determination of compressive modulus and hydraulic permeability. Journal of biomechanics. 2005 Nov 1;38(11):2164-71.

Perie DS, Maclean JJ, Owen JP, Iatridis JC. Correlating material properties with tissue composition in enzymatically digested bovine annulus fibrosus and nucleus pulposus tissue. Annals of biomedical engineering. 2006 May;34(5):769-77.

Pezowicz CA, Robertson PA, Broom ND. Intralamellar relationships within the collagenous architecture of the annulus fibrosus imaged in its fully hydrated state. Journal of anatomy. 2005 Oct;207(4):299-312.

Pezowicz CA, Robertson PA, Broom ND. The structural basis of interlamellar cohesion in the intervertebral disc wall. Journal of anatomy. 2006 Mar;208(3):317-30.

Pfirrmann CW, Metzdorf A, Zanetti M, Hodler J, Boos N. Magnetic resonance classification of lumbar intervertebral disc degeneration. Spine. 2001 Sep 1;26(17):1873-8.

Pflaster DS, Krag MH, Johnson CC, Haugh LD, Pope MH. Effect of test environment on intervertebral disc hydration. Spine. 1997 Jan 15;22(2):133-9.

Pokharna HK, Phillips FM. Collagen crosslinks in human lumbar intervertebral disc aging. Spine. 1998 Aug 1;23(15):1645-8.

Reddy GK, Stehno-Bittel L, Enwemeka CS. Glycation-induced matrix stability in the rabbit achilles tendon. Archives of biochemistry and biophysics. 2002 Mar 15;399(2):174-80.

Reddy GK. Cross-linking in collagen by nonenzymatic glycation increases the matrix stiffness in rabbit achilles tendon. Experimental diabesity research. 2004 Apr 1;5(2):143-53.

Roberts S, Menage J, Urban JP. Biochemical and structural properties of the cartilage end-plate and its relation to the intervertebral disc. Spine. 1989 Feb 1;14(2):166-74.

Robinson JR. Control of water content of respiring kidney slices by sodium chloride and polyethylene glycol. The Journal of physiology. 1978 Sep 1;282(1):285-94.

Roeder BA, Kokini K, Sturgis JE, Robinson JP, Voytik-Harbin SL. Tensile mechanical properties of three-dimensional type I collagen extracellular matrices with varied microstructure. Journal of biomechanical engineering. 2002 Apr 1;124(2):214-22.

Roughley PJ, Alini M, Antoniou J. The role of proteoglycans in aging, degeneration and repair of the intervertebral disc. Biochemical Society Transactions. 2002 Nov;30(6):869-74.

Safa BN, Meadows KD, Szczesny SE, Elliott DM. Exposure to buffer solution alters tendon hydration and mechanics. Journal of biomechanics. 2017 Aug 16;61:18-25.

Samouillan V, Delaunay F, Dandurand J, Merbahi N, Gardou JP, Yousfi M, Gandaglia A, Spina M, Lacabanne C. The use of thermal techniques for the characterization and selection of natural biomaterials. Journal of functional biomaterials. 2011 Sep;2(3):230-48.

Schiller LR, Emmett M, Santa Ana CA, Fordtran JS. Osmotic effects of polyethylene glycol. Gastroenterology. 1988 Apr 1;94(4):933-41.

Schmidt H, Schilling C, Reyna AL, Shirazi-Adl A, Dreischarf M. Fluid-flow dependent response of intervertebral discs under cyclic loading: on the role of specimen preparation and preconditioning. Journal of biomechanics. 2016 Apr 11;49(6):846-56.

Schroeder Y, Sivan S, Wilson W, Merkher Y, Huyghe JM, Maroudas A, Baaijens FP. Are disc pressure, stress, and osmolarity affected by intra-and extrafibrillar fluid exchange?. Journal of Orthopaedic Research. 2007 Oct;25(10):1317-24.

Screen HR, Chhaya VH, Greenwald SE, Bader DL, Lee DA, Shelton JC. The influence of swelling and matrix degradation on the microstructural integrity of tendon. Acta biomaterialia. 2006 Sep 1;2(5):505-13.

Screen HR, Shelton JC, Chhaya VH, Kayser MV, Bader DL, Lee DA. The influence of noncollagenous matrix components on the micromechanical environment of tendon fascicles. Annals of biomedical engineering. 2005 Aug;33(8):1090-9.

Showalter BL, Beckstein JC, Martin JT, Beattie EE, Orías AA, Schaer TP, Vresilovic EJ, Elliott DM. Comparison of animal discs used in disc research to human lumbar disc: torsion mechanics and collagen content. Spine. 2012 Jul 1;37(15):E900.

Singh RB, Barden A, Mori T, Beilin L. Advanced glycation end-products: a review. Diabetologia. 2001 Feb;44(2):129-46.

Sivan SS, Tsitron E, Wachtel E, Roughley P, Sakkee N, Van Der Ham F, Degroot J, Maroudas A. Age-related accumulation of pentosidine in aggrecan and collagen from normal and degenerate human intervertebral discs. Biochemical Journal. 2006 Oct 1;399(1):29-35.

Skaggs DL, Weidenbaum M, Iatridis JC, Ratcliffe A, Mow VC. Regional variation in tensile properties and biochemical composition of the human lumbar anulus fibrosus. Spine. 1994 Jun 1;19(12):1310-9.

Snedeker JG, Gautieri A. The role of collagen crosslinks in ageing and diabetes-the good, the bad, and the ugly. Muscles, ligaments and tendons journal. 2014 Jul;4(3):303.

Stegemann H, Stalder K. Determination of hydroxyproline. Clinica chimica acta. 1967 Nov 1;18(2):267-73.

Svensson RB, Mulder H, Kovanen V, Magnusson SP. Fracture mechanics of collagen fibrils: influence of natural cross-links. Biophysical journal. 2013 Jun 4;104(11):2476-84.

Svensson RB, Smith ST, Moyer PJ, Magnusson SP. Effects of maturation and advanced glycation on tensile mechanics of collagen fibrils from rat tail and Achilles tendons. Acta biomaterialia. 2018 Apr 1;70:270-80.

Sverdlik A, Lanir Y. Time-dependent mechanical behavior of sheep digital tendons, including the effects of preconditioning. Journal of biomechanical engineering. 2002 Feb 1;124(1):78-84.

Takahashi S, Suzuki A, Toyoda H, Terai H, Dohzono S, Yamada K, Matsumoto T, Yasuda H, Tsukiyama K, Shinohara Y, Ibrahim M. Characteristics of diabetes associated with poor improvements in clinical outcomes after lumbar spine surgery. Spine. 2013 Mar 15;38(6):516-22.

Tavakoli J, Amin DB, Freeman BJ, Costi JJ. The biomechanics of the inter-lamellar matrix and the lamellae during progression to lumbar disc herniation: which is the weakest structure?. Annals of biomedical engineering. 2018 Sep;46(9):1280-91.

Taylor D, O'Mara N, Ryan E, Takaza M, Simms C. The fracture toughness of soft tissues. Journal of the mechanical behavior of biomedical materials. 2012 Feb 1;6:139-47.

Thorpe CT, Screen HR. Tendon structure and composition. Metabolic influences on risk for tendon disorders. 2016:3-10.

Tsai TT, Ho NY, Lin YT, Lai PL, Fu TS, Niu CC, Chen LH, Chen WJ, Pang JH. Advanced glycation end products in degenerative nucleus pulposus with diabetes. Journal of Orthopaedic Research. 2014 Feb;32(2):238-44.

Urban JP, Maroudas A. Swelling of the intervertebral disc in vitro. Connective tissue research. 1981 Jan 1;9(1):1-0.

Urban JP, Maroudas A. The measurement of fixed charged density in the intervertebral disc. Biochimica et Biophysica Acta (BBA)-General Subjects. 1979 Aug 6;586(1):166-78.

Urban JP, McMullin JF. Swelling pressure of the lumbar intervertebral discs: influence of age, spinal level, composition, and degeneration. Spine. 1988 Feb 1;13(2):179-87.

Urban JP, Roberts S. Degeneration of the intervertebral disc. Arthritis Res Ther. 2003 Jun;5(3):1-1.

Urban JP. Fluid and solute transport in the inter-vertebral disc. PhD thesis, University of London. 1977.

Veres SP, Robertson PA, Broom ND. ISSLS prize winner: microstructure and mechanical disruption of the lumbar disc annulus: part II: how the annulus fails under hydrostatic pressure. Spine. 2008 Dec 1;33(25):2711-20.

Vernon-Roberts B, Moore RJ, Fraser RD. The natural history of age-related disc degeneration: the pathology and sequelae of tears. Spine. 2007 Dec 1;32(25):2797-804.

Verzijl N, DeGroot J, Zaken CB, Braun-Benjamin O, Maroudas A, Bank RA, Mizrahi J, Schalkwijk CG, Thorpe SR, Baynes JW, Bijlsma JW. Crosslinking by advanced glycation end products increases the stiffness of the collagen network in human articular cartilage: a possible mechanism through which age is a risk factor for osteoarthritis. Arthritis & Rheumatism. 2002 Jan;46(1):114-23.

Viguet-Carrin S, Roux JP, Arlot ME, Merabet Z, Leeming DJ, Byrjalsen I, Delmas PD, Bouxsein ML. Contribution of the advanced glycation end product pentosidine and of maturation of type I collagen to compressive biomechanical properties of human lumbar vertebrae. Bone. 2006 Nov 1;39(5):1073-9.

Vlassara H, Palace MR. Diabetes and advanced glycation endproducts. Journal of internal medicine. 2002 Feb;251(2):87-101.

Von Forell GA, Hyoung PS, Bowden AE. Directional failure of tendons in the presence of a notch defect. InMechanics of Biological Systems and Materials, Volume 4 2014 (pp. 11-14). Springer, Cham.

Wagner DR, Reiser KM, Lotz JC. Glycation increases human annulus fibrosus stiffness in both experimental measurements and theoretical predictions. Journal of biomechanics. 2006 Jan 1;39(6):1021-9.

Watanabe H, Yamada Y, Kimata K. Roles of aggrecan, a large chondroitin sulfate proteoglycan, in cartilage structure and function. The journal of biochemistry. 1998 Oct 1;124(4):687-93.

Werbner B, Lee M, Lee A, Yang L, Habib M, Fields AJ, O'Connell GD. Non-enzymatic glycation of annulus fibrosus alters tissue-level failure mechanics in tension. Journal of the Mechanical Behavior of Biomedical Materials. 2021 Nov 20:104992.

Werbner B, Spack K, O'Connell GD. Bovine annulus fibrosus hydration affects rate-dependent failure mechanics in tension. Journal of biomechanics. 2019 May 24;89:34-9.

Werbner B, Zhou M, McMindes N, Lee A, Lee M, O'Connell GD. Saline-polyethylene glycol blends preserve in vitro annulus fibrosus hydration and mechanics: An experimental and finite-element analysis. Journal of the Mechanical Behavior of Biomedical Materials. 2021 Nov 2:104951.

Werbner B, Zhou M, O'Connell G. A novel method for repeatable failure testing of annulus fibrosus. Journal of biomechanical engineering. 2017 Nov 1;139(11).

White III AA, Panjabi MM. Clinical biomechanics of the spine.

Wilder DG, Pope MH, Frymoyer JW. The biomechanics of lumbar disc herniation and the effect of overload and instability. Journal of spinal disorders. 1988 Jan 1;1(1):16-32.

Wilke HJ, Neef P, Caimi M, Hoogland T, Claes LE. New in vivo measurements of pressures in the intervertebral disc in daily life. Spine. 1999 Apr 15;24(8):755-62.

Woessner Jr JF. The determination of hydroxyproline in tissue and protein samples containing small proportions of this imino acid. Archives of biochemistry and biophysics. 1961 May 1;93(2):440-7.

Wu JJ, Eyre DR, Slayter HS. Type VI collagen of the intervertebral disc. Biochemical and electron-microscopic characterization of the native protein. Biochemical Journal. 1987 Dec 1;248(2):373-81.

Yamamoto N, Hayashi K. Mechanical properties of rabbit patellar tendon at high strain rate. Biomedical materials and engineering. 1998 Jan 1;8(2):83-90.

Yao H, Justiz MA, Flagler D, Gu WY. Effects of swelling pressure and hydraulic permeability on dynamic compressive behavior of lumbar annulus fibrosus. Annals of biomedical engineering. 2002 Nov;30(10):1234-41.

Yoon JH, Halper J. Tendon proteoglycans: biochemistry and function. J Musculoskelet Neuronal Interact. 2005 Mar 1;5(1):22-34.

Żak M, Pezowicz C. Analysis of the impact of the course of hydration on the mechanical properties of the annulus fibrosus of the intervertebral disc. European Spine Journal. 2016 Sep;25(9):2681-90.

Zhou M, Lim S, O'Connell GD. A Robust Multiscale and Multiphasic Structure-Based Modeling Framework for the Intervertebral Disc. Frontiers in Bioengineering and Biotechnology. 2021 Jun 7;9:452.

Zitnay JL, Weiss JA. Load transfer, damage, and failure in ligaments and tendons. Journal of Orthopaedic Research. 2018 Dec;36(12):3093-104.

9. Appendix A: AF Tissue-Level Sample Preparation and Tensile Testing Protocol

University of California, Berkeley
Berkeley Biomechanics Lab

Author: Benjamin Werbner
Date Authored: 10/20/2019
Last Updated: 03/12/2020

Summary: The following protocol describes the methods for the preparation and tensile failure testing of tissue-level annulus fibrosus (AF) specimens from bovine caudal spine sections.

I. Dissection of Intervertebral Discs (IVDs) from Bovine Coccygeal Spine Sections

Materials: Fresh or thawed bovine coccygeal spine sections (thaw overnight in fridge or for ~3hrs in a well-sealed zip-top bag submerged in water), dissection pads, #22 and #11 scalpels, dissection forceps

1. Prepare a working surface for dissection by taping down two overlapping absorbent pads.
2. Begin making long cuts parallel to the long axis of the spine using #22 scalpel, working from lateral to medial but stopping short of the sagittal centerline. Stabilize the spine with the non-dominant hand, or if you prefer use three-tooth dissection forceps. Use these long cuts to peel off long, continuous pieces of muscle along the spine length. Recall the morphology of the transverse, dorsal vertebral processes and try to work around them without dulling the scalpel blade trying to cut bone.
3. As you remove the bulk of the supporting muscle, gently flex the spine back and forth in the frontal plane to get a sense of where the discs are; the spine will flex around the disc at each joint. As you get closer to the disc, use a finger with medium pressure to palpate the dorsal aspect along the sagittal centerline to identify where the dorsal process extends over the protected cavity containing the disc.
4. Once you've identified the dorsal opening between bones where the disc will be, switch over to the #11 and make scooping cuts, primarily in the frontal plane, and in the transverse plane, i.e. with the blade perpendicular to the long axis, working your way ventrally toward the disc. Make these cuts successively smaller and more conservative until you see the shiny pinkish-white tissue of the longitudinal ligament and outer AF, but don't go too far into the white of the AF.
5. Once you have exposed a small portion of the disc outer surface, begin to rotate the spine and use the #11 blade to gently 'scoop' all of the tissue tangent to the disc around its circumference, until you can see the shiny smooth pink surrounding the disc around its full circumference.
6. Use medium-hard pressure with dissecting forceps or your fingernail to palpate precisely where the hard bone/endplate ends and the softer disc begins. Place the scalpel a few millimeters on the bone side of the interface and gently press down, advancing forward a small amount each time until you begin to cut the soft disc tissue.
7. Having identified the disc-endplate boundary, begin making many small, conservative cuts in the transverse plane with the scalpel, scraping the end plate to get as much disc tissue off without gouging the disc surface. Gently lift one end of the spine off the table so that the weight of the spine induces slight tension on the dorsal side and helps 'peel' the disc away from the endplate as you continue to cut along the endplate boundary in the transverse plane.
8. Begin rotating the angle of approach and work your way around successively larger arcs of the disc, making small, scraping cuts at the bone-disc interface. Recall that the endplate tends to be quite convex, so be sure to angle the scalpel blade accordingly to optimize the thickness of undamaged disc tissue that can be harvested.
9. Once the first aspect is detached, flip the spine, and do the same on the other side; this may be slightly more challenging because you don't have the weight of the spine to tension the cut.

10. Wrap the dissected disc in gauze dampened with PBS, place in a 3x4" zip top bag, label with the spine ID (date of dissection) and disc number (C1-C4), and freeze at -20°C.

II. Cryo-stage Microtome Isolation of Tissue-Level Specimens from IVDs

Materials: Fresh or frozen intact IVDs, #22 scalpel, NEG-50 frozen section embedding medium

1. Turn on microtome with switch on back of control console.
2. Use plastic pipette to deposit a thin layer of embedding media (NEG-50 gel) onto center of microtome stage covering the area of the disc.
3. Place frozen disc with the smoother, more evenly dissected aspect down and the more unevenly dissected side facing up to start.
4. Make sure to press the disc down tightly and flat against the stage before temperature drops below 0°C and media hardens.
5. Wait for disc to freeze *through the thickness*, then begin microtoming using one to three strokes at a time. Remember not to slam microtome back against the stop closest to you while advancing it, as this can damage the spring.
6. When entire top surface of disc is smooth and free of nicks or defects (Fig. 1), continue microtoming a little more until the disc measures around 7.5-8mm in height. Check the height as shown in Fig. 2.

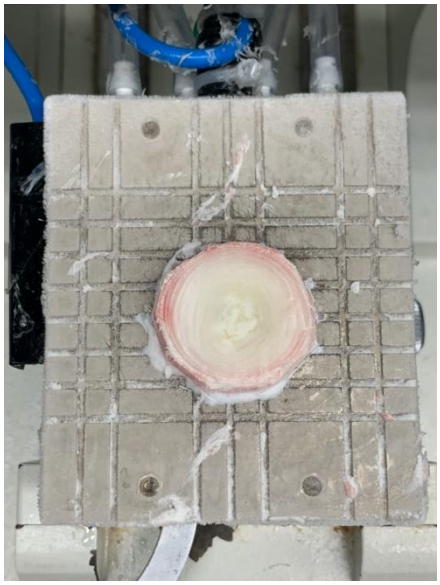

Fig. 1: Disc superior surface free of defects

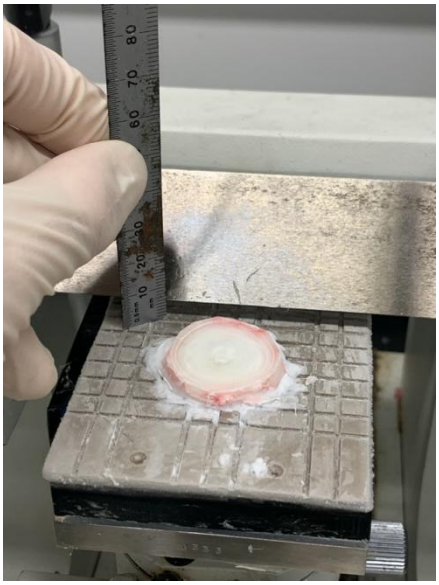

Fig. 2: Measuring disc height via blade height

7. When content with the first side, hold the 'Thaw' button on the front of the control console. When the media thaws (around 0°C), flip the disc over, potentially adding a little more media under if necessary. Make sure to press the disc down so the microtomed side is tight against the stage.
8. Wait for disc to freeze through the thickness, then begin microtoming using 1-3 strokes at a time.
9. Microtome until the disc height reaches 5mm, measuring as shown in Fig. 2.
10. Hold the 'Thaw' button until the temperature reaches about -3°C; this will make the disc easier to cut through without breaking it loose from the stage.
11. Use the reusable yellow 10 mm biopsy punch to remove most of the nucleus from the disc, and then make four parallel cuts using a #22 scalpel so isolate the longest and cleanest sections of AF, as shown in Fig. 3. Recap punch.
12. Thaw the stage and remove all the tissue pieces, setting them aside on a dissection pad to thaw. Wipe the stage clean with a Kimwipe.

13. Discard the outermost tissue and place the inner tissue sections in a 1.5ml biochem tube labelled with the disc ID.
14. When slightly thawed/relaxed, place the two AF tissue pieces in some embedding media, lengthwise on the stage (long axis perpendicular to blade) with the inner-AF sides facing up to start.
15. Wait for the samples to freeze all the way through; this takes several minutes so occupy yourself otherwise and don't rush it. When frozen through again, microtome the slices down to ~4mm.
16. Thaw the stage and flip the samples over, allow them to refreeze, and microtome them down until they are exactly 2mm thick. They should appear as in Fig. 4.
17. Thaw and remove the samples from the stage and clean the stage and blade with a damp paper towel while the samples thaw slightly on the dissection pad.

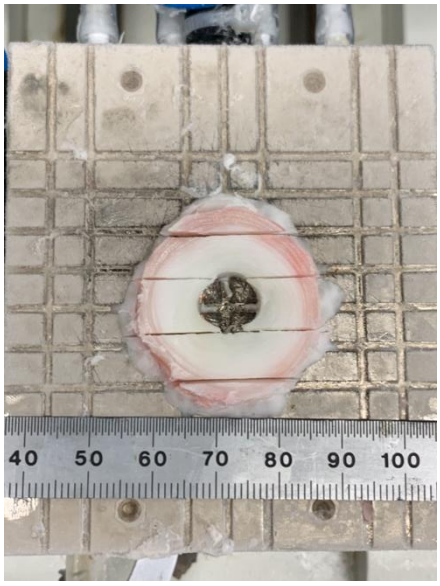

Fig. 3: IVD with nucleus pulposus removed and cuts to isolate anterior/posterior AF

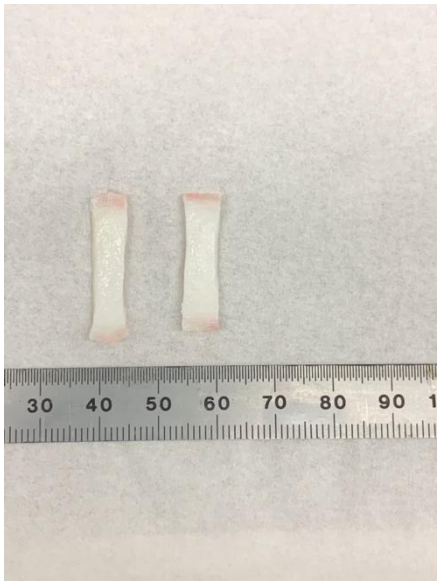

Fig. 4: Prepared tensile specimens (unnotched)

III. Notching for Repeatable Tensile Failure

Materials: Tissue-level AF specimen, 3D printed notching jigs and razor blades

1. Place the samples in the 3-piece depth-notching jig (Fig. 5) and smooth it down to ensure that it is flush in the bottom of the channel, and not sticking up on either edge. Ensure that the sample mid-length is centered over the cutting location on the jig.
2. Place the retaining pieces on the jig, and holding them down, smoothly and in one continuous motion slide a flat razor blade across the sample surface through the opening in the jig, and then slide the razor blade back. You should have a depth-notch with only 1mm of thickness remaining.
3. Remove the sample from this jig and place them back on the microtome stage, with the depth notch centered over one of the horizontal channels in the stage. Do not use any embedding media.
4. Turn on the stage, and just after the samples start to stick to the surface and freeze through the thickness, use the double-razor width-notching jig (Fig. 6) to cut through the existing depth notch, with the opening centered on the sample mid-length, until the razors go all the way through the tissue and into the channel in the stage. You should be able to see through to confirm that only ~1.25mm of sample width remains in the notch. See Fig. 7 for a summary schematic of the notch geometry.

5. Thaw and remove the samples from the stage, place in white weigh boat, and rinse briefly with PBS from squirt bottle. Mix around to make sure samples are clean and then remove from PBS and blot totally dry with a Kimwipe.

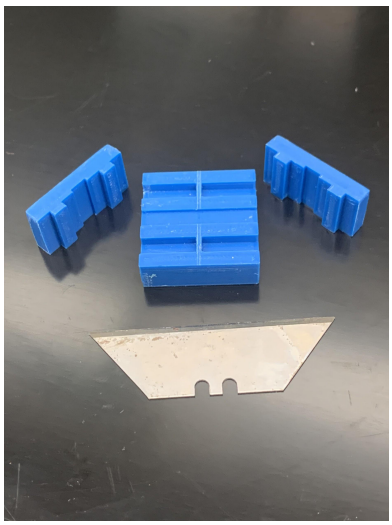

Fig. 5: Depth-notch jig

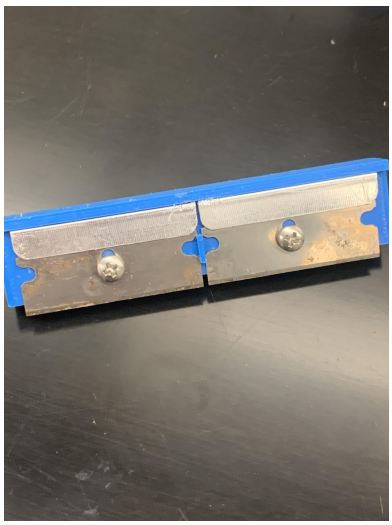

Fig. 6: Width-notch jig

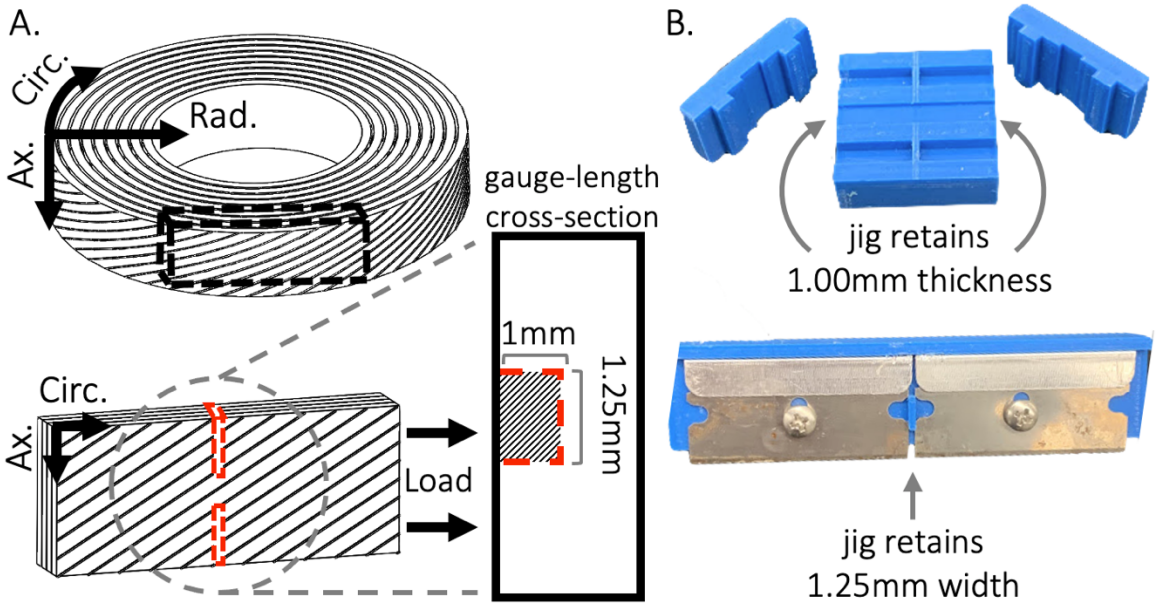

Fig. 7: Summary schematic of tensile specimen notch geometry

IV. Equilibrium Hydration/In Vitro Disease Model Treatment

Materials: Saline-polyethlyene glycol blend (SPEG), methylglyoxal, chABC, or other treatment solutions

1. Weigh and record the sample fresh weight and the soak solution that is to be used.
2. Pipette 5ml of buffer solution into a 15ml soak tube labeled with the sample ID. Buffer solutions are described elsewhere in detail.
3. Place the sample in the tube of solution and either leave on counter near scale for room temperature samples or place in tube stand in water bath set to 50°C if treatment requires. Make sure there is

sufficient water in the bath and supplement with DI water from pump in TE room if necessary. Hold the 'Set' button and adjust the temperature on the water bath to achieve 50°C.
4. Note the time and be sure to prepare to test 18 hours later.
5. ~~~~~~~~~~~~~~~~~~~~ 18 hours later ~~~~~~~~~~~~~~~~~~~~
6. Remove sample from soak solution by gently using the long tweezers.
7. Blot the sample totally dry with a Kimwipe (when you flip it no fluid outline should be deposited).
8. Record the soaked weight of the sample.
9. You may want to put the sample back into the soak tube while you set up the machine and get the grips ready for testing.

V. Shimadzu Mechanical Tester and PointGrey Camera Setup

1. To install the lower tension grip, first thread the locking collar onto the lower grip, then place the grip post into the mount at the base of the water bath. Make sure the grip is positioned such that the front surface of the sample will face forward. Place the pin through the grip mount and post, and thread down the locking collar to secure the grip on the mount.
2. Turn on the Shimadzu with the toggle switch on the front left of the machine.
3. Wait ~10sec for the machine to boot up and then open the Trapezium X program on the Shimadzu computer. The username is 'admin' and the password is 'admin'.
4. Click 'Select Method and Test' and choose the appropriate method ('AF_Tension_Low' or 'AF_Tension_High')
5. Right-click the Force display in the top left corner and click 'Calibration.' Do not disturb the machine at all during calibration. Once the machine beeps after calibration, confirm the load is at zero; the machine is now prepared for mechanical testing.
6. Mount the camera arm near the Shimadzu by lining up the mounting bracket with the clear tape between the computer and the machine. Gripping only the arm and not the camera itself, position the camera 'horizontally' in front of the water bath, parallel to the ground and aimed at about 1" above the bottom grip.
7. Plug the camera USB cord into the Instron computer and open the PointGrey FlyCap software (blue/yellow diamond icon). Select the 'Grasshopper' camera and click 'OK.'
8. Click the Record button (red circle) at the top of the window. Click 'Browse' and create a separate folder labeled with the sample ID for each mechanical test performed. Select this directory to save your image files.
9. For high-rate testing, change the image capture options to 'Capture once every 100 ms from a run of 100000 ms.' For low-rate testing, set to 'Capture once every 60,000 ms from a run of 12000000 ms.'
10. Now click back to the first option and input '1,' i.e. 'Capture 1 frames.' We use this option to take a still image of the specimen with a ruler before testing.
11. For the other options, select 'Streaming' and change the file type to 'TIFF.'

VI. Gripping and Testing

1. When the machine, cameras, and computer are ready to test, remove the first sample from its soak tube and dry it off completely using a Kimwipe.
2. Using tweezers, place the sample into the first set of grips (will be the bottom grip), placing the end of the sample in the teeth of the grip so that only clean AF gauge length remains. Place the notched side of the specimen facing forward. Grip the sample anticipating a gauge length of ~10mm.
3. Carefully and evenly close the first set of grips on the sample by slowly but firmly squeezing the toothed area between the fingers on one hand. Hold the grips tight this way while beginning to tighten the screws with your free hand.

4. Tighten the first screw until some resistance is felt, then tighten the other, and alternate progressively until both screws are tight, making sure the sample remains in the correct position while tightening. Confirm that the length of the sample is perpendicular to the top of the grips.
5. Place the bottom grip with the sample in the lower jaws of the machine, making sure that the grips are aligned horizontally and that the sample is centered in the grips. Tighten the lower jaw to clamp the lower grip in place.
6. Loosen the screws of the top grip somewhat and clamp the loose top grip in the upper jaws of the machine. Right click the 'Load' display and click 'To zero' to balance the load or do so using the button on the machine. Confirm that the load reads zero with the upper grip installed.
7. Manually jog the crosshead down and carefully guide the free end of the sample into the open serrated area of the upper grip using tweezers. Make sure the sample is straight and that sufficient material is gripped within the teeth. Again, pinch the grip with one hand around the serrated area and alternately tighten the screws until the sample is tightly and securely clamped in the upper grip as well. If the Load display reads more than about 0.5N, you may need to adjust the sample in the grips or the grips in the jaws to make sure everything is straight and relaxed but avoid unscrewing the grip screws once they have been tightened if possible.
8. When the load is confirmed to be near zero, right click the Displacement display and click 'To Zero' to balance the extension or use the button on the machine to do so.
9. Confirm that the load is near zero, the displacement is zero, and that the camera is positioned correctly and in focus.
10. Point the lamp at the sample and hold the ruler in the same plane as the sample front surface, confirm that 'Capture 1 frames' is selected, and click the 'Capture' button in the bottom right corner of the PointGrey camera software. It is essential that we have a clear picture of each sample with the ruler before testing begins (Fig. 8). Bring the mouse from the Instron computer over toward the Shimadzu to be able to take the picture and hold the ruler at the same time.
11. Now click over to 'Capture once every XXX ms from a run of XXX ms.'
12. Click the 'Start Test' button in the Shimadzu software, and then click 'Start Test' in the Shimadzu popup while clicking 'Capture' on the camera computer.

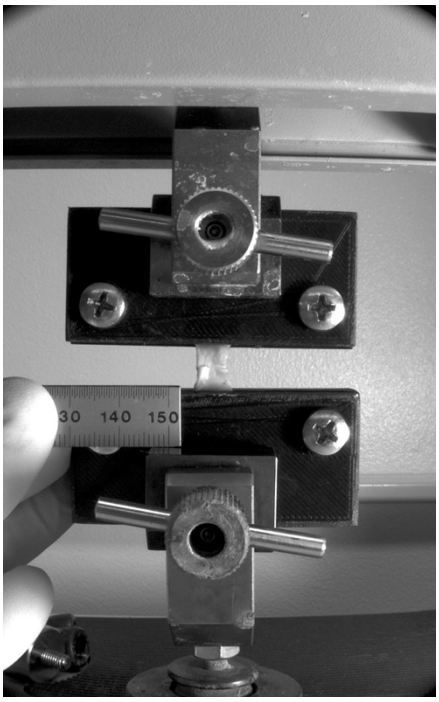

Fig. 8: Gripped sample with scale bar. Every tested sample must have this photo.

VII. Data Export, Shimadzu Breakdown, and Failed Specimen Storage

1. After the test has completed, click ‘Stop Recording’ in the camera software and ‘Stop Test’ on the Shimadzu computer.
2. On the Shimadzu computer, click ‘File’ -> ‘Export’ -> ‘Raw Data’. Make sure you are in the right folder and name the CSV file with the sample ID and click ‘Save.’ For low-rate tests, in may take a minute for this file to save, so do not click around too much until you are sure that the file has finished exporting.
3. Raise the crosshead up about 3-4” and remove both grips.
4. Loosen grips and remove failed specimens.
5. If you are finished testing for the day, close the Trapezium software and turn off the Shimadzu. Close the PointGrey software on the Instron computer and disconnect the camera USB.
6. Copy both the mechanical testing data and the photos for the day onto the O’Connell Lab external hard drive (usually found in this room or attached to the middle room computer).
7. For each sample, record in the spreadsheet whether the sample failed at the mid-length or at the grips.
8. Weigh two purple 1.5ml centrifuge tubes and label each tube with its empty weight and the name of the sample that will go inside. Note that since we retain two tissue sections per sample, the tube will be labeled with something like ‘042018-1-D2-S2-1’ or ‘103120-2-D1-S1-2’.
9. Using a scalpel, cut the crimped sections off the two specimen halves and retain two ~50-80 mg tissue sections from the failed sample, ideally from either side of the failure site or mid-length. Try to aim for consistent wet weights when possible.
10. Gently blot off each tissue section using a Kimwipe, place each section in a centrifuge tube, and note the combined weight on the tube exterior and in the Tissue Inventory spreadsheet.
11. Place the tubes together in the small zip-top bag labeled with the disc name or in a storage box in the freezer with the other retained specimen sections and update the lab notebook spreadsheet with the status of the sample and any notes that you made during the preparation and testing procedure.